CIVIL ENGINEERING STUDIES
STRUCTURAL RESEARCH SERIES NO. 324

ANALYSIS OF ELASTO-PLASTIC SHELL STRUCTURES

by
N. A. SHOEB
and
W. C. SCHNOBRICH

A Report on a Research
Program Carried Out
under
National Science Foundation
Grant No. GK-538

UNIVERSITY OF ILLINOIS
URBANA, ILLINOIS
AUGUST, 1967

ANALYSIS OF ELASTO-PLASTIC SHELL STRUCTURES

by

N. A. Shoeb

and

W. C. Schnobrich

A Report on a Research
Program Carried Out
under
National Science Foundation
Grant No. GK-538

University of Illinois
Urbana, Illinois
August, 1967

ACKNOWLEDGMENT

This report was prepared as a doctoral dissertation by Mr. N. A. Shoeb. The work was under the supervision of Dr. W. C. Schnobrich. The research has been partially supported by the National Science Foundation under Research Grant NSF-GK 538.

The authors wish to express their thanks to the staff of the Department of Computer Science for their cooperation in the use of the IBM 7094-1401 computer system (supported partially by a grant from the National Science Foundation under Grant NSF-GP 700).

TABLE OF CONTENTS

TABLE OF CONTENTS (cont'd)

LIST OF TABLES

LIST OF FIGURES

LIST OF FIGURES (cont'd)

LIST OF FIGURES (cont'd)

LIST OF FIGURES (cont'd)

1. INTRODUCTION

1.1. Object and Scope

Beginning with the design of the first shell roof structure[22]* and continuing to the present day, engineers have based their design of shell structures on the classical theory of elasticity. Experience has shown that employing elastic design procedures usually provides structures that are adequate under service loads. Some engineers,[1,21,25] however, prefer ultimate load methods for the design of reinforced concrete shells. Johansen[21] for example feels that it is irrational to solve the shell by a fine mathematical work based on the theory of elasticity and then sum up the tensile stresses into a tensile force and determine the reinforcement by dividing this tensile force by the working stress, ignoring the fact that the deformation and the working stress do not correspond. He thus suggests that the working load must be fixed according to the ultimate load. Limit analysis techniques have also been investigated for shells of homogeneous materials. With a limit analysis, upper and lower bound solutions are sought. For the most part these solutions have only been found for rotationally symmetric shells. The one exception to this is the paper by Fialko.[14] He investigated upper and lower bound solutions for a cylindrical shell roof under radial loading.

There remains a gap in the knowledge of the behavior of shell structures for the whole region between the elastic limit and the

---

* Numbers in parentheses refer to entries in the List of References.

ultimate load. The redistribution of stresses in the shell after exceeding the elastic limit and the elasto-plastic response are phases that need closer investigation.

The object of this investigation is to study the behavior of a cylindrical shell roof between the end of the elastic stage and the final ultimate capacity. To achieve this purpose a mathematical model is used to replace the continuum. By the use of electronic computers this model makes it possible to simulate an actual experimental test in the laboratory. The model consists of rigid bars joined together by deformable nodes. The nodes are of the sandwich type and their outer layers bear the material properties of the shell. This model is adaptable for any kind of shallow shell rectangular in plan form but it will be used here only for cylindrical shells as an example to demonstrate the applicability of the method. Different boundary conditions are formulated for the model. The displacements in the model are defined so that it is possible for all forces to be found at each node. This feature is particularly desirable in solving an elastic-plastic problem.

The material is assumed elastic perfectly plastic. In the elastic range it is assumed to obey Hooke's law. For the determination of the initiation of the plastic flow the Mises-Hencky yield criterion is used. In the plastic range an incremental form of the Prandtl-Reuss relations, modified for the state of plane stress, is used. By increasing the load in small finite increments it is possible to trace the progression of yield zones in the shell. For each load increment all the displacements, forces, and moments are determined in the model. The load displacement characteristic is thus studied. Due to the

complexity of the problem an extensive program for the IBM 7094 computer is developed to handle all the calculations.

Two illustrative problems are presented in Chapter 6. The first is a single barrel cylindrical shell simply supported at its ends and with its longitudinal edges free. The second problem is that of a multiple barrel shell also simply supported at both ends.

Since the design objective is to utilize the material fully, an understanding of the behavior of shell structures is invaluable, as the usual theory of elasticity does not provide an adequate guide. However, with an elasto-plastic analysis, small plastic strains might be allowed in an effort to use the material more efficiently.

1.2. Nomenclature

The symbols used in this study are defined when they first appear. For convenience they are summarized below.

e = mean normal strain

e_x, e_y, e_z = deviatoric strain components

E = modulus of elasticity

G = modulus of rigidity

h = thickness of shell

J_2 = the second stress invariant

k = yield stress in simple shear

K = bulk modulus = $\frac{E}{3(1-2\nu)}$

L_x, L_y = grid length in the x and y directions, respectively

M_x, M_y = moments about the x and y axes, respectively

M_{xy} = twisting moment

N_x, N_y = axial forces in the x and y-directions, respectively

N_{xy} = in plane shearing force

p = uniform applied load

Q_y = normal shearing force perpendicular to the y-axis

R = radius of shell

s = mean normal stress

s_x, s_y, s_z = deviatoric stress components

t = spacing of layers

u, v, w = displacements in the x, y and z directions, respectively

W = work performed by stresses during plastic distortion

$\overline{X}, \overline{Y}, \overline{Z}$ = external loads in the x, y and z directions, respectively

β = angle between rigid bars in the yz plane

γ_{xy} = shearing strain

ϵ_x, ϵ_y = strains in the x and y-directions, respectively

θ = rotation of rigid bars

ν = Poisson's ratio

σ_x, σ_y = stresses in the x and y-directions, respectively

τ_{xy} = shearing stress

φ = half the opening angle of the shell

κ_x, κ_y = curvatures in the x and y-directions, respectively

κ_{xy} = twisting curvature

2. DESCRIPTION OF THE MODEL

2.1. General

In the analysis of plates, shells, and similar complex structures, the concept of using a physical analogue lends itself readily to the solution of such problems. In the application of the analogue method the continuous medium of the structure is replaced by a model which consists of rigid bars joined by deformable nodes. The nodes possess the desired material properties of the medium. Such a model was used by Schnobrich[34] for the analysis of cylindrical shells, assuming the material to be elastic. In that model the normal stresses were defined at one set of points, while the shear stresses were defined at yet a different set of points. Although the model functioned very satisfactorily in the elastic region, the separation of the extensional elements from the shear elements renders that particular model inconvenient for an extension of the study into the plastic range of material behavior.

Another model, which may be considered a superposition of two of the previous models, was developed later by Mohraz and Schnobrich.[27] This later model is used in this work because of its inherent advantages. The most important advantage insofar as this study is concerned is that the extensional as well as the shear stresses are found at the same node. This makes it convenient to apply a yield criterion to the nodes.

2.2. Description of the Model

The model consists of rigid bars connected together by deformable nodes, Fig. 1. This model is suitable for the analysis of any shell rectangular in plan, but it is used here only for cylindrical shells. The bars are arranged in a rectangular pattern. The transverse bars form chords of the arc of the cylinder, while the longitudinal bars lie along the generators. The connections where the two sets of bars intersect between the nodes are made such as to allow their independent movement in the radial direction. However, the connection is such that a rotation of one bar does twist the other crossing bar.

The nodes are of the sandwich type, i.e. composed of two deformable elements at the extreme fibers separated by a distance t. The two deformable elements enclose a rigid core as shown in Fig. 2. The top and bottom layers of the nodes are assumed in a state of plane stress. The core material is assumed to carry the vertical shear and does not yeild or fail. The extensional and shear stiffnesses of a strip of the shell with a length L_x, a width $L_y/2$ and a thickness of $h/2$ are concentrated at both the top and bottom layers of the node. These layers possess all the material properties of the prototype. The spacing t between the two facings is equal to $h/\sqrt{3}$ when the bending stiffness furnished by the sandwich shell is equated to the bending stiffness of a solid elastic shell of thickness h. If the moment furnished by the sandwich shell is equated to the fully plastic moment in a solid shell, t is then found to be equal to $h/2$. Solutions based on either equivalent thickness held fixed during the entire loading process or on a variable equivalent thickness changing when plastic action

starts should not differ from each other by any appreciable amount. Therefore in this study t is chosen equal to $h/\sqrt{3}$ and is kept constant throughout both the elastic and plastic phases.

The system of notation used to identify the different points on the model is shown in a plan view in Fig. 3. Any node at which the strains, stresses, forces, and moments are sought will always be designated ij.

2.3. Coordinate System

In the analysis of cylindrical shells it is convenient to use a moving triad of orthogonal axes as the coordinate system. When the origin is placed at a deformable node then the x-axis is in the longitudinal direction, the y-axis in the direction of the tangent, and the z-axis normal to the tangent. This system of axes is shown in Fig. 4 with their positive directions indicated.

2.4. Displacements

The components of displacement of the shell are defined as follows (Figs. 3 and 4):

a. The "u" displacements are parallel to the x-axis and are defined at the intersections of the rigid bars.

b. The "v" displacements are parallel to the y-axis and are defined at the intersections of the rigid bars.

c. The "w" displacements are parallel to the z-axis and are defined at the deformable nodes.

2.5. External Loads

Loads applied to the shell are reduced to a number of concentrated loads acting at the points where the corresponding displacements are defined. Figure 3 shows the load contribution areas for the different components of the concentrated loads. One loading of particular interest in regard to shell roofs is a uniform load acting vertically downward on the shell. Such a load has two components: one in the direction of the normal to the shell (z-direction), and the other in the tangential direction (y-direction).

2.6. Internal Forces and Their Sign Convention

The positive directions of σ_x, σ_y, and τ_{xy} for both the top and bottom layers of a node are shown in Fig. 5a. Also the forces N_x, N_y, and N_{xy} have the same positive direction as their corresponding stresses. The positive directions for the moments are as shown in Figs. 5b and 5c.

2.7. Strain-Displacement Relations for the Model

The strains which are required are those of the top and bottom layers of a node. These strains are defined in terms of the displacements of the middle surface. Although there is no deformable layer at the middle surface it is still convenient to define a pseudo set of mid-surface strains and curvatures and use them to find the strains at the top and bottom layers. These pseudo mid-surface strains and curvatures are established by the geometry of deformation of the nodes. They are similar to the finite difference form of the strains

and curvatures developed about the middle surface of a real continuous shell. Referring to Fig. 3, the mid-surface extensional and shearing strains for a typical interior node ij are:[27]

$$\epsilon_{xij} = \frac{1}{L_x}(u_{i+1j} - u_{i-1j})$$

$$\epsilon_{yij} = \frac{1}{L_y \cos\frac{\beta}{2}}(v_{ij+1} - v_{ij-1}) - \frac{1}{R\cos\frac{\beta}{2}} w_{ij} \qquad (2.1)$$

$$\gamma_{xyij} = \frac{1}{L_y}(u_{ij+1} - u_{ij-1}) + \frac{1}{L_x}(v_{i+1j} - v_{i-1j})$$

The bending and twisting curvatures in terms of the rotation of the rigid bars are:

$$\kappa_{xij} = \frac{1}{L_x}(\theta_{xi+1j} - \theta_{xi-1j})$$

$$\kappa_{yij} = \frac{1}{L_y}(\theta_{yij+1} - \theta_{yij-1}) \qquad (2.2)$$

$$\kappa_{xyij} = \frac{1}{L_y}(\theta_{xij+1} - \theta_{xij-1}) + \frac{1}{L_x}(\theta_{i+1j} - \theta_{i-1j})$$

The rotations of the different bars in terms of the displacements are found to be:

$$\theta_{xi+1j} = \frac{1}{L_x}(w_{i+2j} - w_{ij})$$

$$\theta_{xi-1j} = \frac{1}{L_x}(w_{ij} - w_{i-2j})$$

$$\theta_{yij+1} = \frac{1}{L_y}\left[\frac{L_y}{R\cos\frac{\beta}{2}} v_{ij+1} + \frac{1}{\cos\frac{\beta}{2}}(w_{ij+2} - w_{ij})\right] \qquad (2.3)$$

$$\theta_{yij-1} = \frac{1}{L_y}\left[\frac{L_y}{R\cos\frac{\beta}{2}} v_{ij-1} + \frac{1}{\cos\frac{\beta}{2}}\left(w_{ij} - w_{ij-2}\right)\right]$$

Substituting the above expressions for the rotations into Eqs. (2.2) the expressions for the curvatures, κ_{xij} and κ_{yij}, can be rewritten as:

$$\kappa_{xij} = \frac{1}{L_x^2}\left(w_{i+2j} - 2w_{ij} + w_{i-2j}\right)$$

$$\kappa_{yij} = \frac{1}{L_y^2}\left[\frac{L_y}{R\cos\frac{\beta}{2}}\left(v_{ij+1} - v_{ij-1}\right) + \frac{1}{\cos\frac{\beta}{2}}\left(w_{ij+2} - 2w_{ij} + w_{ij-2}\right)\right] \tag{2.4}$$

Expressions similar to Eqs. (2.3) and necessary for the determination of the twisting curvature are likewise easily formulated. The resulting twist-displacement equation thus found is:

$$\kappa_{xyij} = \frac{1}{L_x R\cos\frac{\beta}{2}}\left(v_{i+1j} - v_{i-1j}\right) + \frac{1}{L_x L_y}\left(1 + \frac{1}{\cos\frac{\beta}{2}}\right)\left(w_{i+1j+1} - w_{i-1j+1} - w_{i+1j-1} + w_{i-1j-1}\right) \tag{2.5}$$

The strains in the top and bottom layers are related to the mid-surface strains and curvatures by:

$$\begin{aligned}
\epsilon^{T}_{xij} &= \epsilon_{xij} + \frac{t}{2}\kappa_{xij} \\
\epsilon^{B}_{xij} &= \epsilon_{xij} - \frac{t}{2}\kappa_{xij} \\
\epsilon^{T}_{yij} &= \epsilon_{yij} + \frac{t}{2}\kappa_{yij} \\
\epsilon^{B}_{yij} &= \epsilon_{yij} - \frac{t}{2}\kappa_{yij}
\end{aligned} \tag{2.6}$$

$$\gamma^{T}_{xyij} = \gamma_{xyij} + \frac{t}{2}\kappa_{xyij}$$

$$\gamma^{B}_{xyij} = \gamma_{xyij} - \frac{t}{2}\kappa_{xyij}$$

Substituting Eqs. (2.1), (2.4), and (2.5) in the above equations, the expressions for the top and bottom strains are found to be:

$$\epsilon^{T}_{xij} = \frac{1}{L_x}(u_{i+1j}-u_{i-1j}) + \frac{t}{2L_x^2}(w_{i+2j}-2w_{ij}+w_{i-2j})$$

$$\epsilon^{B}_{xij} = \frac{1}{L_x}(u_{i+1j}-u_{i-1j}) - \frac{t}{2L_x^2}(w_{i+2j}-2w_{ij}+w_{i-2j})$$

$$\epsilon^{T}_{yij} = \frac{1}{L_y \cos\frac{\beta}{2}}(1+\frac{t}{2R})(v_{ij+1}-v_{ij-1}) + \frac{t}{2L_y^2\cos\frac{\beta}{2}}(w_{ij+2}-2w_{ij}+w_{ij-2}) - \frac{1}{R\cos\frac{\beta}{2}}w_{ij}$$

$$\epsilon^{B}_{yij} = \frac{1}{L_y \cos\frac{\beta}{2}}(1-\frac{t}{2R})(v_{ij+1}-v_{ij-1}) - \frac{t}{2L_y^2\cos\frac{\beta}{2}}(w_{ij+2}-2w_{ij}+w_{ij-2}) - \frac{1}{R\cos\frac{\beta}{2}}w_{ij} \qquad (2.7)$$

$$\gamma^{T}_{xyij} = \frac{1}{L_y}(u_{ij+1}-u_{ij-1}) + \frac{1}{L_x}(1+\frac{t}{2R\cos\frac{\beta}{2}})(v_{i+1j}-v_{i-1j}) + \frac{t}{2L_xL_y}(1+\frac{1}{\cos\frac{\beta}{2}})(w_{i+1j+1}-w_{i-1j+1}-w_{i+1j-1}+w_{i-1j-1})$$

$$\gamma^{B}_{xyij} = \frac{1}{L_y}(u_{ij+1}-u_{ij-1}) + \frac{1}{L_x}(1-\frac{t}{2R\cos\frac{\beta}{2}})(v_{i+1j}-v_{i-1j}) - \frac{t}{2L_xL_y}(1+\frac{1}{\cos\frac{\beta}{2}})(w_{i+1j+1}-w_{i-1j+1}-w_{i+1j-1}+w_{i-1j-1})$$

where the superscripts T and B stand for the top and bottom layers of the node, respectively. In the above equations cos $\beta/2$ will be assumed equal to 1 as $\beta/2$ is small, and it was found that the final results are affected only slightly by this approximation.

As the load on the shell is increased progressively the displacements increase incrementally. Thus Eqs. (2.1), (2.2), and (2.7) are used in an incremental form, i.e., $\Delta\epsilon$ and $\Delta\kappa$ instead of ϵ and κ and also Δu, Δv, and Δw instead of u, v, and w.

All the above strain displacement relations may be presented in the form of operators. The operators for the top and bottom strains (Eq. (2.7) with cos $\beta/2 = 1$) are shown in Figs. 6a, 6b, and 6c.

3. RELATIONS IN THE ELASTIC AND PLASTIC PHASES OF THE MATERIAL

3.1. General

In this study the deformable material of the nodes is assumed to be elastic-perfectly plastic. To make such an assumption it is necessary to define three essential aspects of material behavior:

1) The stress-strain relations in the elastic region.

2) A yield criterion that defines the limit of elasticity under any combination of stresses.

3) The stress-strain relations in the plastic region.

The stress state at a point of a body when referred to cartesian coordinates is described mathematically by a stress tensor. Geometrically this state of stress can be represented by a point plotted in "stress space." The coordinates of the point are the components of the stress tensor, and the vector from the origin to the stress point is called the stress vector. In general, there are nine components of stress, but considering moment equilibrium of an element of the material it follows that the stress tensor is symmetric. Thus only six components of the stress are independent. A change in a state of stress is represented by a vector from one point in the stress space to another.

In the stress space the mathematical expression defining the limit of elasticity is represented by a surface which is called the yield surface. This surface encloses a region in which only elastic changes in the strain occur. For a perfectly plastic material the yield

surface is fixed in this stress space. A stress point cannot be located outside the surface. When the stress vector reaches a point on the surface further changes must be associated with movement along or a return inside the yield surface. Plastic deformation occurs for movements on the yield surface.

3.2. Elastic Stress-Strain Relations

In the elastic region of the material behavior Hooke's law is assumed, thus the stresses are linearly proportional to the strains. The following relations between the stresses and strains are expressed in an incremental form to suit the method of analysis used in this study. For a state of plane stress the incremental stress-strain relations are:

$$\Delta\sigma_x = \frac{E}{1-\nu^2}(\Delta\epsilon_x + \nu\,\Delta\epsilon_y)$$

$$\Delta\sigma_y = \frac{E}{1-\nu^2}(\Delta\epsilon_y + \nu\,\Delta\epsilon_x) \qquad (3.1)$$

$$\Delta\tau_{xy} = \frac{E}{2(1+\nu)}\Delta\gamma_{xy}$$

To apply these relations to either the top or bottom layer of a node the corresponding strains should be used.

3.3. Yield Criterion

The yield criterion is the condition defining the limit of elasticity under any combination of stresses. It is represented by a surface in the stress space. The yield criterion which is assumed here is the Von Mises yield criterion. It states that plastic flow will

start if the second stress invariant J_2 reaches the value k^2, where k is the yield limit in simple shear. This simple shear yield limit is expressible as:

$$k = \frac{\sigma_o}{\sqrt{3}}$$

where σ_o is the yield stress of the material in simple tension. If J_2 is less than k^2 this means that the point is still elastic.

The yield criterion is applied in this problem to both the top and bottom layers of each node to check whether or not the specific layer has yielded.

For a state of plane stress the yield criterion reduces to:

$$\frac{1}{3}(\sigma_x^2 + \sigma_y^2 - \sigma_x\sigma_y) + \tau_{xy}^2 = k^2 \qquad (3.2)$$

The above equation is represented by the surface shown in Fig. 7a when the coordinate axes are taken to be σ_x, σ_y and τ_{xy}. If the surface is cut by the plane $\tau_{xy} = 0$, the relation between σ_x and σ_y is represented by the ellipse shown in Fig. 7b. If the surface is cut by the plane $\sigma_y = 0$, the relation between σ_x and τ_{xy} is represented by the ellipse shown in Fig. 7c.

3.4. Plastic Stress-Strain Relations

In the case of a perfectly plastic material once the stress vector touches the yield surface plastic flow takes place. During plastic flow the rate of change of the plastic strain is, at any

instant, proportional to the instantaneous stress deviation. This is known as the Prandtl-Reuss theory.[19,20] To present the stress-strain relations based on that theory it is convenient to first define the following quantities.

The mean normal stress (when $\sigma_z = 0$):

$$s = \frac{1}{3}(\sigma_x + \sigma_y) \tag{3.3}$$

The deviatoric stress components:

$$s_x = \sigma_x - s, \qquad s_y = \sigma_y - s, \qquad s_z = \sigma_z - s = -s \tag{3.4}$$

The mean normal strain:

$$e = \frac{1}{3}(\epsilon_x + \epsilon_y + \epsilon_z) \tag{3.5}$$

The deviatoric strain components:

$$e_x = \epsilon_x - e, \qquad e_y = \epsilon_y - e, \qquad e_z = \epsilon_z - e \tag{3.6}$$

Only those relations which are of use in the case of plane stress problems are written below. Also, to suit the numerical technique used in the analysis, the relations are presented in an incremental form rather than the rate form. In their general incremental form these relations are:[20]

$$\Delta s_x = 2G(\Delta e_x - \frac{\Delta W}{2k^2} s_x)$$

$$\Delta s_y = 2G(\Delta e_y - \frac{\Delta W}{2k^2} s_y) \qquad (3.7)$$

$$\Delta \tau_{xy} = G(\Delta \gamma_{xy} - \frac{\Delta W}{k^2} \tau_{xy})$$

where G is the shear modulus:

$$G = \frac{E}{2(1+\nu)}$$

ΔW is the incremental form of the rate at which the stresses do work during plastic flow in connection with the change of shape. In its general form ΔW is equal to:

$$\Delta W = s_x \Delta e_x + s_y \Delta e_y + s_z \Delta e_z + \tau_{yz} \Delta \gamma_{yz} + \tau_{zx} \Delta \gamma_{zx} + \tau_{xy} \Delta \gamma_{xy}$$

By its nature ΔW is essentially a positive quantity during plastic flow. In the case of plane stress problems τ_{yz} and τ_{zx} are zero and the expression reduces to:

$$\Delta W = s_x \Delta e_x + s_y \Delta e_y + s_z \Delta e_z + \tau_{xy} \Delta \gamma_{xy} \qquad (3.8)$$

Substituting Eqs. (3.4) and (3.6) into Eq. (3.8) and then using Eqs. (3.3) and (3.5) the expression for ΔW is reduced to the following:

$$\Delta W = \sigma_x \Delta \epsilon_x + \sigma_y \Delta \epsilon_y + \tau_{xy} \Delta \gamma_{xy} - 3s\Delta e$$

but

$$\Delta e = \frac{\Delta s}{3K}$$

where K is the bulk modulus and is equal to:

$$K = \frac{E}{3(1-2\nu)}$$

Thus:

$$\Delta W = \sigma_x \Delta\epsilon_x + \sigma_y \Delta\epsilon_y + \tau_{xy}\Delta\gamma_{xy} - \frac{s\Delta s}{K} \tag{3.9}$$

If complete incompressibility is assumed K tends to ∞ and the last term in Eq. (3.9) becomes zero.

To reduce Eqs. (3.7) to the special case of plane stress the following procedure is adopted.[23] Equations (3.4) are written in the incremental form and the stresses placed on the left-hand side of the equation with the following result:

$$\begin{aligned} \Delta\sigma_x &= \Delta s_x + \Delta s = \Delta s_x + \frac{\Delta\sigma_x + \Delta\sigma_y}{3} \\ \Delta\sigma_y &= \Delta s_y + \Delta s = \Delta s_y + \frac{\Delta\sigma_x + \Delta\sigma_y}{3} \end{aligned} \tag{3.10}$$

Equation (3.9) is substituted in Eqs. (3.7) then the resulting expressions substituted in Eqs. (3.10). Thus, two equations in two unknowns, $\Delta\sigma_x$ and $\Delta\sigma_y$, result. Upon solving these two equations the following expressions for $\Delta\sigma_x$ and $\Delta\sigma_y$ are obtained.

$$\begin{aligned} \Delta\sigma_x = C_A \Bigg[&\Delta\epsilon_x \left(4 - \frac{\sigma_x^2}{k^2} + \frac{4G}{3K}\frac{\tau_{xy}^2}{k^2}\right) + \Delta\epsilon_y \left(2 - \frac{\sigma_x\sigma_y}{k^2} - \frac{4G}{3K}\frac{\tau_{xy}^2}{k^2}\right) \\ &+ \Delta\gamma_{xy}\left(-\frac{\sigma_x\tau_{xy}}{k^2} + \frac{2G}{3K}\frac{(\sigma_y-\sigma_x)}{k^2}\tau_{xy}\right)\Bigg] \end{aligned} \tag{3.11}$$

$$\Delta\sigma_y = C_A \left[\Delta\epsilon_x\left(2 - \frac{\sigma_x\sigma_y}{k^2} - \frac{4G}{3K}\frac{\tau_{xy}^2}{k^2}\right) + \Delta\epsilon_y\left(4 - \frac{\sigma_y^2}{k^2} + \frac{4G}{3K}\frac{\tau_{xy}^2}{k^2}\right)\right.$$
$$\left. + \Delta\gamma_{xy}\left(-\frac{\sigma_y\tau_{xy}}{k^2} + \frac{2G}{3K}\frac{(\sigma_x-\sigma_y)}{k^2}\tau_{xy}\right)\right] \qquad (3.12)$$

Where

$$C_A = \frac{G}{1 + \frac{2G}{3K}\left(2 - 1.5\frac{s^2}{k^2}\right)}$$

Now, Δs is easily obtained by substituting Eqs. (3.11) and (3.12) in Eq. (3.3) in its incremental form:

$$\Delta s = \frac{C_A}{3}\left[\Delta\epsilon_x\left(6 - \frac{\sigma_x^2}{k^2} - \frac{\sigma_x\sigma_y}{k^2}\right) + \Delta\epsilon_y\left(6 - \frac{\sigma_y^2}{k^2} - \frac{\sigma_x\sigma_y}{k^2}\right)\right.$$
$$\left. - \Delta\gamma_{xy}\frac{\tau_{xy}}{k^2}(\sigma_x+\sigma_y)\right] \qquad (3.13)$$

Also, the expression for ΔW is obtained by substituting Eq. (3.13) into Eq. (3.9):

$$\Delta W = \frac{C_A}{G}\left[\Delta\epsilon_x\left(\sigma_x + \frac{2G}{3K}(\sigma_x-\sigma_y)\right) + \Delta\epsilon_y\left(\sigma_y + \frac{2G}{3K}(\sigma_y-\sigma_x)\right)\right.$$
$$\left. + \Delta\gamma_{xy}\tau_{xy}\left(1 + \frac{4G}{3K}\right)\right] \qquad (3.14)$$

Substitution of Eq. (3.14) into $\Delta\tau_{xy}$ of Eqs. (3.7) gives:

$$\Delta\tau_{xy} = C_A \left[\Delta\epsilon_x\left(-\frac{\sigma_x\tau_{xy}}{k^2} + \frac{2G}{3K}\frac{(\sigma_y-\sigma_x)}{k^2}\tau_{xy}\right)\right.$$

$$+ \Delta\epsilon_y\left(-\frac{\sigma_y\tau_{xy}}{k^2} + \frac{2G}{3K}\frac{(\sigma_x-\sigma_y)}{k^2}\tau_{xy}\right)$$

$$\left. + \Delta\gamma_{xy}\left(1 - \frac{\tau_{xy}^2}{k^2} + \frac{4G}{3K}\left(1 - \frac{\tau_{xy}^2}{k^2} - 0.75\,\frac{s^2}{k^2}\right)\right)\right] \qquad (3.15)$$

When $\Delta\sigma_x$, $\Delta\sigma_y$, $\Delta\tau_{xy}$, Δs, or ΔW are used for either the top or bottom layer of a node the corresponding top or bottom strains and stresses are used in their corresponding equations.

For complete incompressibility $K \to \infty$, and Eqs. (3.11), (3.12), (3.15), (3.13), and (3.14) simplify to the following form:

$$\Delta\sigma_x = G\left[\Delta\epsilon_x\left(4 - \frac{\sigma_x^2}{k^2}\right) + \Delta\epsilon_y\left(2 - \frac{\sigma_y\sigma_x}{k^2}\right) + \Delta\gamma_{xy}\frac{(-\tau_{xy}\sigma_x)}{k^2}\right]$$

$$\Delta\sigma_y = G\left[\Delta\epsilon_x\left(2 - \frac{\sigma_y\sigma_x}{k^2}\right) + \Delta\epsilon_y\left(4 - \frac{\sigma_y^2}{k^2}\right) + \Delta\gamma_{xy}\frac{(-\tau_{xy}\sigma_y)}{k^2}\right]$$

$$\Delta\tau_{xy} = G\left[\Delta\epsilon_x\left(\frac{-\tau_{xy}\sigma_x}{k^2}\right) + \Delta\epsilon_y\frac{(-\tau_{xy}\sigma_y)}{k^2} + \Delta\gamma_{xy}\left(1 - \frac{\tau_{xy}^2}{k^2}\right)\right] \qquad (3.16)$$

$$\Delta s = \frac{G}{3}\left[\Delta\epsilon_x\left(6 - \frac{\sigma_x^2}{k^2} - \frac{\sigma_x\sigma_y}{k^2}\right) + \Delta\epsilon_y\left(6 - \frac{\sigma_y^2}{k^2} - \frac{\sigma_x\sigma_y}{k^2}\right)\right.$$

$$\left. + \Delta\gamma_{xy}\frac{\tau_{xy}}{k^2}(\sigma_x+\sigma_y)\right]$$

$$\Delta W = \sigma_x\,\Delta\epsilon_x + \sigma_y\,\Delta\epsilon_y + \tau_{xy}\,\Delta\gamma_{xy}$$

3.5. Summary of Stress-Strain Relations

The stress-strain relations in their incremental form may be represented for both the top and bottom layers of a node in the following form:

$$\begin{aligned} \Delta\sigma_x &= C_{11}\,\Delta\epsilon_x + C_{12}\,\Delta\epsilon_y + C_{13}\,\Delta\gamma_{xy} \\ \Delta\sigma_y &= C_{21}\,\Delta\epsilon_x + C_{22}\,\Delta\epsilon_y + C_{23}\,\Delta\gamma_{xy} \\ \Delta\tau_{xy} &= C_{31}\,\Delta\epsilon_x + C_{32}\,\Delta\epsilon_y + C_{33}\,\Delta\gamma_{xy} \end{aligned} \tag{3.17}$$

Where in the elastic range the coefficients C for both the top and bottom layers are:

$$\begin{aligned} C_{11} &= C_{22} = \frac{E}{1-\nu^2} \\ C_{12} &= \frac{E\nu}{1-\nu^2} \\ C_{13} &= C_{23} = 0 \\ C_{33} &= \frac{E}{2(1+\nu)} \end{aligned} \tag{3.17a}$$

and in the plastic range:

$$\begin{aligned} C_{11} &= C_A\left[4 - \frac{\sigma_x^2}{k^2} + \frac{4G}{3K}\frac{\tau_{xy}^2}{k^2}\right] \\ C_{12} &= C_A\left[2 - \frac{\sigma_x\sigma_y}{k^2} - \frac{4G}{3K}\frac{\tau_{xy}^2}{k^2}\right] \\ C_{13} &= C_A\left[-\frac{\sigma_x\sigma_y}{k^2} + \frac{2G}{3K}\frac{(\sigma_y-\sigma_x)}{k^2}\tau_{xy}\right] \end{aligned} \tag{3.17b}$$

$$C_{22} = C_A\left[4 - \frac{\sigma_y^2}{k^2} + \frac{4G}{3K}\frac{\tau_{xy}^2}{k^2}\right]$$

$$C_{23} = C_A\left[-\frac{\sigma_y \tau_{xy}}{k^2} + \frac{2G}{3K}\frac{(\sigma_x - \sigma_y)}{k^2}\tau_{xy}\right]$$

$$C_{33} = C_A\left[1 - \frac{\tau_{xy}^2}{k^2} + \frac{4G}{3K}\left(1 - \frac{\tau_{xy}^2}{k^2} - 0.75\frac{s^2}{k^2}\right)\right]$$

where

$$C_A = \frac{G}{1 + \frac{2G}{3K}\left(2 - 1.5\frac{s^2}{k^2}\right)}$$

It should be noticed that in the elastic range the coefficients C are constants. Also they are equal for the top and bottom layers. However, in the plastic range they are no longer constants as they depend on the stress level. Furthermore, they are no longer equal for the top and bottom layers as the top and bottom stresses, in general, are different.

3.6. Stress-Displacement Relations

In Section 2.7 the strain-displacement relations were obtained and in Section 3.5 the stress-strain relations were presented in their most general form. By combining both these sets of equations the stress-displacement relations result. The six stresses in terms of their displacements are best shown in the form of operators. These operators are listed in Appendix A.

3.7. Force-Displacement Relations

The stresses in the upper and lower facings of the nodes are assumed to be uniformly distributed over the thickness of the facings. Thus the following relations, in their incremental form, for both top and bottom facings are:

$$\begin{aligned} \Delta N_x^T &= \frac{L_y h}{4} \Delta\sigma_x^T \\ &\vdots \\ \Delta N_{xy}^B &= \frac{L_y h}{4} \Delta\tau_{xy}^B \end{aligned} \tag{3.18}$$

Instead of the above equations the forces and moments can be expressed in a manner similar to the finite difference form developed about the middle surface of a real continuous shell. Then the following expressions are defined:

$$\begin{aligned} \Delta N_x &= \Delta N_x^T + \Delta N_x^B = \frac{L_y h}{4} (\Delta\sigma_x^B + \Delta\sigma_x^T) \\ &\vdots \\ \Delta M_x &= -(\Delta N_x^B - \Delta N_x^T) \frac{t}{2} = -\frac{L_y ht}{8} (\Delta\sigma_x^B - \Delta\sigma_x^T) \\ &\vdots \end{aligned} \tag{3.19}$$

A typical operator for any of the above forces involves the displacements shown in Fig. 8. The operators of all the above equations are shown diagramatically in Appendix B. If Eqs. (3.17) are substituted in Eqs. (3.19) the forces and moments are obtained as a function of the top and bottom strains. To illustrate the form of these relations the force N_x is written below:

$$\Delta N_x = \frac{L_y h}{4}\left[C_{11}^T \Delta\epsilon_x^T + C_{12}^T \Delta\epsilon_y^T + C_{13}^T \Delta\gamma_{xy}^T + C_{11}^B \Delta\epsilon_x^B + C_{12}^B \Delta\epsilon_y^B + C_{13}^B \Delta\gamma_{xy}^B\right]$$

But as can be seen from the operators in Appendix B it is also possible to write the forces and moments as a function of the strains and curvature of the middle surface (Eqs. 2.1, 2.4, 2.5). It is more convenient, for the sake of brevity in writing the equations, to first define the following:

$$\chi_x = \frac{t}{2}\kappa_x \quad , \quad \chi_y = \frac{t}{2}\kappa_y \quad , \quad \chi_{xy} = \frac{t}{2}\kappa_{xy} \tag{3.20a}$$

The forces and moments are then expressed as follows:

$$\begin{aligned}
N_x &= L_y \frac{h}{4}\left[A_{11}\epsilon_x + B_{11}\chi_x + A_{12}\epsilon_y + B_{12}\chi_y + A_{13}\gamma_{xy} + B_{13}\chi_{xy}\right] \\
N_y &= L_x \frac{h}{4}\left[A_{21}\epsilon_x + B_{21}\chi_x + A_{22}\epsilon_y + B_{22}\chi_y + A_{23}\gamma_{xy} + B_{23}\chi_{xy}\right] \\
N_{xy} &= L_y \frac{h}{4}\left[A_{31}\epsilon_x + B_{31}\chi_x + A_{32}\epsilon_y + B_{32}\chi_y + A_{33}\gamma_{xy} + B_{33}\chi_{xy}\right] \\
M_x &= L_y \frac{ht}{8}\left[B_{11}\epsilon_x + A_{11}\chi_x + B_{12}\epsilon_y + A_{12}\chi_y + B_{13}\gamma_{xy} + A_{13}\chi_{xy}\right] \\
M_y &= L_x \frac{ht}{8}\left[B_{21}\epsilon_x + A_{21}\chi_x + B_{22}\epsilon_y + A_{22}\chi_y + B_{23}\gamma_{xy} + A_{23}\chi_{xy}\right] \\
M_{xy} &= L_y \frac{ht}{8}\left[B_{31}\epsilon_x + A_{31}\chi_x + B_{32}\epsilon_y + A_{32}\chi_y + B_{33}\gamma_{xy} + A_{33}\chi_{xy}\right]
\end{aligned} \tag{3.20b}$$

where

$$A_{mn} = C_{mn}^{\ T} + C_{mn}^{\ B} \qquad (m \text{ and } n \text{ vary from } 1 \text{ to } 3)$$

$$B_{mn} = C_{mn}^{\ T} - C_{mn}^{\ B}$$

All the above equations could also be written in an incremental form for use in the numerical analysis in this study.

3.8. Equilibrium Equations

The equilibrium equations for the model are best formulated by the principle of virtual work. This principle states that for a system in equilibrium the total work done by both internal and external forces is equal to zero for any arbitrary virtual displacements. This principle is valid regardless of the material properties.

If for a virtual displacement the internal work is equal to I, and the external work done is W', then:

$$I + W' = 0 \tag{3.21}$$

The internal work I is equal to the negative of the product of the internal forces times the displacements plus the product of the moments times the rotations which result from the given virtual displacement:

$$I = - \sum N \delta d - \sum M \delta\theta$$

For convenience in finding the displacements and the rotations, the above equation can also be written as:

$$I = - \sum N(\delta\epsilon\, L) - \sum M(\delta\kappa\, L) \tag{3.22}$$

where $\delta\epsilon$ and $\delta\kappa$ represent the strains and curvatures due to the virtual displacement.

To generate the equilibrium equation in the x-direction joint i+1j is given a virtual displacement δu_{i+1j} while all the other displacement points are restrained from movement. As can be seen from Fig. 9 nodes ij and i+2j will undergo extensional strains while nodes

i+1j+1 and i+1j-1 will be subjected to shearing strains. Because the curvature of the shell is zero in the x-direction no rotation results from the virtual displacement. For a virtual displacement in the axial direction the internal work is:

$$I = -\left[N_{xij}\delta\epsilon_{xij} + N_{xi+2j}\delta\epsilon_{xi+2j}\right] L_x - \left[N_{yxi+1j+1}\delta\gamma_{xyi+1j+1} + N_{yxi+1j-1}\delta\gamma_{xyi+1j-1}\right] L_y \qquad (3.23)$$

From Eqs. (2.1)

$$\begin{aligned} \delta\epsilon_{xij} &= \frac{1}{L_x}\,\delta u_{i+1j} \\ \delta\epsilon_{xi+2j} &= \frac{-1}{L_x}\,\delta u_{i+1j} \\ \delta\gamma_{xyi+1j-1} &= \frac{1}{L_y}\,\delta u_{i+1j} \\ \delta\gamma_{xyi+1j+1} &= \frac{-1}{L_y}\,\delta u_{i+1j} \end{aligned} \qquad (3.24)$$

The external work done by the load $\bar{X}_{i+ij}$ applied to the point i+1j is:

$$W' = \bar{X}_{i+1j}\,\delta u_{i+1j} \qquad (3.25)$$

Substituting Eqs. (3.24) into Eq. (3.23) and adding the resulting expression to Eq. (3.25), the equilibrium equation in the x-direction is obtained in terms of the forces:

$$N_{xi+2j} - N_{xij} + N_{yxi+1j+1} - N_{yxi+1j-1} + \bar{X}_{i+1j} = 0 \qquad (3.26)$$

Similarly for the equilibrium equation in the y-direction joint ij+1 is given a virtual displacement δv_{ij+1}. The internal work will be:

$$I = - \left[N_{yij} \delta\epsilon_{yij} + N_{yij+2} \delta\epsilon_{yij+2} \right] L_y - \left[M_{yij} \delta\kappa_{yij} + M_{yij+2} \delta\kappa_{yij+2} \right] L_y$$
$$- \left[N_{xyi-ij+1} \delta\gamma_{xyi-1j+1} + N_{xyi+1j+1} \delta\gamma_{xyi+1j+1} \right] L_x$$
$$- \left[M_{xyi-1j+1} \delta\kappa_{xyi-1j+1} + M_{xyi+1j+1} \delta\kappa_{xyi+1j+1} \right] L_x \qquad (3.27)$$

From the strain-displacement Eqs. (2.1), (2.4), and (2.5) the incremental strains resulting from the virtual displacement are as follows:

$$\delta\epsilon_{yij} = \frac{1}{L_y \cos \frac{\beta}{2}} \delta v_{ij+1}$$
$$\vdots$$
$$\delta\kappa_{yij} = \frac{-1}{L_y R \cos \frac{\beta}{2}} \delta v_{ij+1} \qquad (3.28)$$
$$\vdots$$
$$\delta\kappa_{xyij} = \frac{1}{L_x R \cos \frac{\beta}{2}} \delta v_{ij+1}$$

The external work will be:

$$W' = \bar{Y}_{ij+1} \delta v_{ij+1} \qquad (3.29)$$

Substituting Eqs. (3.28) into Eqs. (3.27) and adding the result to Eq. (3.29), the equilibrium equation in the y-direction is obtained:

$$\frac{1}{\cos \frac{\beta}{2}} (N_{yij+2} - N_{yij}) + \frac{1}{R \cos \frac{\beta}{2}} (M_{yij} - M_{yij+2}) + N_{xyi+1j+1}$$
$$- N_{xyi-1j+1} + \frac{1}{R \cos \frac{\beta}{2}} (M_{xyi-1j+1} - M_{xyi+1j+1}) + \bar{Y}_{ij+1} = 0 \qquad (3.30)$$

The equilibrium equation in the radial direction is similarly formulated by giving the node ij a virtual displacement δw_{ij}. The resulting equation is:

$$\frac{1}{L_x}\left(M_{xi+2j} - 2M_{xij} + M_{xi-2j}\right) + \frac{1}{L_y \cos\frac{\beta}{2}}\left(M_{yij+2} - 2M_{yij} + M_{yij-2}\right)$$

$$+ \frac{L_y}{R\cos\frac{\beta}{2}}\left(N_{yij}\right) + \left(1 + \frac{1}{\cos\frac{\beta}{2}}\right)\frac{1}{L_y}\left(M_{xyi+1j+1} - M_{xyi-1j+1}\right.$$

$$\left. - M_{xyi+1j-1} + M_{xyi-1j-1}\right) + \bar{Z}_{ij} = 0 \qquad (3.31)$$

The above equilibrium equations are written in terms of the forces and moments. By using the relations previously obtained between the forces and moments, and the displacements, the equilibrium equations are expressed in terms of the various displacements. The forces and displacements involved in the x, y, and z equations are shown diagramatically in Figs. 10a, 10b, 11a, 11b, and 12a, 12b, respectively.

The term $\cos \beta/2$ is assumed equal to one as was mentioned in Section 2.7. Also it should be noted that the equilibrium equations are used in an incremental form as the load is progressively increased. For each load increment Δp the equilibrium equations are formulated for all the grid points of the model. A set of linear algebraic simultaneous equations result in terms of the unknown increments in displacements Δu, Δv, and Δw. Solving these equations the increments in displacements are obtained. Once Δu, Δv, and Δw are known the increments in the strains, stresses, forces, and moments are easily obtained throughout the shell. By adding the increments of displacements, strains,

stresses, forces, and moments to the values previously obtained the final values are obtained for each stage of loading. The numerical technique is described in more detail in Chapter 5.

4. BOUNDARY CONDITIONS

4.1. General

The model used in this investigation is adaptable to a variety of boundary conditions. Of these, the three which are pertinent to this study are presented below. The boundaries considered include a simply-supported edge; a free edge; and a continuous edge.

As shown in Section 3.8, the internal work done due to a virtual displacement can be expressed in terms of strains and curvatures (Eq. 3.22). For both geometric and force boundary conditions the desired representation of the boundary is established by using the appropriate strains and curvatures for those points close to or on the boundary. Hence the only modification needed for the introduction of a boundary edge is on the strains and curvatures existing there.

4.2. Simply-Supported Edge

The simply-supported edge represents the case where the shell is supported by a diaphragm which is infinitely stiff in its own plane, but has no resistance to loads normal to its plane. Assuming the simply-supported edge to be parallel to the y-axis the following conditions must be satisfied along that edge;

$$v = 0, \; w = 0 \tag{4.1}$$

$$N_x = 0, \; M_x = 0 \tag{4.2}$$

The special strain and curvature relations for points on or near the

boundary are derived, taking into consideration these specified stress and displacement values.

4.2.1. Node on Edge

For a node ij on the edge, substitution of Eq. (4.1) in the strain-displacement Eqs. (2.1) and (2.4) determines the strain and curvature directed along the edge. These are:

$$\epsilon_{yij} = 0 \text{ and } \kappa_{yij} = 0 \tag{4.3}$$

In the N_x and M_x expressions of Eqs. (3.20) A_{13}, B_{13}, and B_{11} are equal to zero in the elastic range. When Eqs. (4.2) are used, and ϵ_{yij} and κ_{yij} are substituted into the N_x and M_x expressions of Eqs. (3.20), the strain and curvature in the x-directions become:

$$\epsilon_{xij} = 0 \text{ and } \kappa_{xij} = 0 \tag{4.4}$$

In the plastic range the coefficients A_{13}, B_{13}, and B_{11} can be shown to remain equal to zero for a node on the edge. Thus the above Eq. (4.4) is valid in both the elastic and plastic ranges.

The shearing strain and twisting curvature are obtained by substituting Eq. (4.1) into the third Eqs. of (2.1) and into Eq. (2.5). Since the node represents the material extending one-half spacing in from the edge, $L_x/2$ is used in place of L_x. The appropriate strain and twist relations thus become:

$$\gamma_{xyij} = \frac{1}{L_y}\left(u_{ij+1} - u_{ij-1}\right) + \frac{2}{L_x}\left(-v_{i-1j}\right) \tag{4.5}$$

$$\kappa_{xyij} = \frac{2}{L_x R}\left(-v_{i-1j}\right) + \frac{2}{L_x L_y}\left(-2w_{i-1j+1} + 2w_{i-1j-1}\right) \tag{4.6}$$

4.2.2. Node One-Half Space From Edge

The expressions for ϵ_{xij}, ϵ_{yij}, and κ_{yij} at a node ij one-half space interval from the edge are the same as those of an interior node. Since v and w are zero on the edge, the remaining strain expressions are:

$$\kappa_{xij} = \frac{1}{L_x^2}\left(-3w_{ij} + w_{i-2j}\right) \tag{4.7}$$

$$\gamma_{xyij} = \frac{1}{L_y}\left(u_{ij+1} - u_{ij-1}\right) + \frac{1}{L_x}\left(-v_{i-1j}\right) \tag{4.8}$$

$$\kappa_{xyij} = \frac{1}{L_x R}\left(-v_{i-1j}\right) + \frac{2}{L_x L_y}\left(-w_{i-1j+1} + w_{i-1j-1}\right) \tag{4.9}$$

4.2.3. Node One Space From Edge

All strain and curvature quantities for a node ij one space from the edge are the same as a typical interior node except the expression for the curvature in the x-direction which becomes:

$$\kappa_{xij} = \frac{1}{L_x^2}\left(-2w_{ij} + w_{i-2j}\right) \tag{4.10}$$

4.3. Free Edge

If the edge parallel to the x-axis, i.e. the longitudinal edge, is free then the following conditions must be satisfied along that edge:

$$\begin{aligned} N_y &= 0 \\ N_{yx} &= 0 \\ M_y &= 0 \\ R_y &= 0 \end{aligned} \tag{4.11}$$

where

$$R_y = Q_y + \frac{\partial M_{yx}}{\partial x}$$

and

$$Q_y = \frac{\partial M_y}{\partial y}$$

Some modification in the model is needed along the free edge to make it possible to define the reaction R_y at all points along the edge. This modification requires additional displacements, δ's, along the free edge. These new displacements are defined at the intersection of the rigid bars and are in the radial direction. To account for the extra unknowns additional equations of equilibrium along the edge are developed. These are discussed in Section 4.3.3. The details of the free edge with the necessary modifications are shown in Fig. 13. This detail was first developed by Mohraz and Schnobrich.[27]

4.3.1. Node on Edge

Due to the Kirchhoff-Love assumption of the preservation of normals in the classical theory of plates and shells, the condition that the twisting moment M_{yx} along the free edge be equal to zero cannot be enforced. Instead, the reaction R_y is taken equal to zero. If this assumption is not used and the shear deformation is taken into account, the five stress resultants N_y, M_y, N_{yx}, M_{yx}, and N_{yz} can be equated to zero along the free edge.[16] In this case, the coefficients A_{31}, B_{31}, A_{32}, B_{32}, and B_{33} in the N_{yx} and M_{yx} expressions of Eqs. (3.20) would be equal to zero in both the elastic and plastic ranges. Since N_{yx} and M_{yx} would be equal to zero γ_{yx} and χ_{yx} would also be found equal to zero.

In this study, however, the classical Kirchhoff-Love hypothesis is assumed to be valid, which means that shear deformation is neglected. All the coefficients in the Prandtl-Reuss relations are derived in accord with this assumption. Thus, when A_{31}, B_{31}, A_{32}, B_{32}, and B_{33} in Eqs. (3.20) are calculated they are found to be not equal to zero in the plastic range. The result is that N_{yx}, which was zero in the elastic range, acquires some small value in the plastic range even when γ_{yx} is set to zero.

To obtain the twisting curvature κ_{xyij} at the node ij on the edge the rotations of the bars around that node, Fig. 13, need to be computed first. The rotations about the x-axis of the rigid bars (i+1j-1, i+1j) and (i-1j-1, i-1j) are as follows:

$$\theta_{yi+1j} = \frac{1}{L_y/2} \left(\delta_{i+1j} - w_{i+1j-1} + \frac{L_y}{2R} v_{i+1j}\right) \tag{4.12}$$

$$\theta_{yi-1j} = \frac{1}{L_y/2} \left(\delta_{i-1j} - w_{i-1j-1} + \frac{L_y}{2R} v_{i-1j}\right) \tag{4.13}$$

The rotation about the y-axis of bar (i-1j-1, i+1j-1) is:

$$\theta_{xij} = \frac{1}{L_x} \left(w_{i+1j-1} - w_{i-1j-1}\right) \tag{4.14}$$

The rotations about the y-axis of the two auxiliary bars (i-1,ij) and (ij, i+1j) are:

$$\theta^1_{ij} = \frac{1}{L_x} \left(w_{ij} - \delta_{i-1j}\right)$$

$$\theta^2_{ij} = \frac{1}{L_x} \left(\delta_{i+1j} - w_{ij}\right)$$

thus the average rotation at the node ij is:

$$\theta_{xij} = \frac{1}{2}\left(\theta^{1}_{ij} + \theta^{2}_{ij}\right) = \frac{1}{L_x}\left(\delta_{i+1j} - \delta_{i-1j}\right) \tag{4.15}$$

The twisting curvature is:

$$\kappa_{xyij} = \frac{1}{L_x}\left(\theta_{yi+1j} - \theta_{yi-1j}\right) + \frac{1}{L_y/2}\left(\theta_{xij} - \theta_{xij-1}\right) \tag{4.16}$$

Substituting the values of θ in Eqs. (4.12) through (4.15) into Eq. (4.16) the twisting curvature is obtained:

$$\kappa_{xyij} = \frac{1}{L_x R}\left(v_{i+1j} - v_{i-1j}\right) + \frac{2}{L_x L_y}\left(-2w_{i+1j-1} + 2w_{i-1j-1}\right) + \frac{4}{L_x L_y}\left(\delta_{i+1j} - \delta_{i-1j}\right) \tag{4.17}$$

To obtain the extensional and bending strains ϵ_y and χ_y at the edge, N_y, M_y, and γ_{xy} are set to zero in Eqs. (3.20) in their incremental form. Solving these two simultaneous equations provides $\Delta\epsilon_y$ and $\Delta\chi_y$, in terms of $\Delta\epsilon_x$, $\Delta\chi_x$ and $\Delta\chi_{xy}$:

$$\Delta\epsilon_y = -\alpha_1\Delta\epsilon_x - \alpha_2\Delta\chi_x - \alpha_3\Delta\chi_{xy} \tag{4.18}$$

$$\Delta\chi_y = -\alpha_2\Delta\epsilon_x - \alpha_1\Delta\chi_x - \alpha_4\Delta\chi_{xy} \tag{4.19}$$

where

$$\alpha_1 = \frac{A_{22}A_{12} - B_{22}B_{12}}{A_{22}^2 - B_{22}^2}$$

$$\alpha_2 = \frac{A_{22}B_{12} - B_{22}A_{12}}{A_{22}^2 - B_{22}^2}$$

$$\alpha_3 = \frac{A_{22}B_{23} - B_{22}A_{23}}{A_{22}^2 - B_{22}^2}$$

$$\alpha_4 = \frac{A_{22}A_{23} - B_{22}B_{23}}{A_{22}^2 - B_{22}^2}$$

In the elastic range Eqs. (4.18) and (4.19) reduce to:

$$\epsilon_y = - \nu \epsilon_x$$

$$\chi_y = - \nu \chi_x$$

Now that $\Delta\epsilon_y$ and $\Delta\chi_y$ have been found they are substituted in the expressions of ΔN_x, ΔM_x, and ΔM_{xy} in Eqs. (3.20):

$$\begin{aligned}
\Delta N_x &= \frac{L_y h}{4}\left[\alpha\Delta\epsilon_x + \beta\Delta\chi_x + \gamma_1\Delta\chi_{xy}\right] \\
\Delta M_x &= \frac{L_y ht}{8}\left[\beta\Delta\epsilon_x + \alpha\Delta\chi_x + \gamma_2\Delta\chi_{xy}\right] \\
\Delta M_{yx} &= \frac{L_x ht}{8}\left[\gamma_1\Delta\epsilon_x + \gamma_2\Delta\chi_x + \gamma_3\Delta\chi_{xy}\right]
\end{aligned} \tag{4.20}$$

where

$$\begin{aligned}
\alpha &= A_{11} - A_{12}\alpha_1 - B_{12}\alpha_2 \\
\beta &= B_{11} - A_{12}\alpha_2 - B_{12}\alpha_1 \\
\gamma_1 &= B_{13} - A_{12}\alpha_3 - B_{12}\alpha_4 \\
\gamma_2 &= A_{13} - B_{12}\alpha_3 - A_{12}\alpha_4 \\
\gamma_3 &= A_{33} - B_{23}\alpha_3 - A_{23}\alpha_4
\end{aligned} \tag{4.21}$$

In the elastic range Eqs. (4.20) reduce to:

$$N_x = \frac{L_y h}{2}(1 - \nu^2)\epsilon_x$$

$$M_x = \frac{L_y ht}{4}(1-\nu^2)\chi_x$$

$$M_{yx} = \frac{L_x ht}{4}(\frac{1-\nu}{2})\chi_{xy}$$

An alternative approach would be, of course, to use the stresses rather than the stress resultants. Instead of equating ΔN_y and ΔM_y to zero, $\Delta\sigma_y^T$ and $\Delta\sigma_y^B$ are equated to zero in Eqs. (3.17) and $\Delta\epsilon_y^T$ and $\Delta\epsilon_y^B$ are derived.

4.3.2. Node One-Half Space From Edge

For a node ij one-half space from edge, only the bending curvature κ_{yij} is different from that of an interior node:

$$\kappa_{yij} = \frac{1}{L_y R}(v_{ij+1} - v_{ij-1}) + \frac{1}{L_y^2}(-3w_{ij} + w_{ij-2}) + \frac{2}{L_y^2}\delta_{ij+1} \qquad (4.22)$$

4.3.3. Additional Equilibrium Equations for the Free Edge

Consider the equilibrium of a T-section made of the bars shown in Fig. 14. From the equilibrium of each bar taken separately the following relations can be obtained:

$$Q_{yi+1j} = \frac{1}{L_y/2} M_{yi+1j-1}$$

$$Q'_{1yi+1j} = \frac{1}{L_x/2} M_{yxij} \qquad (4.23)$$

$$Q'_{2yi+1j} = \frac{1}{L_x/2} M_{yx}{}^{i+2j}$$

where

$$M_{yi+1j-1} = \frac{L_x ht}{8}\left[B_{11}\epsilon_x + A_{11}\chi_x + B_{22}\epsilon_y + A_{22}\chi_y + B_{23}\gamma_{xy} + A_{23}\chi_{xy}\right]_{i+1j-1}$$

$$M_{yxij} = \frac{L_x ht}{8}\left[B_{13}\epsilon_x + A_{13}\chi_x + B_{32}\epsilon_y + A_{32}\chi_y + A_{33}\chi_{xy}\right]_{ij} \qquad (4.24)$$

$$M_{yxi+2j} = \frac{L_x ht}{8}\left[B_{13}\epsilon_x + A_{13}\chi_x + B_{32}\epsilon_y + A_{32}\chi_y + A_{33}\chi_{xy}\right]_{i+2j}$$

For equilibrium in the vertical direction:

$$Q_{yij+1} + Q'_{2yij+1} - Q'_{1yij+1} = 0 \qquad (4.25)$$

Combining Eqs. (4.23), (4.24) and (4.25) the additional equilibrium equation at the free edge can be written as:

$$\frac{L_x}{2L_y}\left[B_{11}\epsilon_x + A_{11}\chi_x + B_{22}\epsilon_y + A_{22}\chi_y + B_{23}\gamma_{xy} + A_{23}\chi_{xy}\right]_{i+1j-1}$$

$$+ \frac{1}{2}\left[B_{13}\epsilon_x + A_{13}\chi_x + B_{32}\epsilon_y + A_{32}\chi_y + A_{33}\chi_{xy}\right]_{i+2j}$$

$$- \frac{1}{2}\left[B_{13}\epsilon_x + A_{13}\chi_x + B_{32}\epsilon_y + A_{32}\chi_y + A_{33}\chi_{xy}\right]_{ij} = 0 \qquad (4.26)$$

4.4. Continuous Edge

For a shell that is continuous in the transverse direction and symmetrically loaded, the edge conditions at the junction between two successive interior shells are:

the horizontal displacement normal to the junction, $v = 0$

the rotation in the transverse direction, $\theta_y = 0$

the shearing force, $N_{xy} = 0$

the vertical reaction = 0

The second condition, that of θ_y being zero, does not remain valid once plastic action takes place along the continuous edge. It is replaced by the condition of symmetry of the deflections on both sides of the continuous edge.

Due to the sharp break in curvature at the junction between the two shells some modifications are necessary in the nodes along the edge. The top and bottom layers of such nodes are placed in the horizontal direction. The detail of one of these boundary nodes and the bars connected to it is shown in Fig. 15. From this figure it is noted that the spacing between the two layers of the node becomes equal to $\frac{t}{\cos B/2 \cos \gamma}$. In the equations that follow $\cos \beta/2$ is approximated by being considered equal to unity, so the spacing is taken as $\frac{t}{\cos \gamma}$. Also shown in Fig. 15 is the geometry of displacements at that particular node. Nodes which are one-half spacing on either side of the junction between the two shells are joined together by a horizontal bar as shown in Fig. 16. This manner of connecting the nodes is in agreement with the boundary conditions as described above and is found to yield good correlation between the two systems of nodes as explained in Section 5.5. When the number of spacings increases in the transverse direction, then in the limit these two nodes joined by the horizontal bar will be almost like one of those nodes on the junction between the two shells.

The strains and curvatures for the nodes on or close to the continuous edge are as described below.

4.4.1. Node on Edge

For a node ij on the boundary between the two shells, the extensional strain ϵ_{xij} and the bending curvature κ_{xij} remain the same as those of a typical interior node. It need only be noted that to get the strains at the top and bottom layers of a node due to bending κ_{xij} is multiplied by $\frac{t}{2 \cos \gamma}$ instead of the usual $\frac{t}{2}$. Due to symmetry about the boundary line between the two bays, the shearing strain γ_{xyij} and the twisting curvature κ_{xyij} are equal to zero along the edge:

$$\begin{aligned} \gamma_{xyij} &= 0 \\ \kappa_{xyij} &= 0 \end{aligned} \tag{4.27}$$

Referring to Fig. 15, the extensional strain in the y-direction is:

$$\epsilon_{yij} = \frac{1}{L_y \cos\gamma} (v_{ij+1} - v_{ij-1}) + \frac{2w_{ij} \tan \gamma}{L_y}$$

Because of symmetry $v_{ij+1} = -v_{ij-1}$ thus:

$$\epsilon_{yij} = \frac{1}{L_y \cos \gamma} (-2v_{ij-1}) + \frac{2w_{ij} \tan \gamma}{L_y} \tag{4.28}$$

The rotation of the rigid bar joining the two nodes ij-2 and ij is:

$$\theta_{yij-1} = \frac{1}{L_y} \left[\frac{w_{ij}}{\cos \gamma} - w_{ij-2} - v_{ij-1} (\tan \gamma - \tan \beta/2) \right] \tag{4.29}$$

The curvature in the y-direction is:

$$\kappa_{yij} = \frac{1}{L_y} (\theta_{yij+1} - \theta_{yij-1})$$

From symmetry considerations $\theta_{yij+1} = -\theta_{yij-1}$ thus:

$$\kappa_{yij} = \frac{1}{L_y}\left(-2\theta_{yij-1}\right)$$

Using Eq. (4.34) the following expression for the curvature κ_{yij} results:

$$\kappa_{yij} = \frac{1}{L_y^2}\left[\frac{-2w_{ij}}{\cos\gamma} + 2w_{ij-2} + 2v_{ij-1}\left(\tan\gamma - \tan\beta/2\right)\right] \qquad (4.30)$$

4.4.2. Node One-Half Space from Edge

For a node ij one-half space from the continuous edge, the strains ϵ_{xij}, γ_{xyij}, and the curvature κ_{xij} remain as those of a typical interior node. New expressions must be found for the remaining strain quantities. Referring to Fig. 16, the extensional strain in the y-direction is:

$$\epsilon_{yij} = \frac{1}{L_y\cos\gamma_a}\left(-v_{ij-1}\right) + \frac{w_{ij}\tan\gamma_a}{L_y} \qquad (4.31)$$

For the curvature in the y-direction, both θ_{yij+1} and v_{ij+1} are set to zero, then:

$$\kappa_y = \frac{1}{L_y^2\cos\gamma_a}\left[\frac{-w_{ij}}{\cos\gamma_a} + w_{ij-2} + v_{ij-1}\left(\tan\gamma_a - \tan\beta/2\right)\right] \qquad (4.32)$$

For the twisting curvature κ_{xyij}, the rotations θ_{yi+1j} and θ_{yi-1j} have expressions similar to those in Eq. (4.34). κ_{xyij} is therefore equal to:

$$\kappa_{xyij} = \frac{1}{L_x L_y}\left[-(\tan\gamma - \tan\beta/2)(v_{i+1j}-v_{i-1j}) + \frac{2}{\cos\gamma}(w_{i+1j+1}-w_{i-1j+1}) + 2(-w_{i+1j-1}+w_{i-1j-1})\right] \tag{4.33}$$

As in Section 4.4.1, to get the strains resulting from the curvatures at the top and bottom layers of a node the curvatures are multiplied by $\frac{t}{2\cos\gamma_a}$ instead of t/2.

4.4.3. Node One Space From Edge

For a node ij one space from the edge, the expressions for the curvatures κ_{yij} and κ_{xyij} must be modified. All the other strains and the remaining curvature in the x-direction are like those of a typical interior node. The rotation θ_{yij+1} needed to get the curvature in the y-direction has an expression similar to the one in Eq. (4.34). Thus κ_{yij} becomes:

$$\kappa_{yij} = \frac{1}{L_y^2}\left[\frac{w_{ij+2}}{\cos\gamma} - 2w_{ij} + w_{ij-2} - v_{ij+1}(\tan\gamma - \tan\beta/2) - \frac{L_y}{R}v_{ij-1}\right] \tag{4.34}$$

The modified twisting curvature is:

$$\kappa_{xyij} = \frac{1}{L_x L_y}\left(1 + \frac{1}{\cos\gamma_a}\right)(w_{i+1j+1}-w_{i-1j+1}) + \frac{2}{L_x L_y}(w_{i-1j-1}-w_{i+1j-1}) + \frac{1}{L_x L_y}(\tan\gamma_a - \tan\beta/2)(v_{i-1j} - v_{i+1j}) \tag{4.35}$$

5. NUMERICAL TECHNIQUE

5.1. The Numerical Procedure

The numerical procedure used in this study to follow the behavior of the shell through both the elastic and plastic phases and to trace the progression of yielding is described herein.

Initially a unit load is applied to the model. For this load the top and bottom layers of all the nodes are elastic. Equilibrium equations are formulated and solved to obtain the displacements throughout the model. From the displacements the strains and hence the stresses of both layers of each node are found. Also, the stress resultants or mid-surface forces and moments are obtained.

The load is then increased to a level such that the layer which is closest to the yield surface is stressed to yielding. This is achieved by calculating the quantity J_2 for both layers of all nodes and choosing the largest J_2 to determine the required load level for first yielding. The load initiating yielding is given by:

$$p = \frac{k}{\sqrt{J_2}_{\text{max.}}} 1 \qquad (5.1)$$

The load is increased incrementally from this load level on, stressing layers to yield. For each load increment the equilibrium equations are formulated, using the appropriate coefficients considering whether the top or bottom layer at any particular node is elastic or plastic. Solving these equations the increments in displacements are

obtained, after which the increments in the strains and stresses are found for both the top and bottom layers. The increments in the displacements, strains, and stresses are then added to previous values to obtain current values. Before any load increment is applied the status--whether elastic or plastic--of both layers of each node is known. After the load increment is applied the status of each layer must be checked at the increased load level. If either layer of a node was elastic before the increase in the load, there are three possibilities regarding its state of stress after the load is increased. These are:

(i) the layer remains elastic--i.e., the state of stress represented by a point in the stress space is inside the yield surface.

(ii) the layer becomes plastic--i.e., the stress point lies on the yield surface within the prescribed tolerances.

(iii) the stress point overshoots the yield surface.

This third possibility means that the load increment was larger than that which would bring the state of stress of that particular layer to the yield surface. In such a case the load increment needs to be reduced, and this is done by an interpolation procedure described in Section 5.2.

Another situation arises while checking the status of the layers that were already plastic before the load was increased. During the increase in the load the stress point is supposed to move on the yield surface, but due to the incremental nature of the problem the stress point moves along a tangent to the yield surface. If the stress

point movement away from the yield surface is beyond the specified tolerance it must be brought back to the surface. The method by which this is achieved is described in Section 5.3. Also the positiveness of ΔW is checked for all plastic layers to ensure that no unloading occurred.

A general flow diagram illustrating the sequence of computations for the problem is shown in Fig. 17.

5.2. Initiation of Yielding

As was mentioned in Section 5.1, when the load level is increased a stress point initially inside the yield surface may overshoot it. When this overshooting exceeds a specified small tolerance a new reduced load increment is determined by linear interpolation, that is:

$$\Delta p_{new} = \frac{k^2 - J_2'}{J_2 - J_2'} \Delta p' \qquad (5.2)$$

where

J_2' is the yield function at the previous load level ($J_2' < k^2$)

J_2 is the yield function at the present load level ($J_2 > k^2$)

$\Delta p'$ is the load increment which caused J_2 to exceed k^2

The incremental stresses and displacements which are the result of the excessive load increment are therefore scaled down by the factor $\Delta p_{new}/\Delta p'$ before being added to the previous values of the stresses and displacements to obtain their new values. As a matter of course the layers which were elastic are rechecked for yielding at this new load level.

5.3. Correction Procedure for Plastic Stresses

For the layers which become plastic, the state of stress represented by a point in the stress space should, under increasing load, move on the yield surface. However, due to the incremental nature of the problem, the stress point moves along the tangent to the surface as shown in Fig. 18. This moves the stress point away from the yield surface $J_2 = k^2$.

If the departure exceeds a selected small allowable tolerance the state of stress must be brought back to the surface or else the error which keeps accumulating would become excessive. Techniques for bringing the state of stress back to the yield surface along the gradient have been used before.[32,23] A different formulation of the same scheme is developed below.

The yield surface in the case of plane stress is represented by the quadratic equation:

$$J_2 = \frac{1}{3}\left(\sigma_x^2 - \sigma_x\sigma_y + \sigma_y^2\right) + \tau_{xy}^2 = k^2 \tag{5.3}$$

Let the coordinates of the uncorrected stress point lying outside the surface be $(\sigma_{x1}, \sigma_{y1}, \tau_{xy1})$. The components of the gradient vector to the surface are:

$$\frac{\partial J_2}{\partial \sigma_x} = \frac{1}{3}\left(2\sigma_x - \sigma_y\right)$$

$$\frac{\partial J_2}{\partial \sigma_y} = \frac{1}{3}\left(2\sigma_y - \sigma_x\right) \tag{5.4}$$

$$\frac{\partial J_2}{\partial \tau_{xy}} = 2\tau_{xy}$$

Knowing the components of the gradient and the coordinates of a point outside the surface, the equation of the normal to the surface which passes through that point can be written as:

$$\frac{\sigma_x - \sigma_{x1}}{\frac{\partial J_2}{\partial \sigma_x}\Big|_{\sigma_{x1},\sigma_{y1},\tau_{xy1}}} = \frac{\sigma_y - \sigma_{y1}}{\frac{\partial J_2}{\partial \sigma_y}\Big|_{\sigma_{x1},\sigma_{y1},\tau_{xy1}}} = \frac{\tau_{xy} - \tau_{xy1}}{\frac{\partial J_2}{\partial \tau_{xy}}\Big|_{\sigma_{x1},\sigma_{y1},\tau_{xy1}}} \tag{5.5}$$

Substituting Eqs. (5.4) into Eqs. (5.5) the equation of the normal becomes:

$$\frac{(\sigma_x - \sigma_{x1})}{\frac{1}{3}(2\sigma_{x1} - \sigma_{y1})} = \frac{\sigma_y - \sigma_{y1}}{\frac{1}{3}(2\sigma_{y1} - \sigma_{x1})} = \frac{\tau_{xy} - \tau_{xy1}}{2\tau_{xy1}} \tag{5.6}$$

Now, it is possible to find the intersection of this normal with the yield surface. Solving Eq. (5.3) together with Eqs. (5.6) for the unknowns σ_x, σ_y, and τ_{xy} the coordinates of two points on the surface are obtained. The two points represent both intersections of the normal with the closed yield surface. It is obvious which is the correct point to use for it will be the closer of the two to the uncorrected point.

5.4. Solution of the Equations

The equilibrium equations in the x, y, and z directions are generated in terms of the displacements as explained in Section 3.8. A set of linear algebraic equations is obtained. The resulting matrix of coefficients is in the form of a banded matrix. The numbering system of the different unknowns is chosen such that the band width is a

minimum. This is done in order to minimize the large number of quantities to be stored in the core of the computer. A Gauss elimination method is employed to solve the equations. The computer program uses an equation solver routine developed by Professor J. W. Melin which can solve up to 450 simultaneous equations without using auxiliary storage.

5.5. Coupling of the Two Systems of the Model

As was mentioned in Section 2.1 the model, as used in this study, can be considered as a superposition of two systems of Schnobrich's model. Figure 19 shows one system with solid circles, the other with hollow circles. In the elastic range, the equilibrium equations of one system are independent of those of the other system. In spite of this the solutions for the two networks were found[27] to be in good agreement with one another for the case where all four boundaries are simply supported. When two opposite edges are free and the remaining two opposite edges simply supported the agreement between the two systems is not quite as good. The deflection along the free edge is found to oscillate between the two systems, Fig. 24. Also if the deflection along a diagonal of one quadrant of the shell is plotted, proceeding from the free edge to the simply supported one, it is found that the oscillations are noticeable close to the free edge but damp out near the simply supported edge, Fig. 25. This phenomenon occurs in the case of the free edge because the free edge is sensitive to the number of grid spacings used, and in effect one system is being solved with a finer mesh than the other. As the fineness of the grid is

increased the results pertaining to the two systems move closer to each other and the oscillation becomes less pronounced.

In the plastic range, the equilibrium equations of the two systems are coupled as can be seen from the operators in Figs. 10, 11, and 12. Even when yielding starts in one system the relative magnitude of the oscillation does not seem to grow much larger although its absolute magnitude does.

In the case of a multiple barrel shell simply supported at both ends the agreement between the two systems in the elastic range is quite good and the oscillations are hardly noticeable. In the plastic range the oscillations become more pronounced. Figure 35 shows the deflection along a diagonal of one quadrant of the shell. Several curves are plotted to show the behavior at different load levels.

6. NUMERICAL RESULTS

6.1. General Remarks

Two illustrative problems are presented in this chapter to demonstrate the success of the model for handling the elasto-plastic analysis of shells. The first problem is that of a cylindrical shell with the transverse edges simply supported and the longitudinal edges free. The second problem is that of a continuous multiple barrel shell. In both cases the loading applied is a uniform increasing load of intensity p lb/ft^2. The loading and geometry are symmetrical about both axes of the shell, so only one quandrant is needed to solve the problems.

Previous work in the area of shell structure analysis is, in general, limited to linearly elastic material behavior. Although some work has been done on the basis of limit analysis it is mostly restricted to rotationally symmetric shells. Thus comparisons with previous works are of necessity quite limited.

6.2. Cylindrical Shell with Two Edges Simply Supported and the Remaining Two Free

The shell considered here is a single bay shell simply supported at both its transverse ends while the longitudinal straight edges are free. The dimensions of the shell are chosen to correspond to those of Example 1 in the ASCE Manual 31.[8] These dimensions are given in Fig. 20. The ratio R/L for this shell is 0.5. Cylindrical

shells are usually described on the basis of this ratio as either long, intermediate, or short. Manual 31 does not make such a fine distinction and categorizes shells as either short or long. The division point between short and long shells occurs at the ratio R/L = 0.6. According to Gibson[15] the shell chosen in this example would be classified an intermediate shell. The classification of the shells as made by various authors is an attempt to distinguish between shells whose primary action is that of a beam from those whose primary action is arching. For this study the intermediate case was chosen in order that the shell have both actions present.

A quadrant of the shell is divided into six spacings in each direction, resulting in 234 unknowns. Poisson's ratio is chosen to be zero. The yield stress σ_o is chosen on the basis of the maximum longitudinal tensile reinforcement in a reinforced concrete shell. For the Manual 31 shell this is about 8% of the sectional area. Thus if the material is considered homogeneous, as is done in this study, an equivalent yield stress may be assumed. If the yield stress for steel is 33 ksi, i.e., 47.5×10^5 lb/ft^2 then the equivalent yield stress is 3.8×10^5 lb/ft^2. In this case the yield limit in simple shear $k = 2.18 \times 10^5$ lb/ft^2. But since the top and bottom stresses in the model are in terms of lb/ft, then σ_o and k are multiplied also by h/2. If kh/2 is designated "SK" then the selected tolerance for yielding is $\pm$ 0.01 SK^2.

A unit load was applied to the shell and increased to get the first layer of a node to yield. Subsequent loading was then progressively increased, successively forcing further layers to yield. At an

applied load of 118.4 lb/ft^2 the first yielding occurred in the bottom layer at the center of the free edge. This layer is subjected to a state of uniaxial tension. Under increasing loads yielding progressed in both the top and bottom layers of the shell. At an applied load of 154.1 lb/ft^2 one top layer on the simply supported edge started to yield due to the presence of maximum shearing stresses. Figures 21a and 21b show the extent of the plastic yielding at different load levels for both the top and bottom layers.

The displacements in the shell increase progressively with the load. A plot showing the load versus the w deflection at the center of the free edge is shown in Fig. 22. The dead load level (27 lb/ft^2) is also marked on Fig. 22 for comparison.

At the load level of 263.1 lb/ft^2 yielding covered a major part of the shell and the deflections became quite large. At that load level a node near the crown started to unload. With further increase in loading two other layers unloaded while several additional nodes yielded. The load increased up to 270.3 lb/ft^2 with a very large increase in deflection. If the modulus of elasticity of the material is taken equal to that of concrete, i.e. 30 x 10^5 psi, then the deflection at the center of the free edge is found to be 37.1 inches. It was decided to stop further loading as it was found that deflections were growing quite rapidly with each further application of small load increments. This load (270.3 lb/ft^2) is considered to be the ultimate load for the shell, as it is apparent that yielding has exhausted the major portion of its load capacity.

A plot of the normal deflection, w, on the section at midspan between the two simply supported edges is shown in Fig. 23 for the different load levels. Also the deflections along the free edge and along a diagonal proceeding from the free edge to the simply supported edge are shown in Fig. 24 and Fig. 25. The variations of the longitudinal force N_x at the midspan section and along the free edge are shown in Fig. 26 and Fig. 27 respectively. From Fig. 26 it is noticed that with the increase in loading and plastic action the position of the neutral axis moves upward towards the crown. Also, in the later stages of loading the stresses on the tension side become almost constant and equal to the yield value in simple tension. On the other hand, the stresses on the compression side cannot reach as high a value as the yield stress since in this zone high transverse stresses occur due to the bending moment M_y. If an ideal stress distribution is assumed, with the stress in compression assumed to be half the stress in tension, the position of the neutral axis corresponds to 1/3 the angle φ measured from the edge. The obtained ultimate load is then 331.1 lb/ft^2. If the stress in compression is assumed to be one third the stress in tension the position of the neutral axis corresponds to 1/4 the angle φ measured from the edge. The obtained ultimate load would then be 261.3 lb/ft^2. This latter value corresponds quite well with the ultimate load obtained in this study. The shearing force N_{xy} along the simply supported edge is shown in Fig. 28. Finally, the variation of the transverse bending moment M_y at the midspan section is shown in Fig. 29 for different load levels.

The displacements and forces in the elastic range agree with those obtained by Mohraz and Schnobrich.[27] Small differences do occur since in this study cos $\beta/2$ is taken to be equal to unity. The results obtained agree quite well with those given by the ASCE Manual.[8] The largest deviation is in the magnitude of the N_x force at the center of the free edge. For the 6 x 6 grid this N_x force for a unit load is 886 lb/ft, while for an 8 x 8 grid it is 949 lb/ft. The corresponding value of N_x obtained from the Manual is 1128 lb/ft. The value of N_x at the edge converges to the "exact" value as the mesh becomes finer. If linear extrapolation is used the value of N_x when the grid size tends to zero is 1030 lb/ft. It should be kept in mind that the values obtained from the Manual are for a sinusoidal load which causes the N_x stress at midspan section to be slightly larger than that resulting from a uniform load. A plot of the N_x force at midspan section comparing the results obtained here with those of the Manual is shown in Fig. 30.

Almost no information exists on which to draw comparisons with the results of this study once plastic action has begun in the shell. The small amount of experimental data that has been published deals with reinforced concrete and microconcrete models.[3,4,5] In these experiments transverse bending moments develop yield line hinges in the shell surface. The model in this study is considered composed of isotropic materials. Choice of the yield properties of the nodes was guided by considerations of the usual longitudinal tensile steel near the free edge. As a consequence, the resulting transverse moment resistance is considerably higher than for most normally reinforced concrete

shells, suppressing any tendency to form yield line hinges. This discrepancy between the model and reinforced shells was realized at the outset of the study. However, as subsequently discussed in Chapter 7, it was decided not to overly complicate the programming effort of this first study. Any comparisons with the limited number of published experimental data must therefore be of a rather gross qualitative, rather than quantitative, nature.

A rigid-plastic analysis of circular cylindrical roof shell structures was performed by Fialko.[14] Fialko sought upper and lower bounds to the ultimate load of the shell when loaded by uniform radial pressure. The yield condition used was a linear yield condition which approximated both the Mises and Tresca conditions. The shear stress does not combine in any of the inequalities of the yield condition, rather, additional bounding planes at $\tau_{xy} = \pm k$ were used. Fialko assumed three different stress fields to get lower bound solutions, selecting the largest. He also assumed three different kinematical fields to obtain upper bound solutions and selected the lowest. All lower bound solutions obtained according to the three assumed stress fields fall below the ultimate load as determined in this investigation. Two of the kinematical fields give upper bounds which lie above the ultimate load. A third kinematical field gives a load which falls below the ultimate load obtained in this study. This third kinematical field does not reflect an increase in the ultimate load when the opening angle φ increases. This is not the case for the type of shell analyzed in which beam type failure is prominent. The difference in loading and yield conditions between the two methods of analysis is another

factor which results in that discrepancy. To investigate the effect of the difference in loading the example presented here is examined for the case of uniform radial loading. This is carried out till the end of the elastic range. For radial loading the transverse moments are higher throughout the shell than those resulting from vertical loading. Also the axial tensile force N_x at the free edge is larger for the shell subjected to radial loading. Consequently the end of the elastic range is 112.2 lb/ft^2 for radial loading versus 118.4 lb/ft^2 for vertical loading. Higher transverse moments and axial force at the free edge will cause the ultimate load to drop. Fialko's third kinematical field is based on the assumption that yield lines will form parallel to the longitudinal edge. Even when the loading and yield conditions used by Failko are incorporated in the computer program of this study it is inconceivable that such yield lines would form. This is simply because the transverse moment is not high enough to form plastic lines parallel to the longitudinal edges.

To investigate the effect of the grid size on the solution an 8 x 8 mesh on one quadrant is also used. The resulting number of unknowns is 408. The problem was run on the computer for 51 cycles of incremental loading. After these 51 cycles the load had reached the value of 238.8 lb/ft^2. The obtained load deflection diagram and yield pattern are almost identical to those obtained from the problem with 6 x 6 grid when compared at the corresponding load level. Thus it is felt unwarranted to run the problem with the finer mesh up to the ultimate load. Any difference between the two ultimate loads is expected to be very small. This can be explained by the fact that the shell is

behaving like a beam. Near the ultimate load a plastic hinge is formed at the center of the shell. The distribution of the longitudinal force N_x does not change significantly by decreasing the grid size.

Convergence has been demonstrated for similar models and similar elasto-plastic analysis in the investigations by Lopez and Ang[24] for square plates, Mohraz and Schnobrich[27] for shell structures, and by Crose and Ang[7] for circular plates considering large deflection effects. In view of these earlier studies no additional investigation is considered necessary for this study.

6.3. Multiple Barrel Shell Simply Supported at Both Ends

The dimensions and the material properties of the shell in this case are the same as those used in Section 6.2 for the single barrel shell. A quadrant of the shell is divided into six spacings in each direction resulting in 222 unknowns. The shell is subjected to an increasing load. The first yielding occurs in the bottom layer at the center of the valley at a load of 188.3 lb/ft^2. With further loading yielding progresses in both the top and bottom layers of the shell. Figure 31 shows this progression. Once the load passes the value of about 400 lb/ft^2 yielding spreads rapidly until it covers the major portion of the shell.

In the case of a multiple barrel shell the maximum deflection is not at the center of the continuous edge but is shifted away from it by about 1/3 of the angle φ. A plot of the load p versus w_{max} is shown in Fig. 32. In the last stages of loading the slope of the load deflection curve becomes very flat, and any small load increment causes

the deflections to increase appreciably. At the load level of 452.1 lb/ft^2 computations are stopped and this load is considered to be the ultimate load for the shell. If as in Section 6.2 the modulus of elasticity of the material is considered equal to that of concrete, then the maximum deflection for the load 452.1 lb/ft^2 is found to be 13.1 inches. At this load level the majority of the top layers and a substantial number of the bottom layers have already yielded.

A plot of the displacement w at the midspan section is shown in Fig. 33. Also the displacement w along the valley and along a diagonal proceeding from the continuous edge to the simply supported edge is shown in Fig. 34 and Fig. 35 respectively. The plot of the displacement along the diagonal shows that, as plastic flow progresses, oscillations between the two systems of nodes develop. This phenomenon has been explained previously in Section 5.5.

The variation of the force N_x at the midspan section is shown in Fig. 36. This closely resembles the ideal plastic stress distribution in the case of beams. If this ideal stress distribution is applied to the shell, i.e. equal tension and compression stresses and a position of the neutral axis corresponding to 1/2 the angle φ, the obtained ultimate load is 451.6 lb/ft^2. This is in very close agreement with the computed value. Figure 37 shows the variation of the N_x force along the valley. Once yielding takes place redistribution of the stresses is possible. In this case, when the N_x force decreases in a certain portion along the valley, it increases along a line parallel to and one spacing away from the valley. The shearing force N_{xy} along the simply supported edge is shown in Fig. 38.

The bottom layers in the midspan section are in a state of biaxial compression. Once these layers yield the stresses in the y-direction decrease to allow for the increase in the stresses in the x-direction so that the state of stress remains on the yield surface. This reduction in the stresses in the y-direction causes the transverse moment M_y to decrease once plastic flow occurs. The variation of the transverse moment M_y at the midspan section for different load levels is shown in Fig. 39. The reduction of M_y can be explained by the fact that the N_x force becomes almost constant on both sides of the midspan section. Just as in any beam, the shearing force, N_{xy}, cannot develop where there is no change in the longitudinal force. Thus the transverse moment decreases since it depends on the shear difference between the two transverse sections. The values of N_x, N_{xy}, and M_y for the nodes of one system of the model are listed in Tables 1, 2, and 3 respectively.

In the elastic range the maximum displacement w in the case of the multiple barrel shell is about one-tenth the value of the maximum displacement in the shell with free edges. At the ultimate load, the maximum displacement w in the case of the multiple barrel shell is about one-third the value of the maximum displacement in the shell with free edges. The ultimate load itself for the multiple barrel shell is 1.67 times that for the single barrel shell. It is thus evident that the multiple barrel shell is far more satisfactory in its serviceability and strength than the single barrel shell.

7. CONCLUSIONS AND RECOMMENDATIONS FOR FUTURE STUDY

The model used in this investigation proved to be successful in handling the analysis of elasto-plastic shells. It simulates a laboratory test through which the behavior of the shell is studied. Laboratory tests are, in general, expensive and cannot cover a wide range of varying parameters. However, such a wide range can be directly covered on the computer by simply varying the input data. The numerical method used proved to be efficient and suitable for programming.

The results obtained for the problems presented as illustrative examples above show clearly that the multiple barrel shell is far better than the single barrel shell in both servicability and ultimate strength. Although the model was used here to solve cylindrical shells it is capable of solving elliptic paraboloids and hyperbolic paraboloids. To arrive at appropriate solutions for these shells entails minor changes in the computer program. Solving such problems will be of interest especially since these shells are usually more uniformly reinforced than are cylindrical shells. Due to this uniformity the obtained results would closely resemble the true behavior of the shells.

In order to provide for the variations in reinforcing steel quantities and placement, orthotropy of the individual nodal layers would be necessary. Also, allowance for differences in the properties of the top and bottom layers at each node would have to be included, as would the variations in the properties with the surface coordinates of

the shell. The inclusion of such differences of material properties for different points of the shell does not pose any difficulty in the theory of application of the model. It does, however, represent a significant programming effort.

Another possible further study is to alter the model to account for the behavior of both the concrete and the steel embodied in it. This could be achieved by changing the formation of the nodes. Yield conditions for reinforced concrete[28,30] and for orthotropic materials can then be used.

The study should also be extended to the large deflection theory of shells to account for the changes in geometry occurring under heavy loading conditions. Such a study is not necessary for the type of cylinders investigated here, but would be for shallow doubly curved shells where significant changes in the radii of curvature might occur.

The boundary conditions of a supporting edge beam should be developed such that it would be possible to trace yielding in both the beam and the shell together.

In conclusion, to achieve the most economical design of shell roofs the methods of analysis should be based on an understanding of all stages of shell behavior. This study of elasto-plastic shell roofs constitutes an important step towards the realization of this goal.

LIST OF REFERENCES

1. Baker, A. L. L., "A Plastic Design Theory for Reinforced and Prestressed Concrete Shell Roofs," Magazine of Concrete Research, No. 4, London, 1950.

2. Baker, A. L. L., "Ultimate Strength Theory for Short Reinforced Concrete Cylindrical Shell Roofs," Magazine of Concrete Research, No. 10, London, 1952.

3. Baker, A. L. L., "Recent Research in Reinforced Concrete, and Its Application to Design," Journal of the Institution of Civil Engineers, Vol. 35, London, 1951.

4. Baker, A. L. L., "Further Research in Reinforced Concrete and Its Application to Ultimate Load Design," Proceedings of the Institution of Civil Engineers, Vol. 2, Part 3, London, 1953.

5. Bouma, A. L., Van Riel, A. C., Van Koten, H. and Beranek, W. J., "Investigations on Models of Eleven Cylindrical Shells Made of Reinforced and Prestressed Concrete," Proceedings of the Symposium on Shell Research, North-Holland Publishing Company, Amsterdam, 1961.

6. Chang, G. C. and Ang, A. H.-S., "Numerical Analysis of Plane Structure - Medium Interaction in Elastic - Perfectly Plastic Media," Civil Engineering Studies, Structural Research Series No. 307, University of Illinois, 1966.

7. Crose, J. G. and Ang, A. H.-S., "A Large Deflection Analysis Method for Transversely Loaded Elastic-Perfectly Plastic Circular Plates," Civil Engineering Studies, Structural Research Series No. 323, University of Illinois, 1967.

8. Design of Cylindrical Concrete Shell Roofs, American Society of Civil Engineers, Manuals of Engineering Practice, No. 31, adopted 1951.

9. Drucker, D. C., "Stress-Strain Relations in the Plastic Range--A Survey of Theory and Experiments," Brown University ONR Report, Contract Number ONR-358, 1950.

10. Drucker, D. C., "A More Fundamental Approach to Plastic Stress--Strain Relations," Proceedings of the First U. S. National Congress of Applied Mechanics, ASME, June 1951.

11. Drucker, D. C., "On Uniqueness in the Theory of Plasticity," Quarter Applied Mathematics, Vol. 14, No. 1, 1956.

12. Drucker, D. C., "A Definition of Stable Inelastic Material," Journal of Applied Mechanics, Vol. 26, March 1959.

13. Drucker, D. C., "Plasticity," Proceedings of the First Symposium on Naval Structural Mechanics, ed. J. N. Goodier and N. J. Hoff, Pergamon Press, New York, 1960.

14. Fialkow, M. N., "Limit Analysis of Simply Supported Circular Shell Roofs," Journal of the Engineering Mechanics Division, Proceedings of ASCE, Vol. 84, July 1958.

15. Gibson, J. E., The Design of Cylindrical Shell Roofs, D. Van Nostrand Company, New Jersey, 1961.

16. Gol'denveizer, A. L., Theory of Elastic Thin Shells, Pergamon Press, New York, 1961.

17. Handelman, G. H. and Lin, C. C., "On the Mechanical Behavior of Metals in the Strain Hardening Range," Quarter of Applied Mathematics, Vol. 4, 1947.

18. Harper, G. N. and Ang, A. H.-S., "A Numerical Procedure for the Analysis of Contained Plastic Flow Problems," Civil Engineering Studies, Structural Research Series No. 266, University of Illinois, 1963.

19. Hill, R., The Mathematical Theory of Plasticity, Oxford University Press, London, 1950.

20. Hodge, P. G., Jr., Limit Analysis of Rotationally Symmetric Plates and Shells, Prentice-Hall, New Jersey, 1963.

21. Johansen, K. W., "Critical Notes on the Calculation and Design of Cylindrical Shells," Third Congress of the International Association for Bridge and Structural Engineers, Final Report, 1948.

22. Lame, G. and Clapeyron, E., "Memoires Sur L'Equilibre Interiur Des Corps Solides Homogenes," Memoires Presentes A L'Academie Des Sciences De L'Institut De France; second series, Vol. 4, 1828.

23. Lopez, L. A., "Flexural Analysis of Elastic-Plastic Rectangular Plates," Ph.D. Thesis, University of Illinois, May 1966.

24. Lopez, L. A. and Ang, A. H.-S., "Flexural Analysis of Elastic-Plastic Rectangular Plates," Civil Engineering Studies, Structural Research Series No. 305, University of Illinois, 1966.

25. Lundgren, H., Cylindrical Shells, Danish Technical Press, Copenhagen, 1951.

26. Mileykovsky, I. E., "Some Problems of Analysis of Reinforced Concrete Cylindrical Shell-Roofs Taking into Account Crack Formation," Non Classical Shell Problems, ed. W. Olszak and A Sawczuk, North-Holland Publishing Company, Amsterdam, 1963.

27. Mohraz, B. and Schnobrich, W. C., "The Analysis of Shallow Shell Structures by a Discrete Element System," Civil Engineering Studies, Structural Research Series No. 304, University of Illinois, March 1966.

28. Morley, C. T., "On the Yield Criterion of an Orthogonally Reinforced, Concrete Slab Element," Journal of the Mechanics and Physics of Solids, Vol. 14, No. 1, January 1966.

29. Newmark, N. M., "Numerical Methods of Analysis of Bars, Plates, and Elastic Bodies," Numerical Methods of Analysis in Engineering, ed. L. E. Grinter, MacMillan Co., New York, 1949.

30. Nielsen, M. P., "Yield Conditions for Reinforced Concrete Shells in the Membrane State," Non Classical Shell Problems, ed. W. Olszak and A. Sawczuk, North-Holland Publishing Company, Amsterdam, 1963.

31. Prager, W. and Hodge, P. G., Theory of Perfectly Plastic Solids, John Wiley and Sons, New York, 1951.

32. Rainer, J. H., "Numerical Calculation of Axi-Symmetric Elastic and Elastic-Perfectly Plastic Wave Motions," Ph.D. Thesis, University of Illinois, 1965.

33. Sawczuk, A., "On Limit Analysis of Anisotropic Plastic Shells," Non Classical Shell Problems, ed. W. Olszak and A. Sawczuk, North-Holland Publishing Company, Amsterdam, 1963.

34. Schnobrich, W. C., "A Physical Analogue for the Numerical Analysis of Cylindrical Shells," Ph.D. Thesis, University of Illinois, June 1962.

TABLE 1. LONGITUDINAL FORCE N_x^* (lb/ft)

IA \ JA	1	3	5	7	9	11	13
$p = 188.3$ lb/ft^2							
1	-38.2	-36.6	-30.5	-16.5	8.5	46.2	96.1
3	-36.8	-35.4	-29.6	-16.3	7.9	44.8	93.9
5	-32.9	-31.7	-27.0	-15.5	6.4	40.7	87.2
7	-26.7	-26.0	-22.7	-13.8	4.1	33.9	75.7
9	-18.7	-18.4	-16.6	-10.9	1.6	24.4	58.6
11	-9.6	-9.5	-8.8	-6.3	-0.08	12.5	34.3
13	0	0	0	0	0	0	0
$p = 412.8$ lb/ft^2							
1	-105.9	-107.1	-92.0	-26.4	106.5	110.5	112.4
3	-103.7	-103.7	-85.6	-24.8	93.8	116.0	112.3
5	-95.9	-93.1	-70.9	-19.5	60.9	117.4	106.4
7	-80.9	-75.7	-55.0	-15.3	39.7	93.7	106.3
9	-58.2	-53.5	-38.3	-11.8	23.7	62.7	92.6
11	-30.3	-27.7	-19.9	-7.1	9.8	30.7	58.8
13	0	0	0	0	0	0	0
$p = 452.1$ lb/ft^2							
1	-123.1	-124.9	-125.5	20.8	112.4	115.4	114.0
3	-119.4	-122.6	-124.0	25.4	108.2	115.1	115.0
5	-113.0	-118.0	-93.5	8.1	94.7	116.0	98.2
7	-102.4	-97.0	-66.1	1.4	62.1	109.3	83.0
9	-75.7	-68.7	-43.6	-2.7	40.6	74.3	76.0
11	-40.5	-35.9	-21.9	-3.3	22.0	32.8	53.3
13	0	0	0	0	0	0	0

* All numbers to be multiplied by 10^3

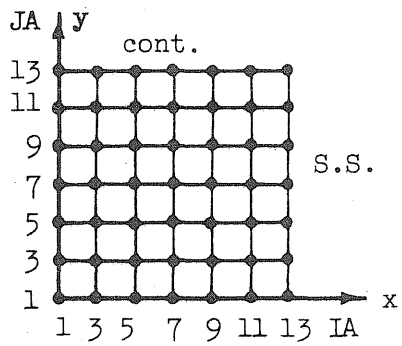

TABLE 2. SHEARING FORCE N^{*}_{xy} (lb/ft)

IA \ JA	1	3	5	7	9	11	13
$p = 188.3$ lb/ft^2							
1	0	0	0	0	0	0	0
3	0	-1.8	-3.3	-3.9	-3.3	-1.6	0
5	0	-3.5	-6.4	-7.9	-7.4	-4.7	0
7	0	-5.0	-9.2	-11.8	-11.7	-7.9	0
9	0	-6.1	-11.5	-15.2	-15.9	-11.7	0
11	0	-7.0	-13.4	-18.0	-19.6	-16.5	0
13	0	-7.6	-15.7	-23.0	-25.3	-16.1	0
$p = 412.8$ lb/ft^2							
1	0	0	0	0	0	0	0
3	0	-3.5	-11.7	-18.2	-4.0	-2.8	0
5	0	-8.5	-19.6	-27.0	-22.1	-1.2	0
7	0	-13.5	-26.3	-33.9	-30.3	-10.7	0
9	0	-17.8	-32.0	-39.0	-36.8	-21.9	0
11	0	-20.9	-36.9	-43.5	-42.0	-34.4	0
13	0	-22.8	-44.7	-60.9	-56.1	-24.4	0
$p = 452.1$ lb/ft^2							
1	0	0	0	0	0	0	0
3	0	-1.3	-4.5	-28.3	-1.4	-8.5	0
5	0	-5.6	-22.5	-37.6	-16.3	-6.7	0
7	0	-14.3	-31.9	-42.3	-34.3	-9.7	0
9	0	-20.9	-36.8	-45.4	-41.3	-22.1	0
11	0	-26.2	-43.5	-50.4	-40.3	-38.7	0
13	0	-35.1	-64.3	-68.3	-64.5	-7.6	0

* All numbers to be multiplied by 10^3

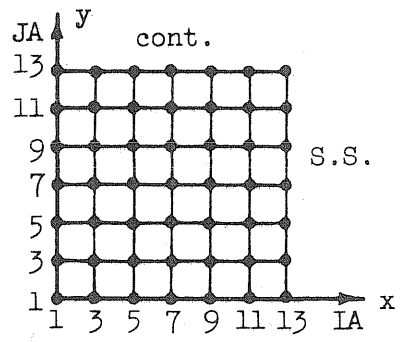

TABLE 3. TRANSVERSE MOMENT M_y^* (lb)

p = 188.3 lb/ft^2							
IA \ JA	1	3	5	7	9	11	13
1	-16.1	-11.5	0.15	12.6	16.8	2.5	-31.3
3	-15.7	-11.2	0.08	12.3	16.4	2.5	-30.7
5	-14.3	-10.3	-.11	11.1	15.3	2.7	-29.0
7	-11.9	-8.7	-.37	9.2	13.3	2.8	-25.9
9	-8.6	-6.4	-.56	6.5	10.2	2.8	-20.8
11	-4.5	-3.4	-.47	3.3	5.7	2.2	-12.8
13	0	0	0	0	0	0	0
p = 412.8 lb/ft^2							
1	-56.0	-43.0	-9.0	36.6	59.6	34.0	-45.2
3	-53.8	-41.1	-6.1	37.7	61.5	30.0	-46.2
5	-49.4	-36.8	-1.9	34.6	52.2	25.7	-59.6
7	-39.2	-27.3	0.10	27.8	38.7	16.3	-58.9
9	-25.8	-18.0	0.34	19.1	26.2	7.2	-48.0
11	-12.7	-9.0	0.02	9.4	13.5	4.0	-29.2
13	0	0	0	0	0	0	0
p = 452.1 lb/ft^2							
1	-33.1	-22.8	1.1	14.6	37.1	36.1	-38.2
3	-44.4	-33.4	-3.6	41.2	50.5	24.3	-37.3
5	-59.2	-45.0	-3.0	49.7	71.2	29.7	-73.6
7	-58.4	-42.4	-0.5	44.0	62.7	24.9	-91.2
9	-45.8	-31.0	0.8	32.0	45.8	11.4	-76.4
11	-22.1	-15.1	0.2	17.0	21.4	57.2	-44.5
13	0	0	0	0	0	0	0

* All numbers to be multiplied by 10^2

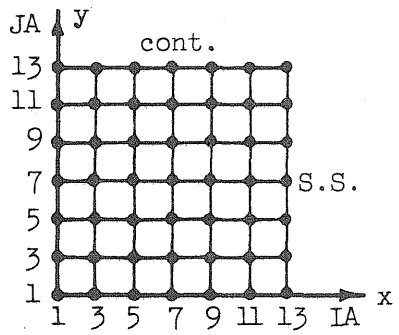

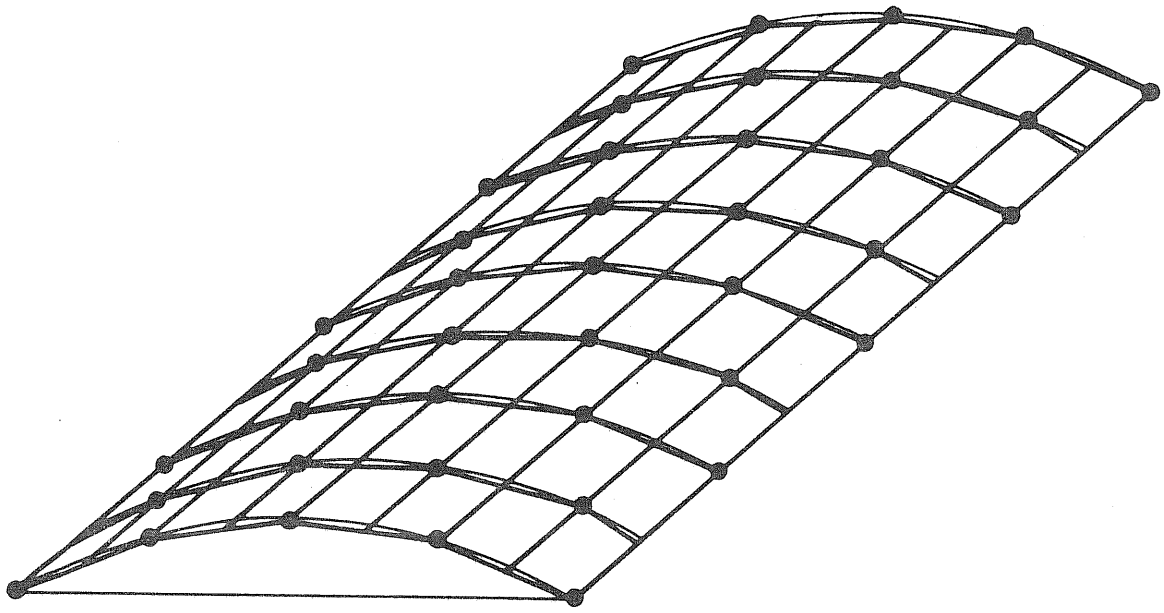

FIG. 1 MODEL REPRESENTATION OF THE SHELL

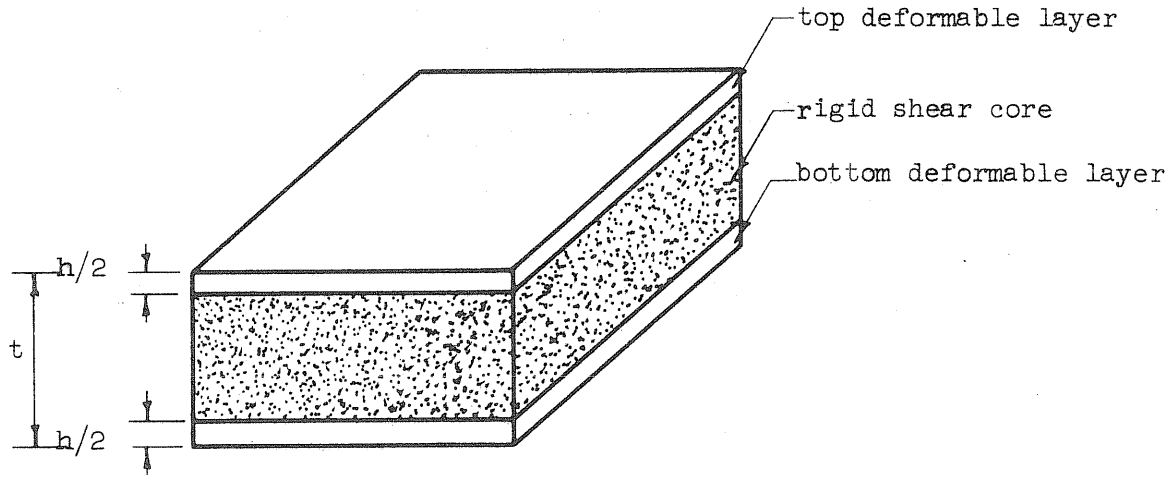

FIG. 2 A TYPICAL NODE

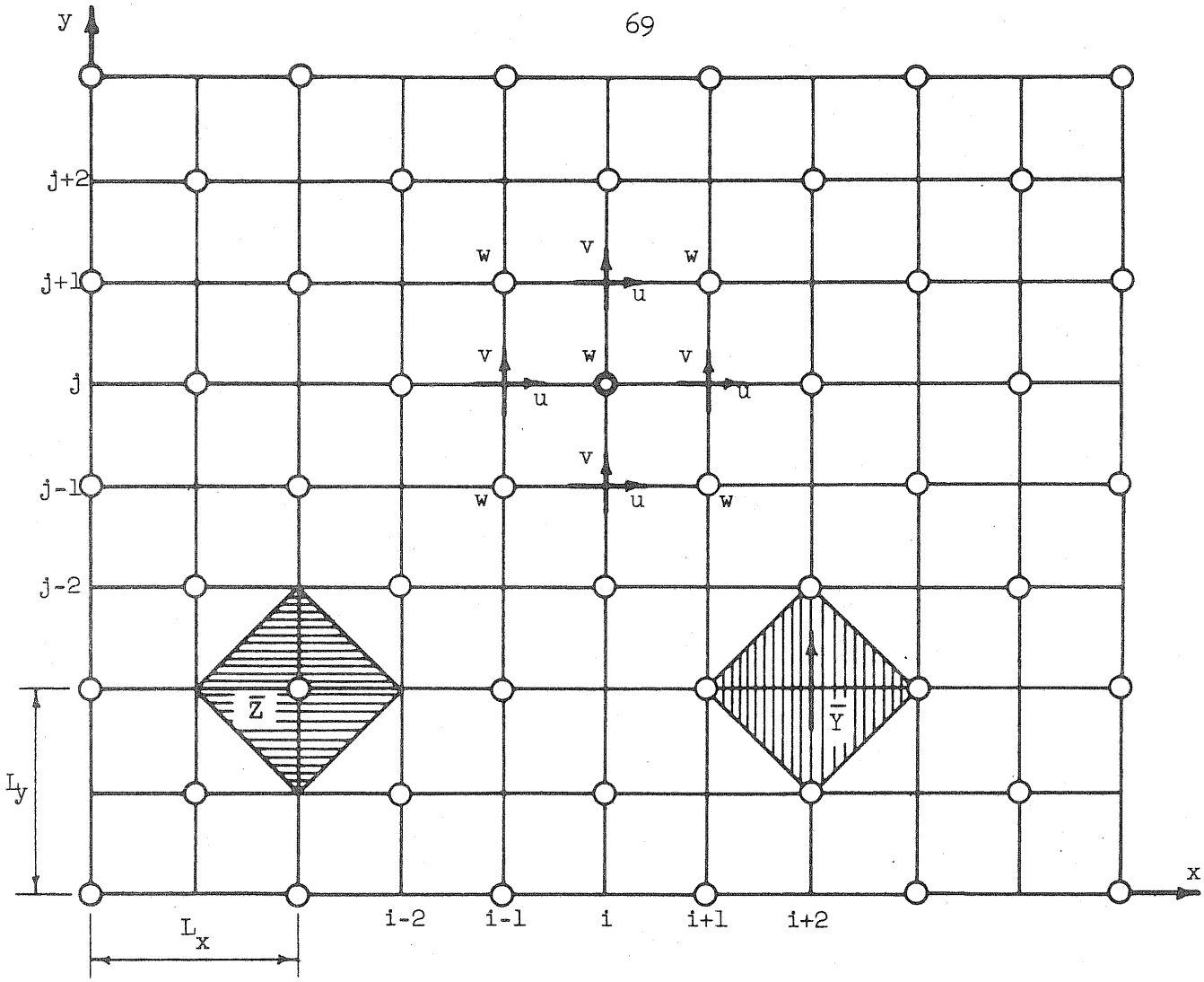

FIG. 3 GRID POINT IDENTIFICATION AND LOAD CONTRIBUTION AREAS

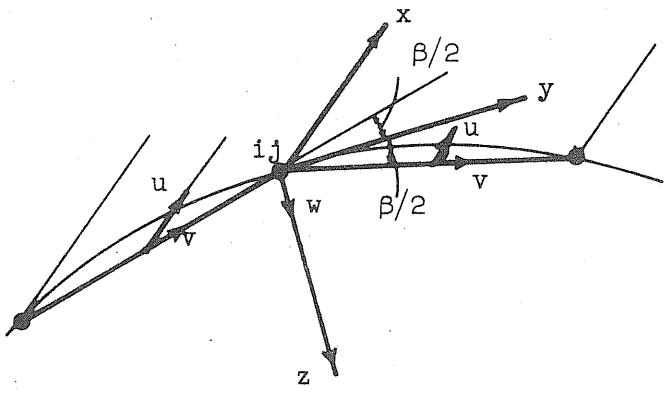

FIG. 4 COORDINATE AXES AND DISPLACEMENTS

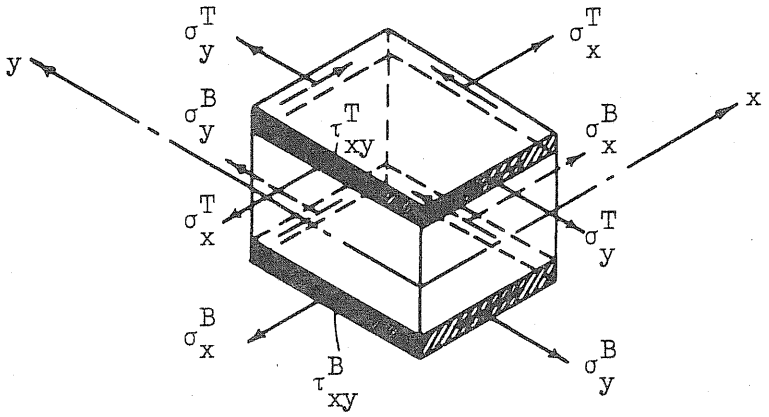

FIG. 5a POSITIVE DIRECTIONS OF THE STRESSES

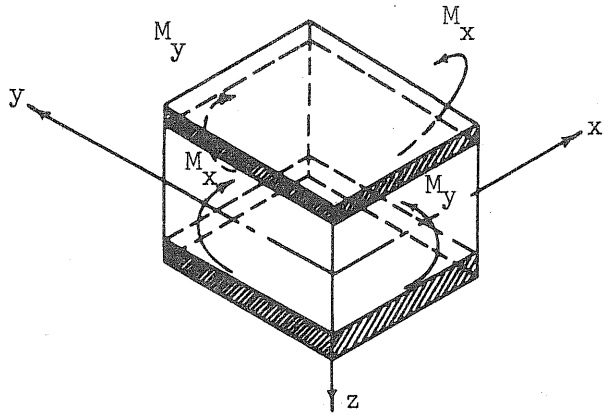

FIG. 5b POSITIVE BENDING MOMENTS

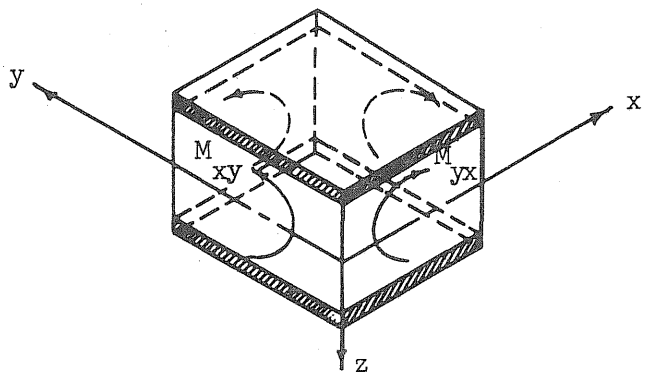

FIG. 5c POSITIVE TWISTING MOMENTS

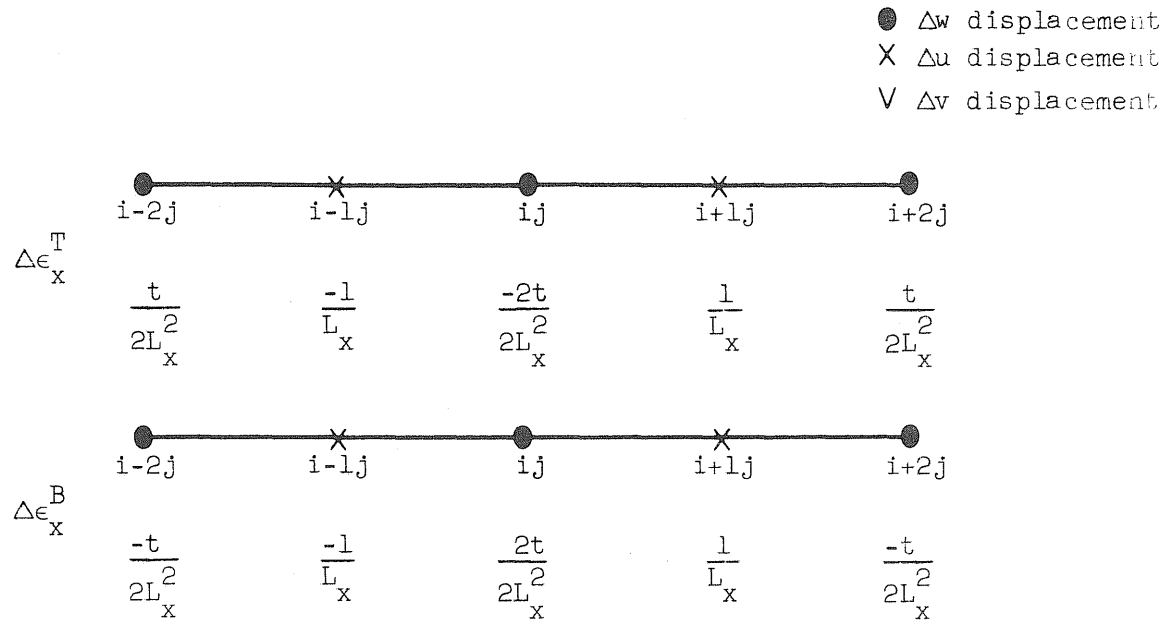

FIG. 6a OPERATORS FOR $\Delta\epsilon_x^T, \Delta\epsilon_x^B$

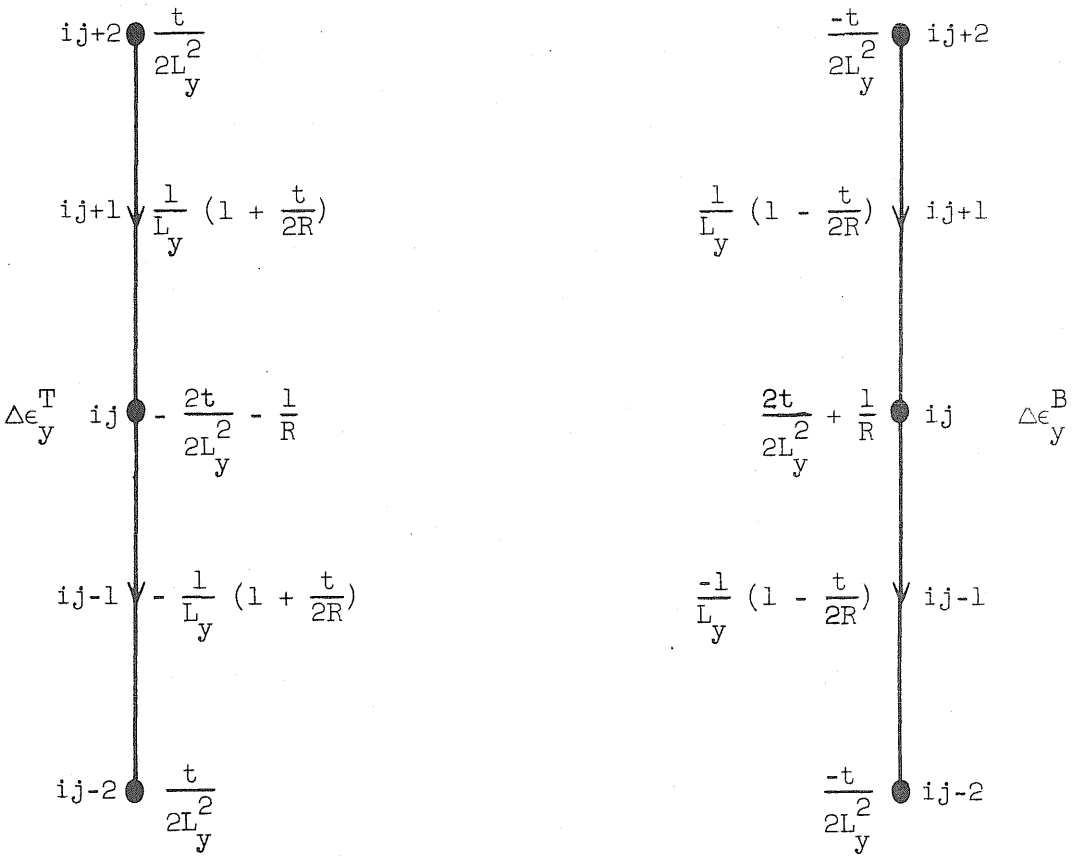

FIG. 6b OPERATORS FOR $\Delta\epsilon_y^T, \Delta\epsilon_y^B$

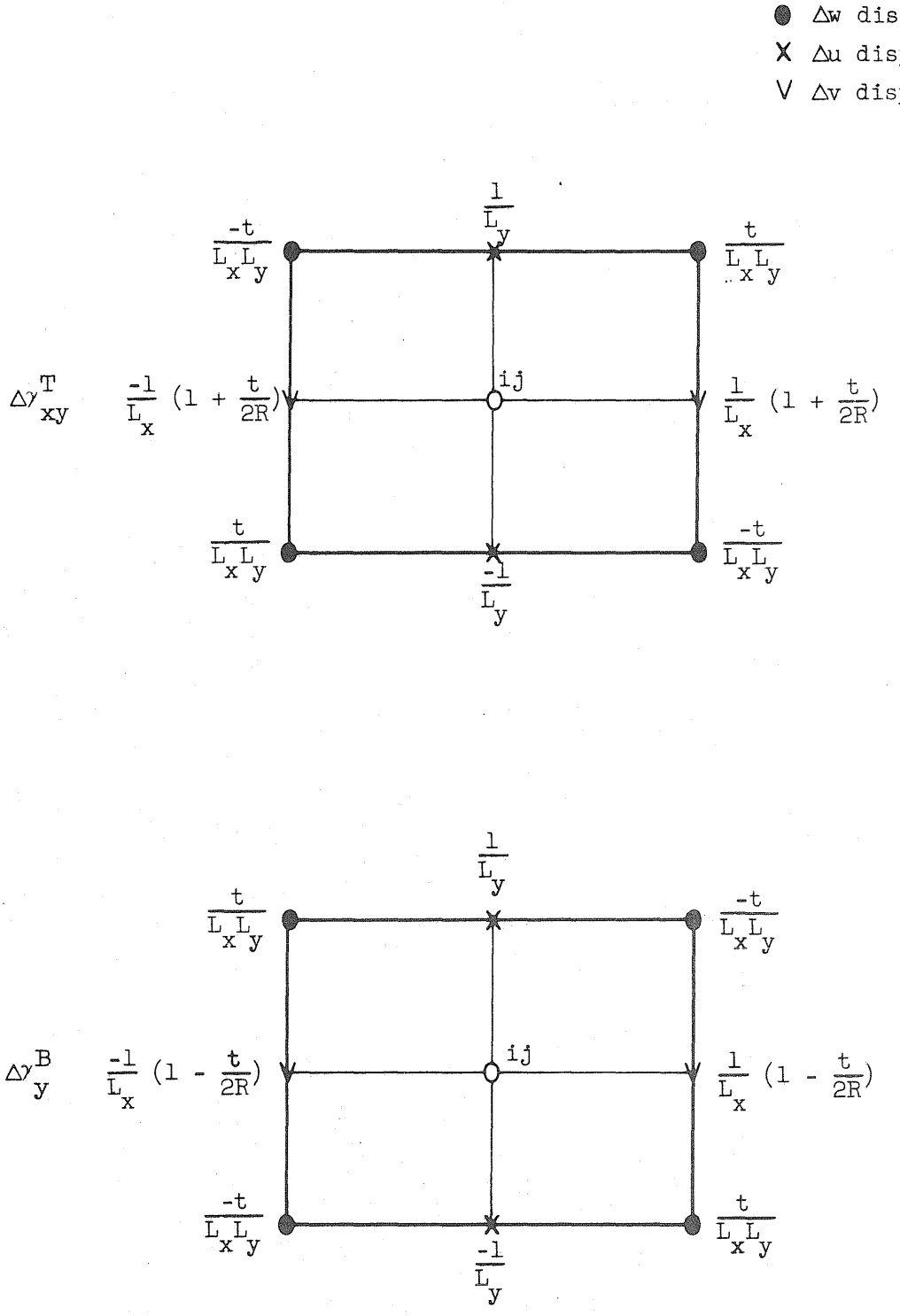

FIG. 6c OPERATORS FOR $\Delta\gamma^T_{xy}$ AND $\Delta\gamma^B_{xy}$

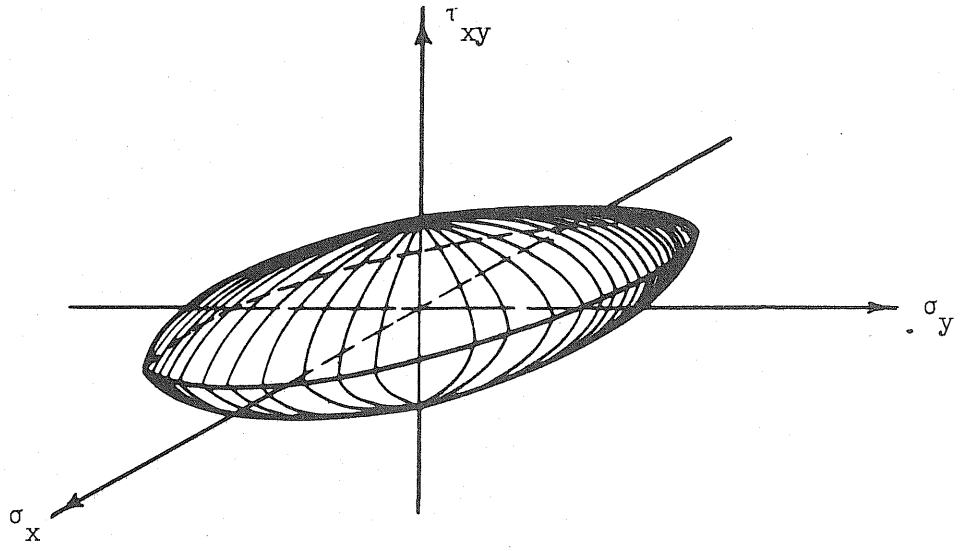

FIG. 7a VON MISES YIELD SURFACE FOR A STATE OF PLANE STRESS

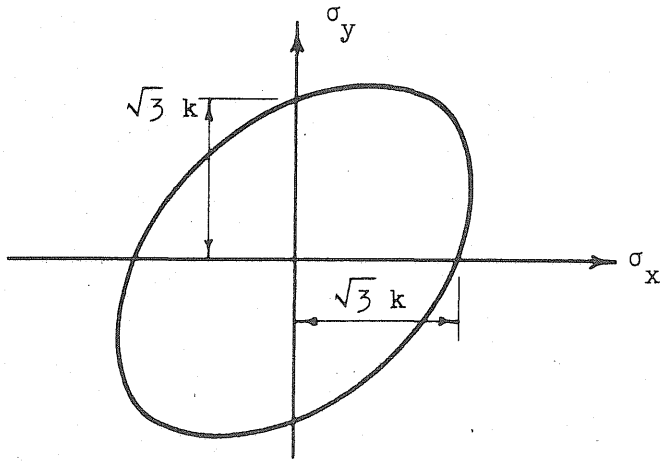

FIG. 7b YIELD LOCUS IN CASE $\tau_{xy} = 0$

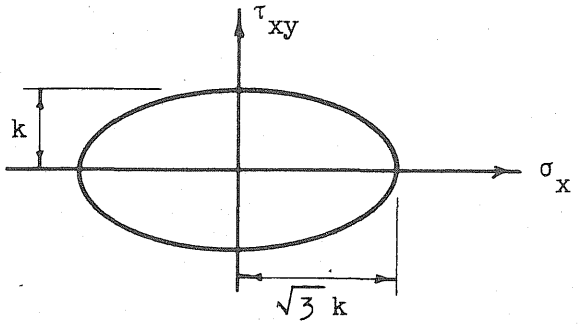

FIG. 7c YIELD LOCUS IN CASE $\sigma_y = 0$

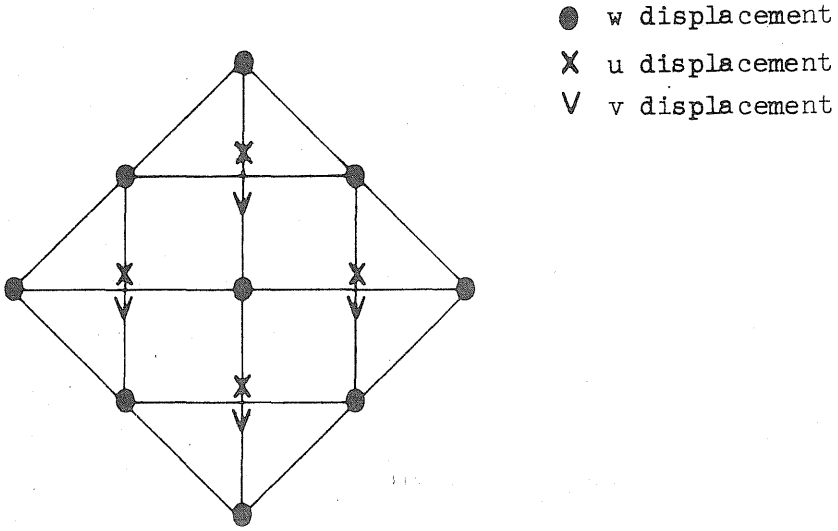

FIG. 8 DISPLACEMENT POINTS ASSOCIATED WITH A TYPICAL OPERATOR FOR FORCES AND MOMENTS

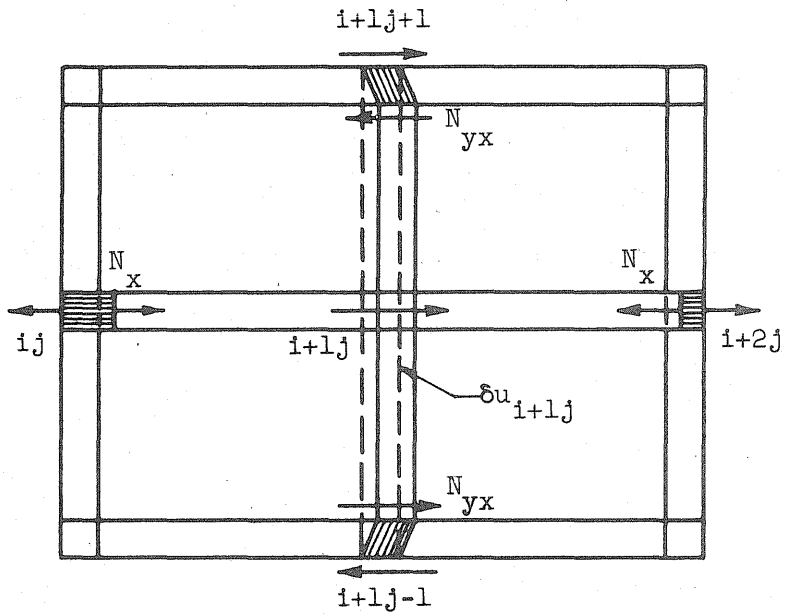

FIG. 9 A VIRTUAL DISPLACEMENT δu_{i+1j}

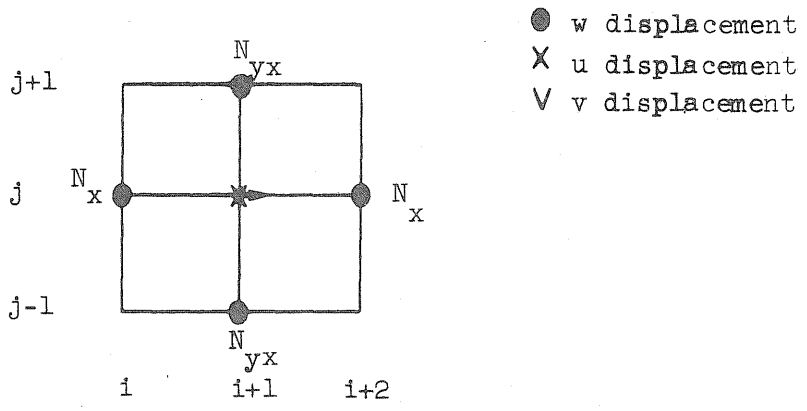

FIG. 10a THE FORCES INVOLVED IN THE EQUILIBRIUM EQUATION IN THE X-DIRECTION

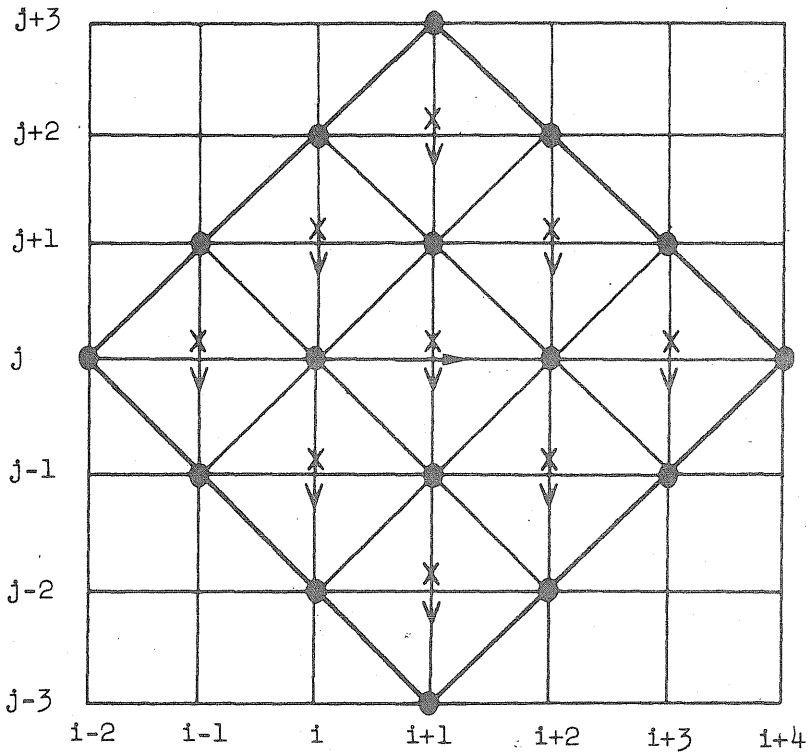

FIG. 10b THE DISPLACEMENTS INVOLVED IN THE EQUILIBRIUM EQUATION IN THE X-DIRECTION

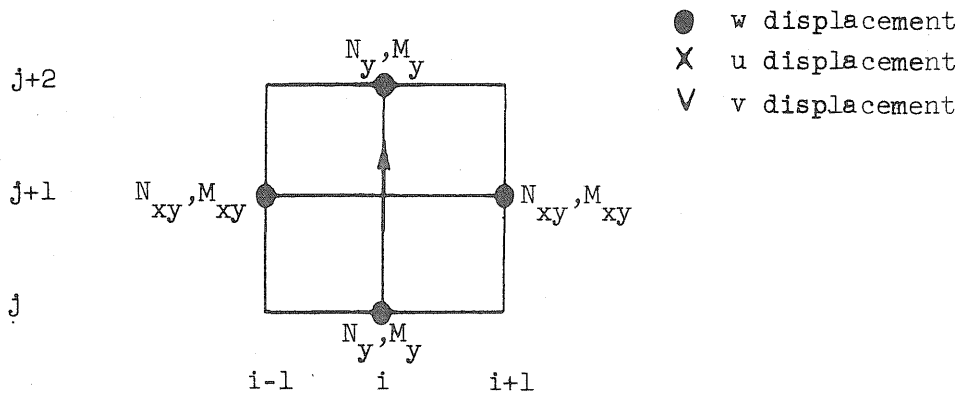

FIG. 11a THE FORCES AND MOMENTS INVOLVED IN THE EQUILIBRIUM EQUATION IN THE Y-DIRECTION

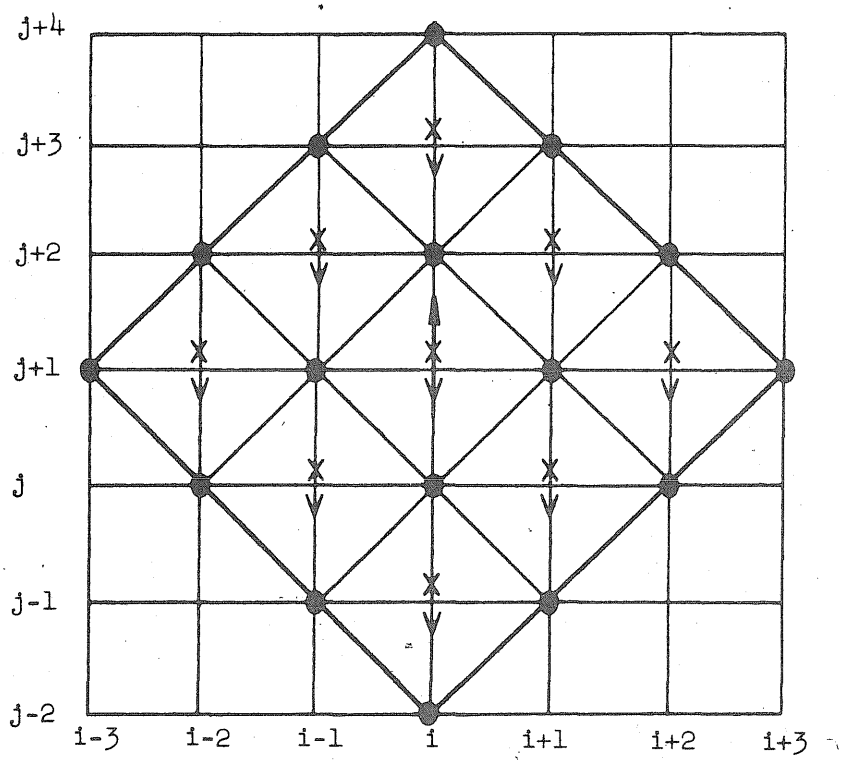

FIG. 11b THE DISPLACEMENTS INVOLVED IN THE EQUILIBRIUM EQUATION IN THE Y-DIRECTION

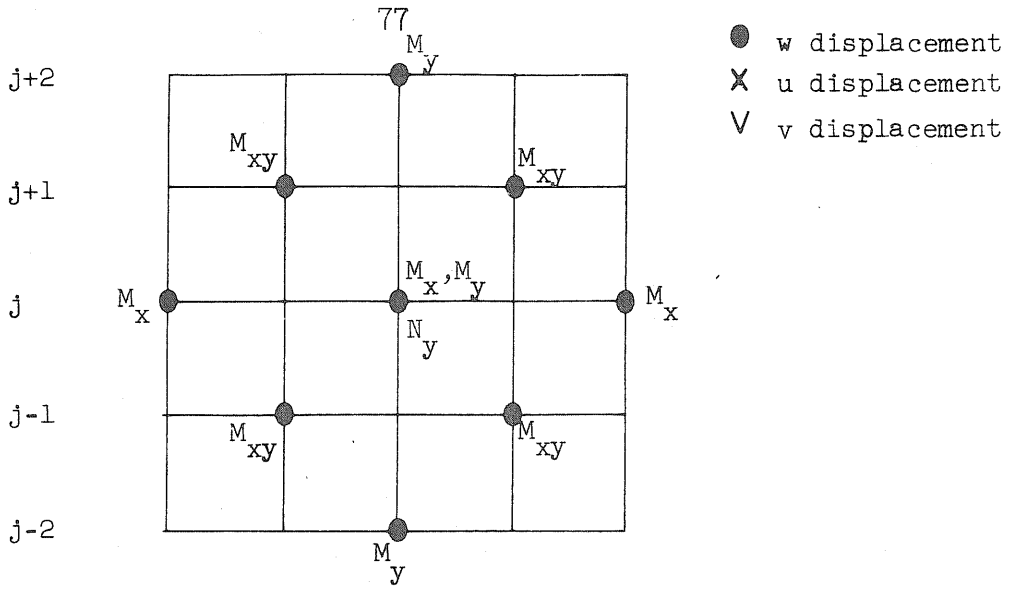

FIG. 12a THE FORCES AND MOMENTS INVOLVED IN THE EQUILIBRIUM EQUATION IN THE W-DIRECTION

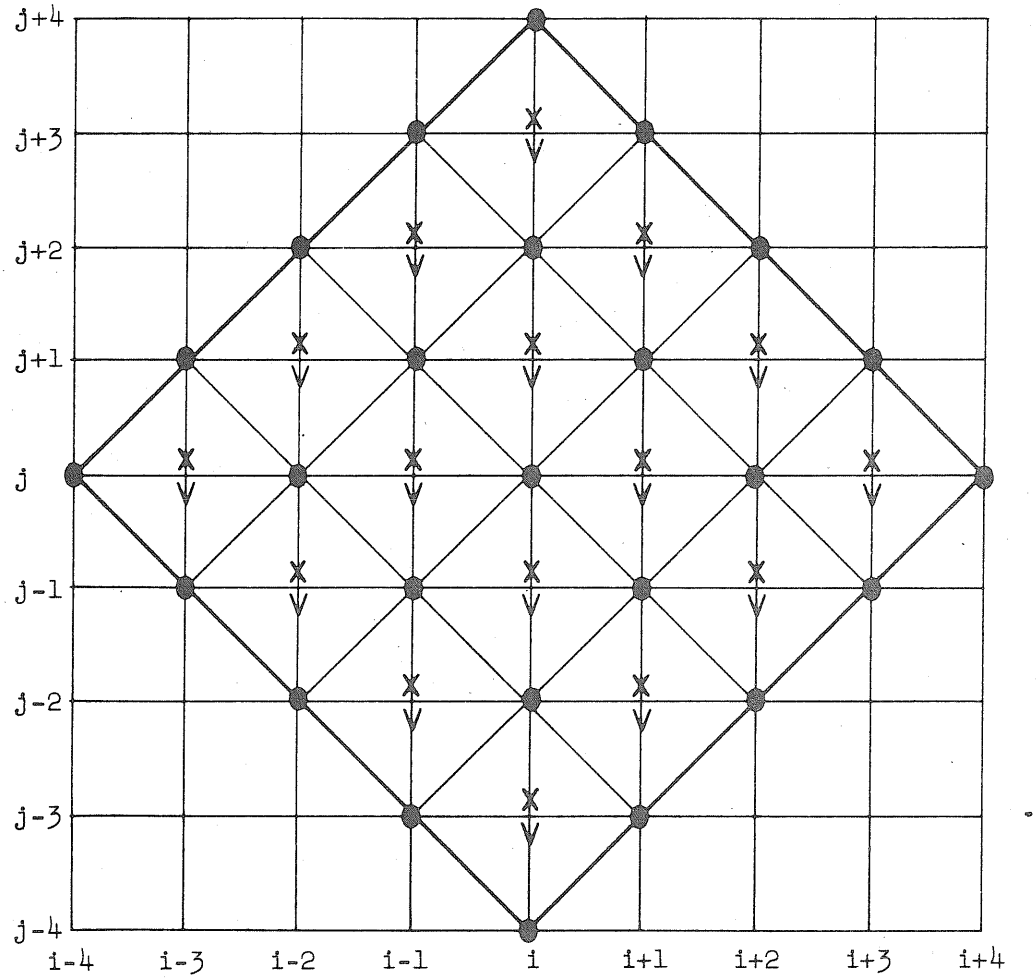

FIG. 12b THE DISPLACEMENTS INVOLVED IN THE EQUILIBRIUM EQUATION IN THE W-DIRECTION

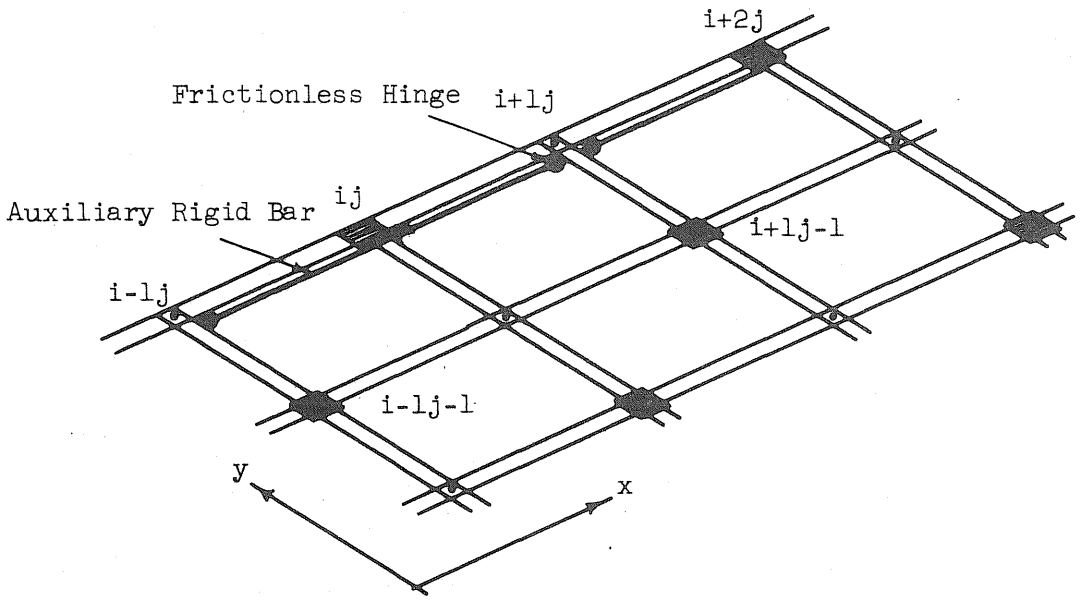

FIG. 13 DETAIL OF MODEL AT A FREE EDGE

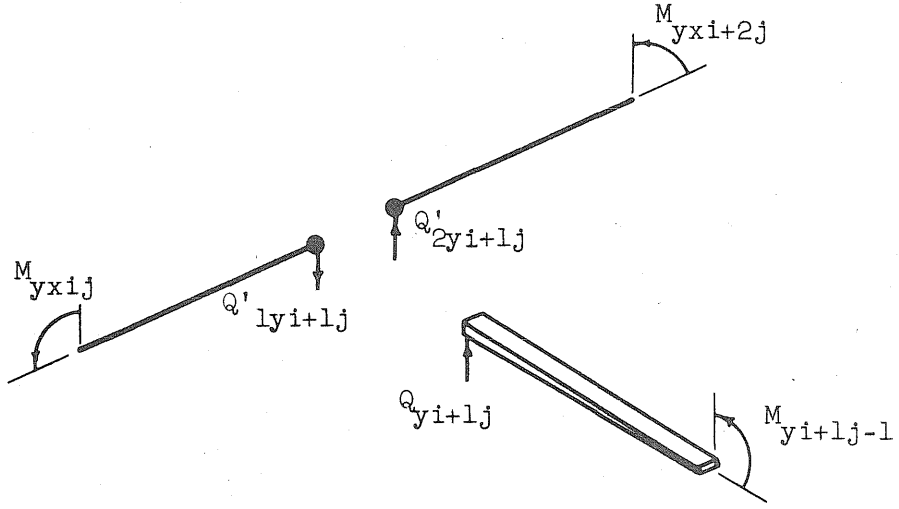

FIG. 14 EQUILIBRIUM OF A T-SECTION AT A FREE EDGE

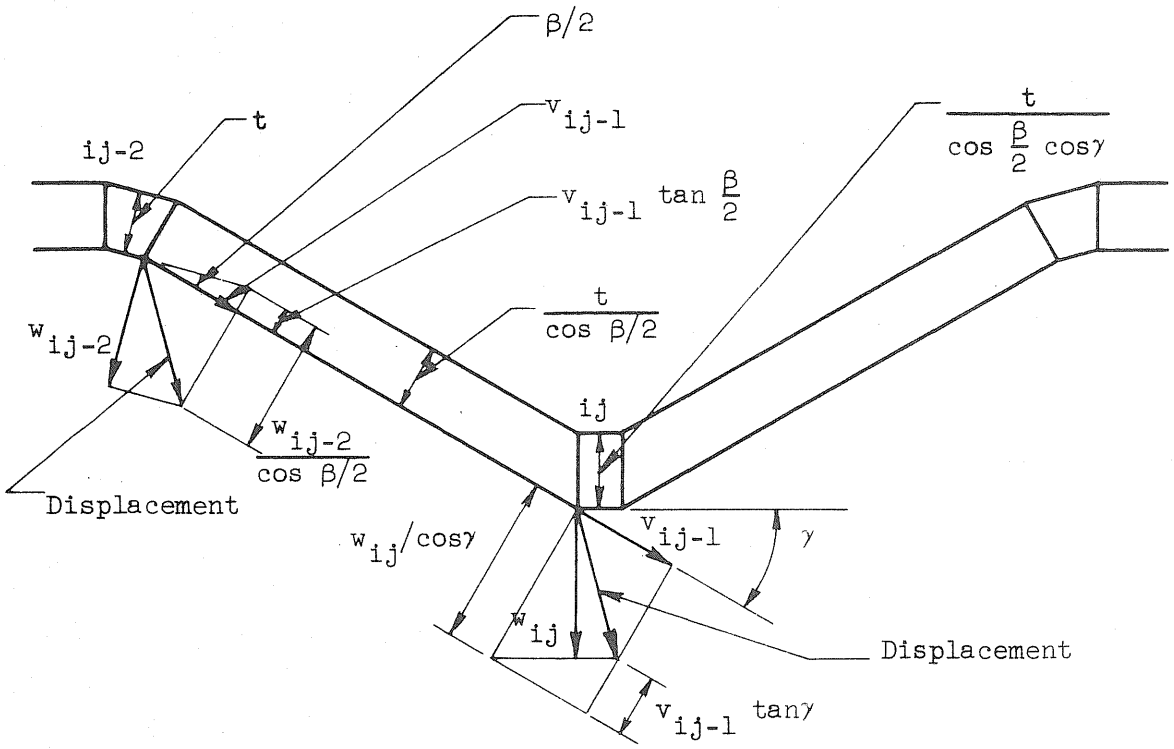

FIG. 15 JUNCTION GEOMETRY AND DISPLACEMENT CONFIGURATION OF TRANSVERSELY CONTINUOUS SHELL

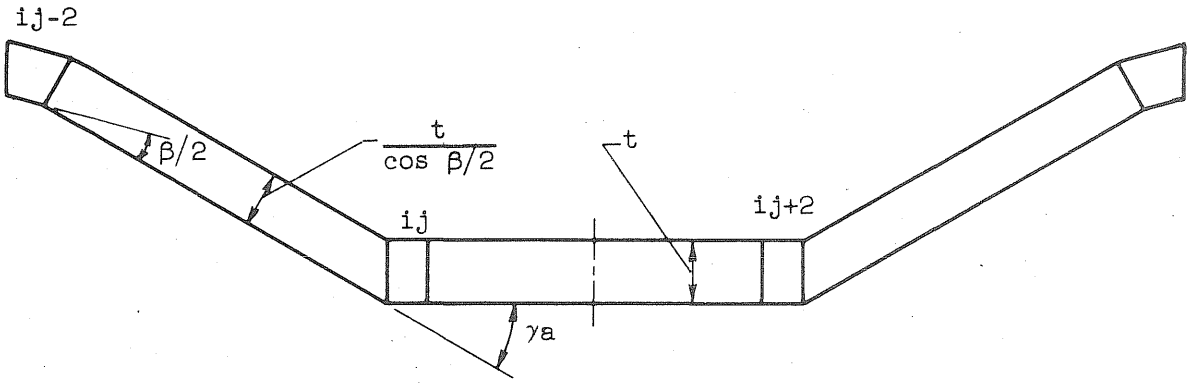

$$\theta_{yij-1} = \frac{1}{L_y}\left[\frac{w_{ij}}{\cos\gamma a} - w_{ij-2} - v_{ij-1}(\tan\gamma - \tan\beta/2)\right]$$

FIG. 16 MODIFIED JUNCTION GEOMETRY OF TRANSVERSELY CONTINUOUS SHELL AT NODES ONE-HALF SPACING FROM VALLEY

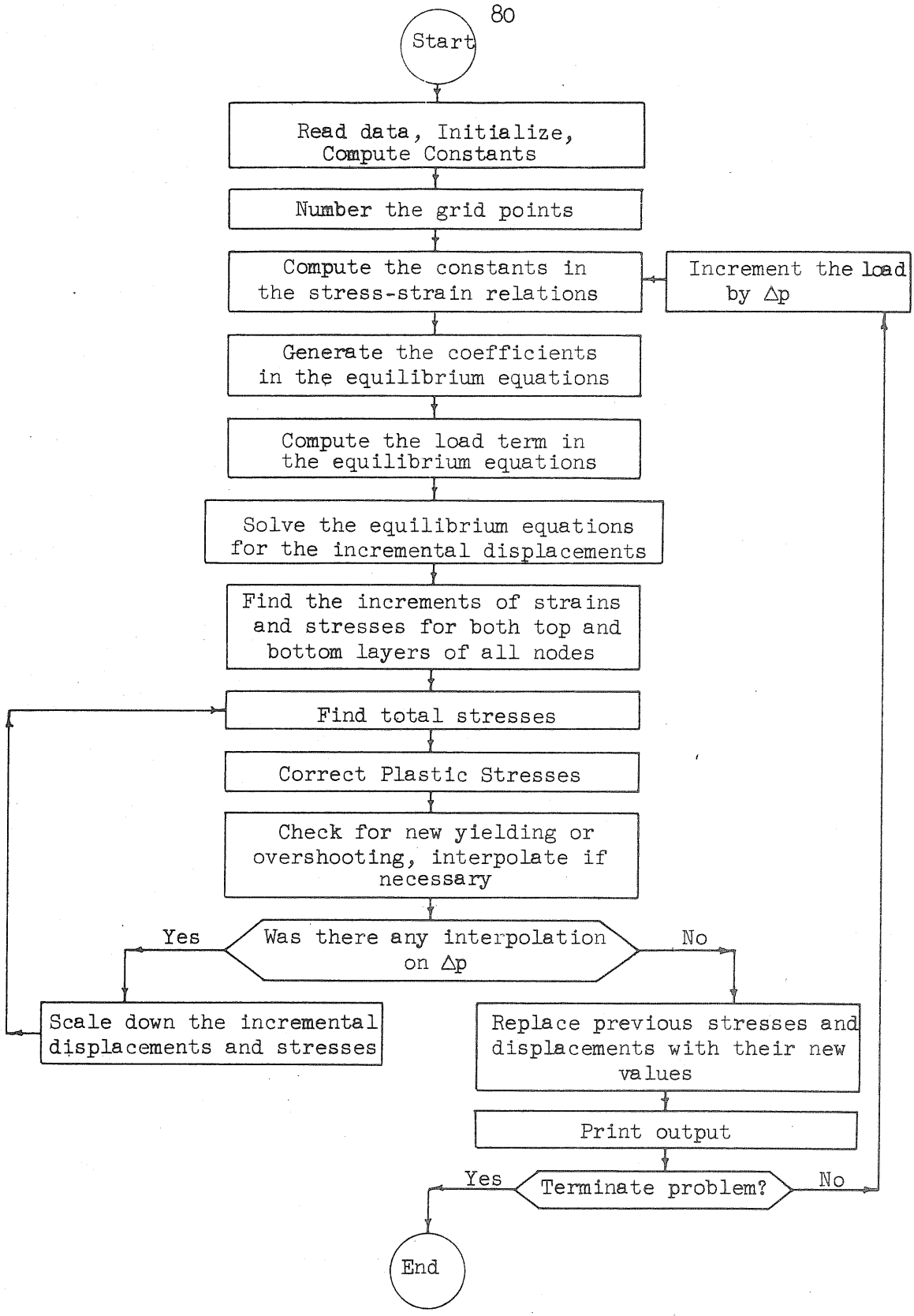

FIG. 17 A GENERAL FLOW DIAGRAM

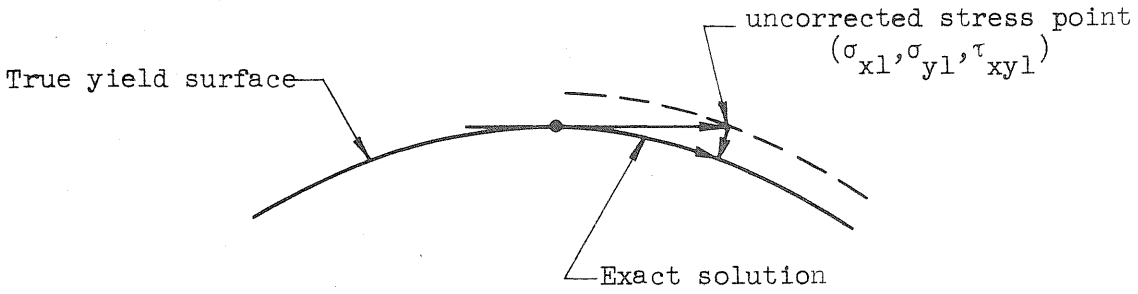

FIG. 18 CORRECTION OF PLASTIC STRESSES

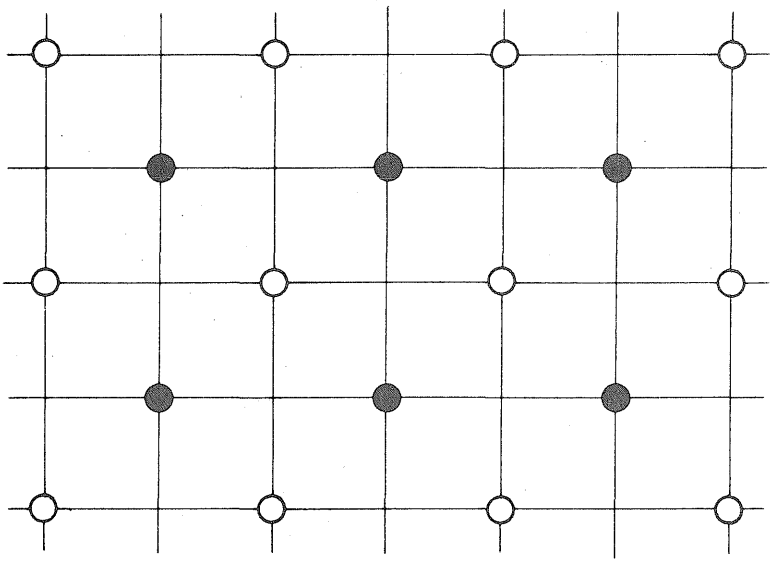

FIG. 19 COUPLING OF THE TWO SYSTEMS IN THE MODEL

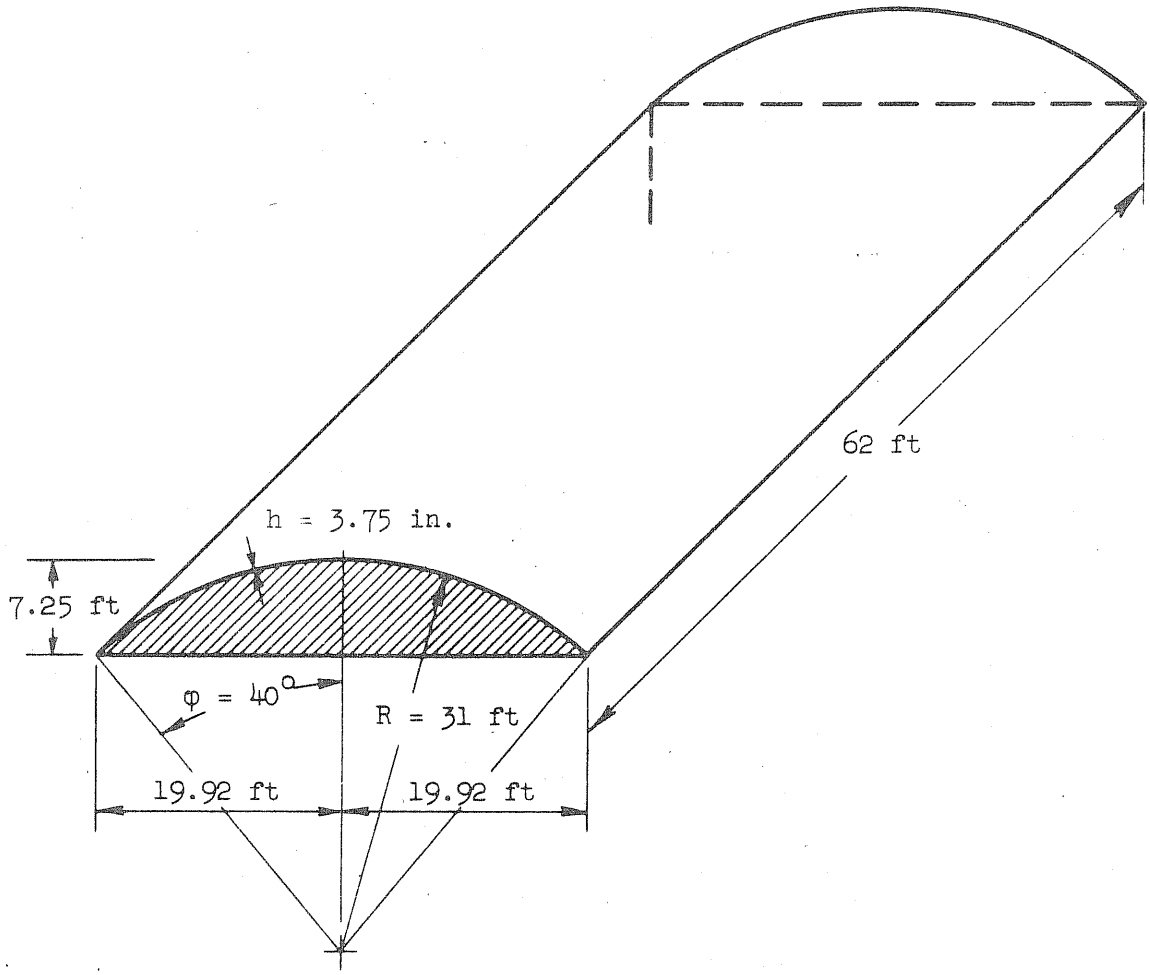

FIG. 20 SIMPLY SUPPORTED CYLINDRICAL SHELL WITH THE LONGITUDINAL EDGES FREE

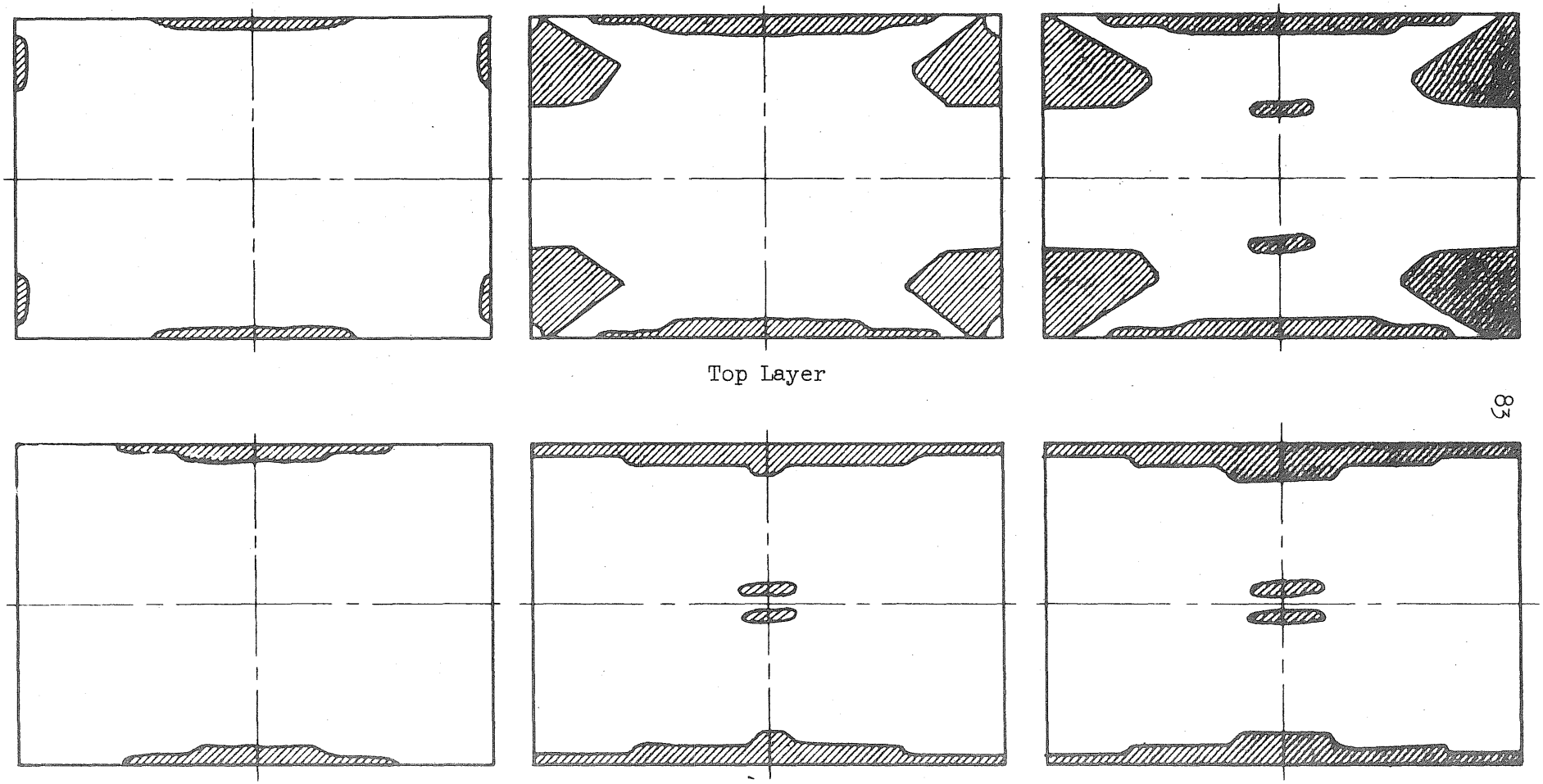

FIG. 21a PROGRESSION OF YIELDING FOR THE CYLINDRICAL SHELL WITH THE FREE LONGITUDINAL EDGES

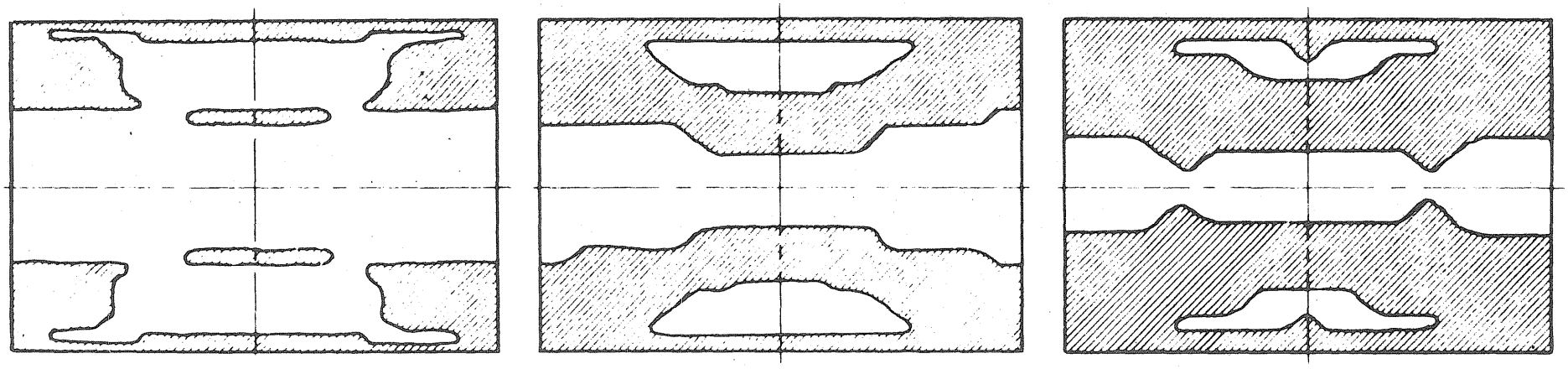

Top Layer

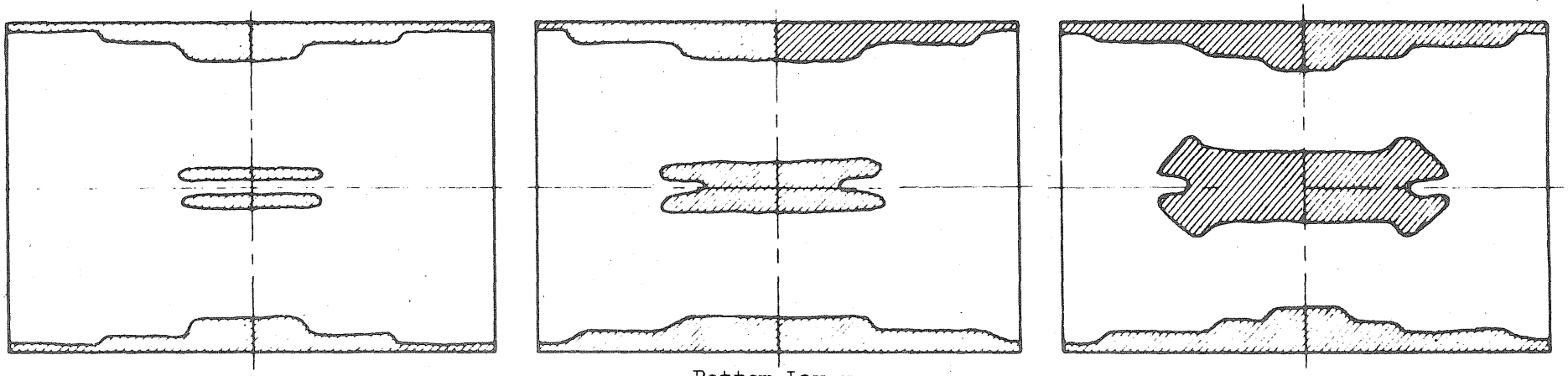

Bottom Layer

p = 234.0 lb/ft^2 p = 248.9 lb/ft^2 p = 263.1 lb/ft^2

FIG. 21a (cont'd) PROGRESSION OF YIELDING FOR THE CYLINDRICAL SHELL WITH THE FREE LONGITUDINAL EDGES

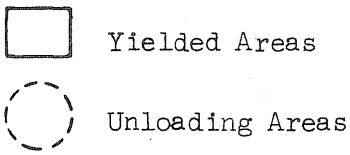

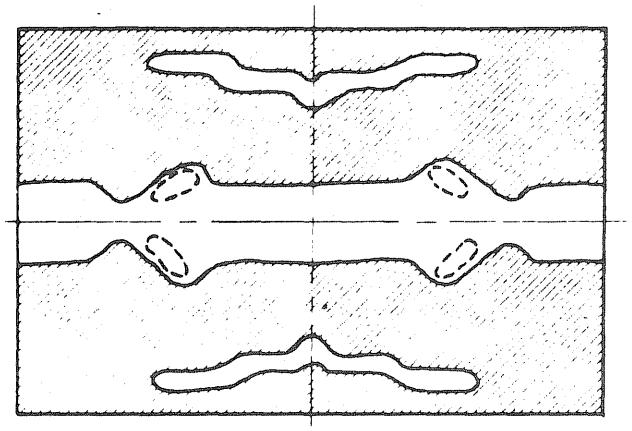

Top Layer

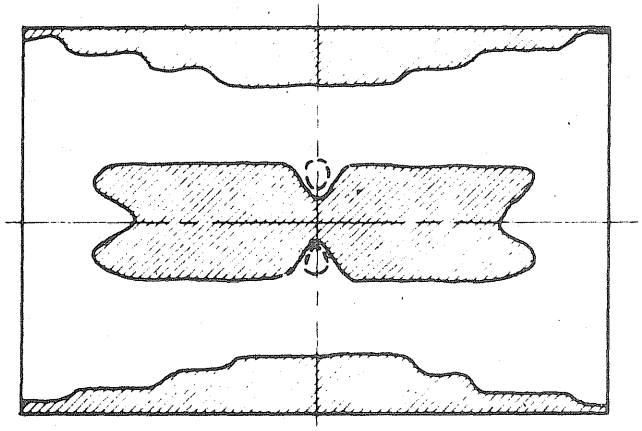

Bottom Layer

$p = 270.3 \text{ lb/ft}^2$

FIG. 21b FINAL STATE OF YIELDING FOR THE CYLINDRICAL SHELL SHOWN IN FIG. 20

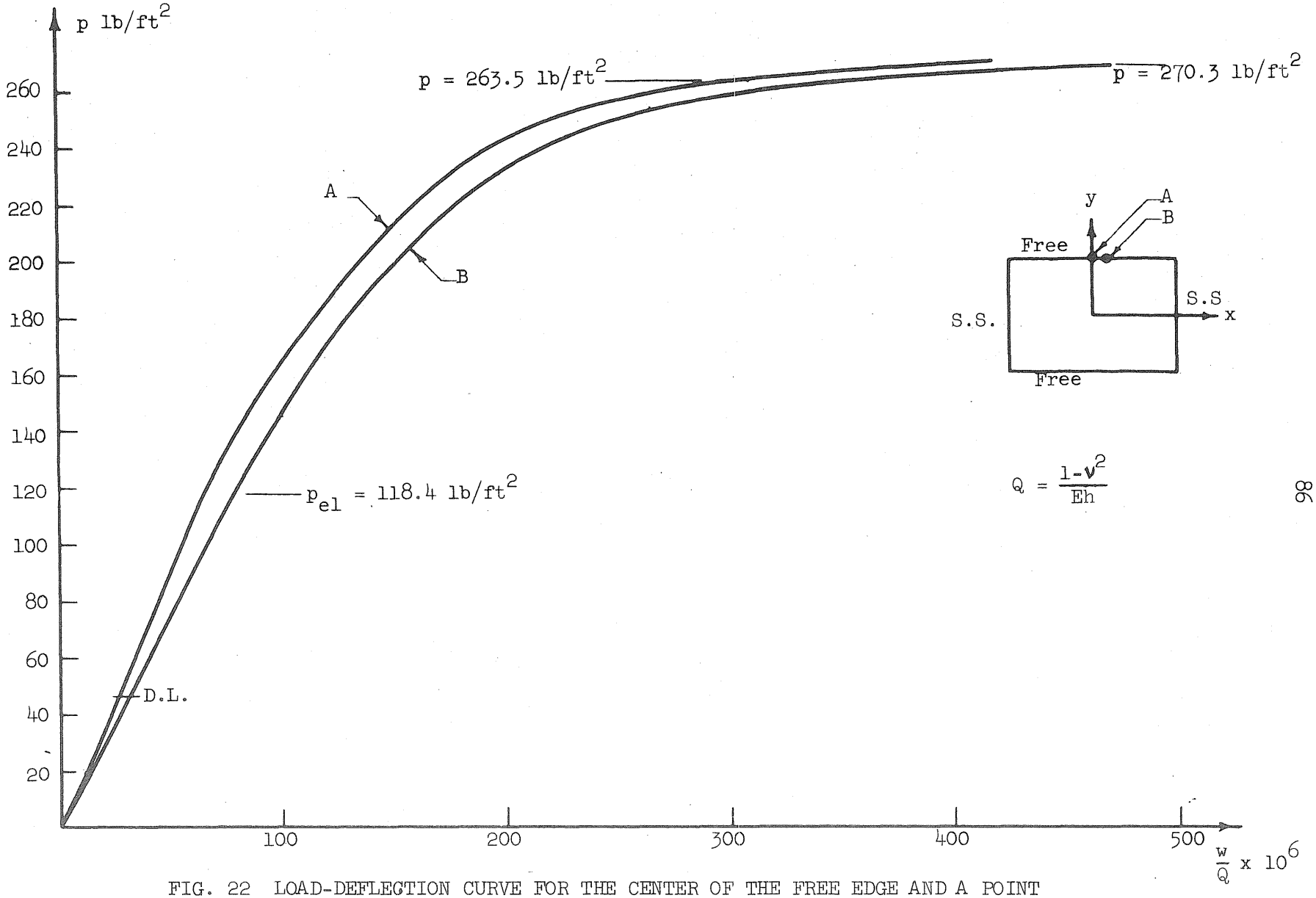

FIG. 22 LOAD-DEFLECTION CURVE FOR THE CENTER OF THE FREE EDGE AND A POINT HALF A SPACE FROM IT

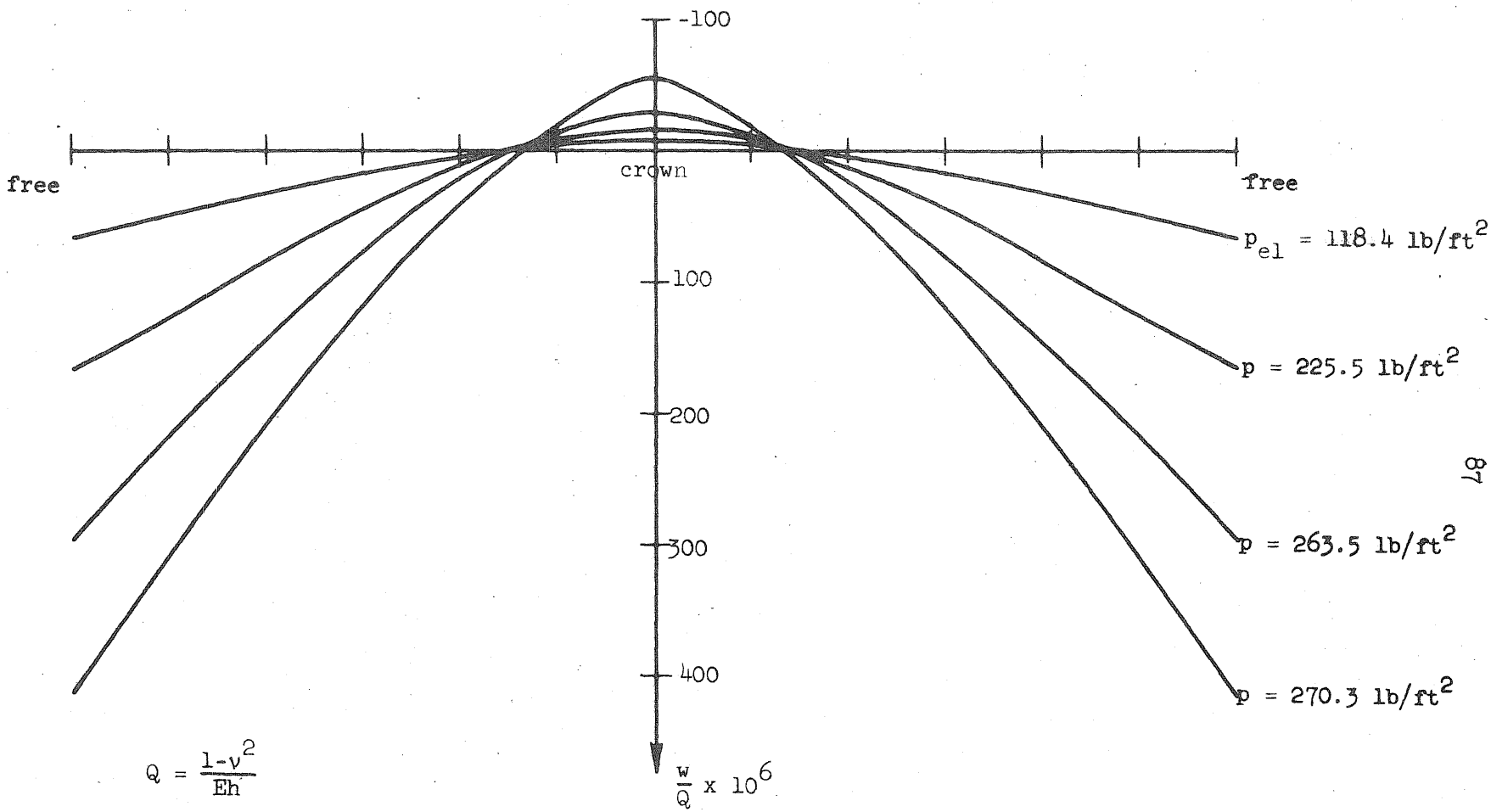

FIG. 23 THE DISPLACEMENT w AT THE MIDSPAN SECTION OF THE CYLINDRICAL SHELL WITH THE FREE LONGITUDINAL EDGES

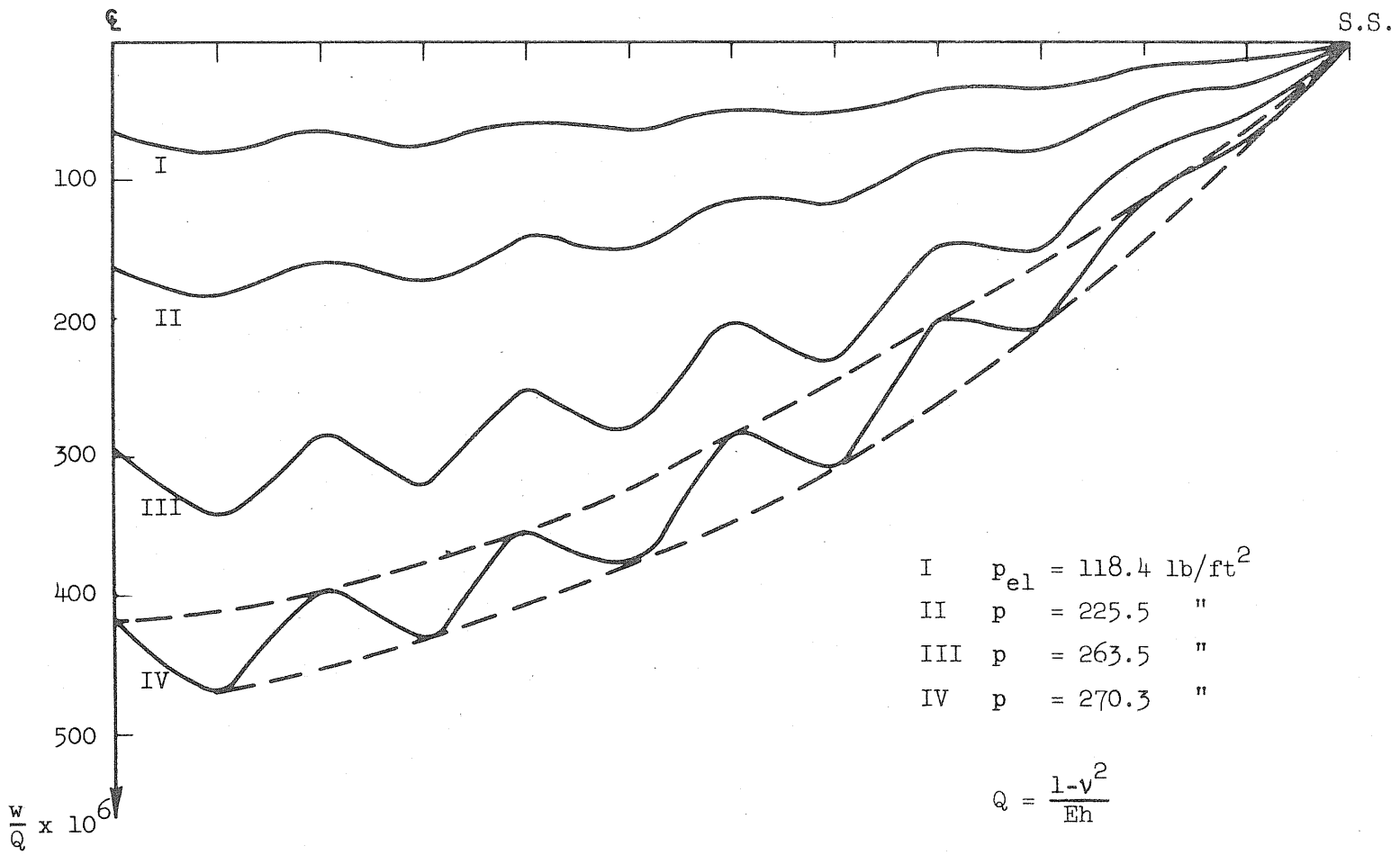

FIG. 24 THE DISPLACEMENT w ALONG THE FREE EDGE

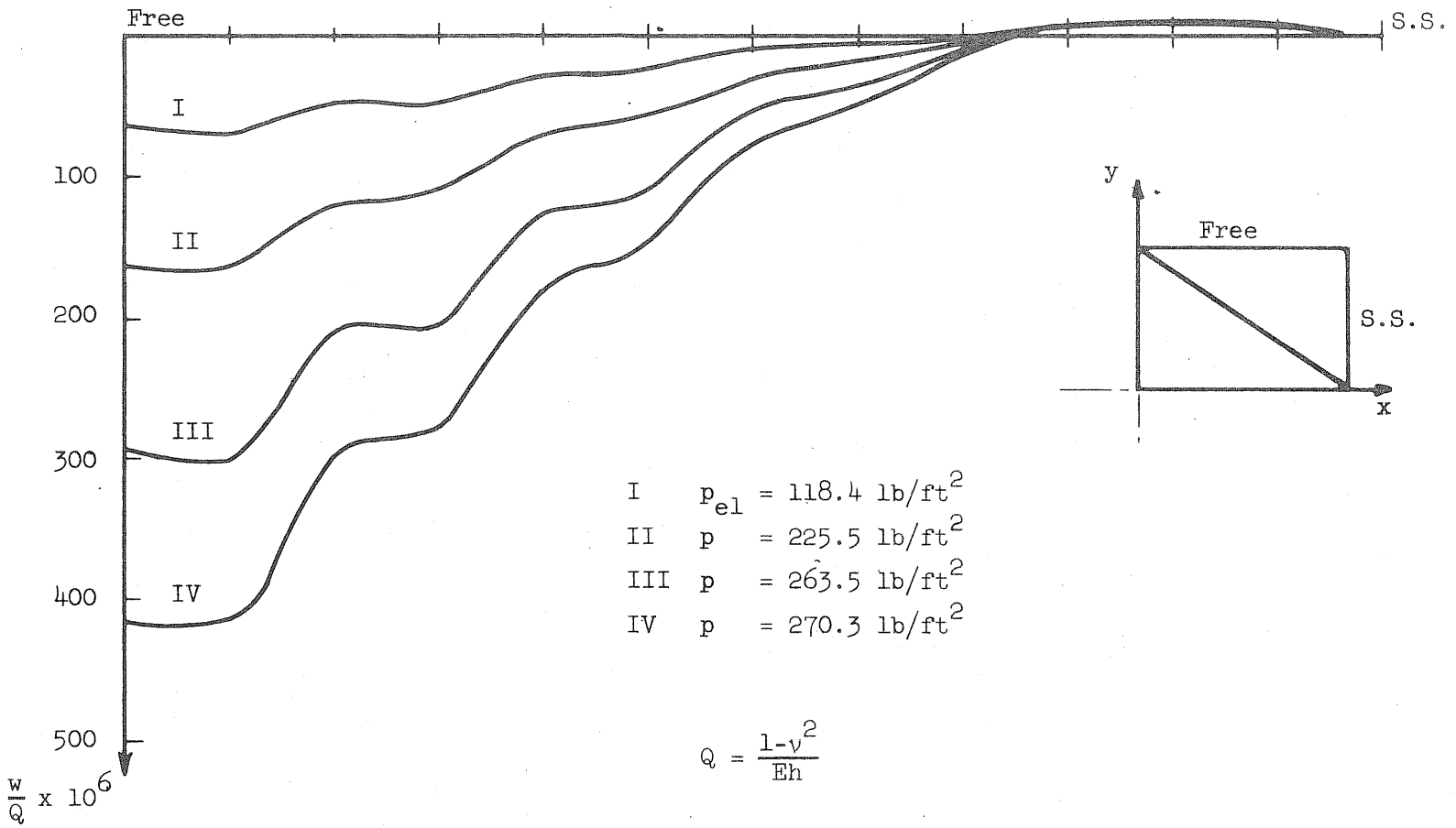

FIG. 25 THE DISPLACEMENT w ALONG A LINE EXTENDING FROM THE FREE EDGE TO THE SIMPLY SUPPORTED EDGE

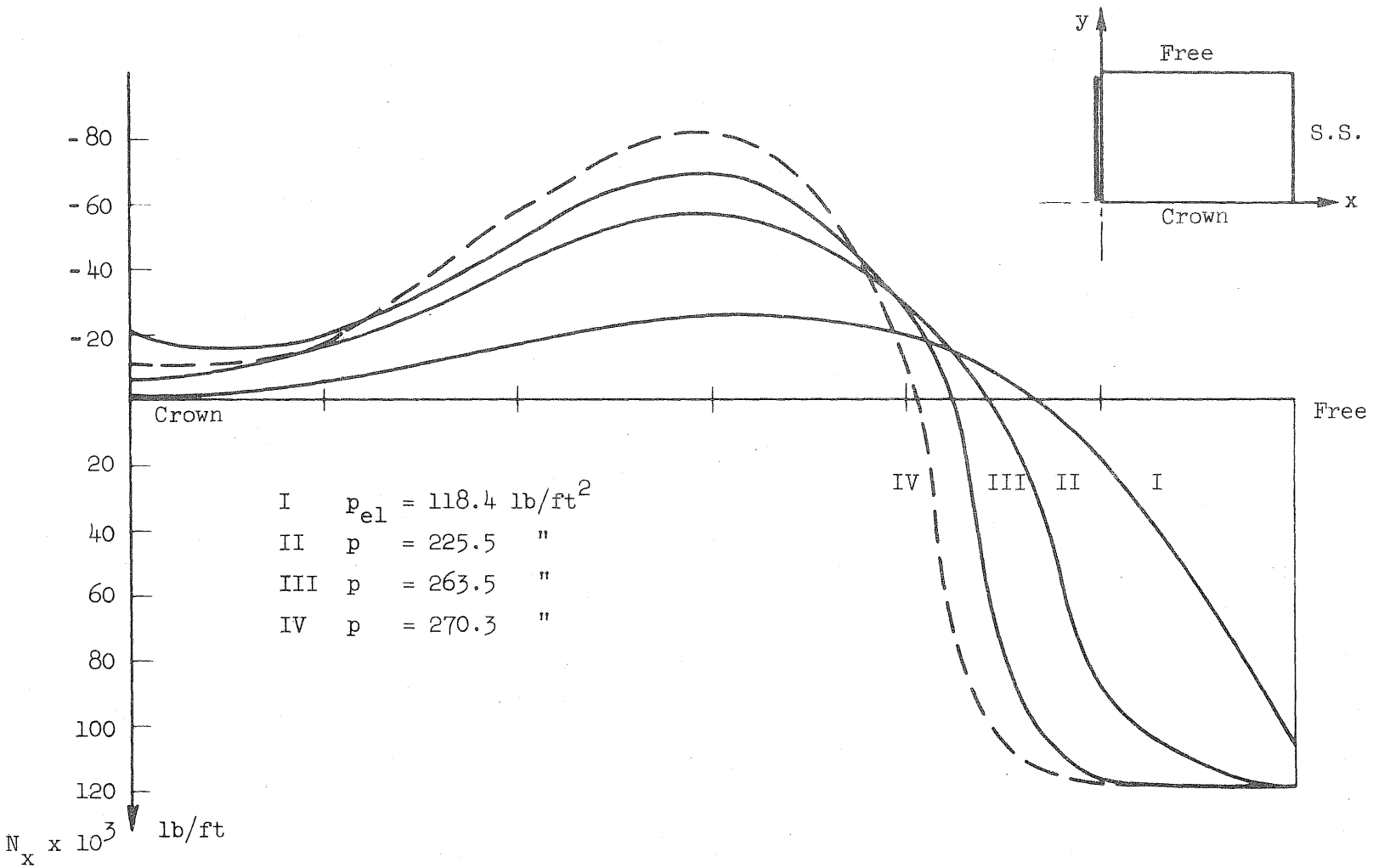

FIG. 26 VARIATION OF THE N_x FORCE AT MIDSPAN SECTION IN THE CYLINDRICAL SHELL WITH FREE LONGITUDINAL EDGES

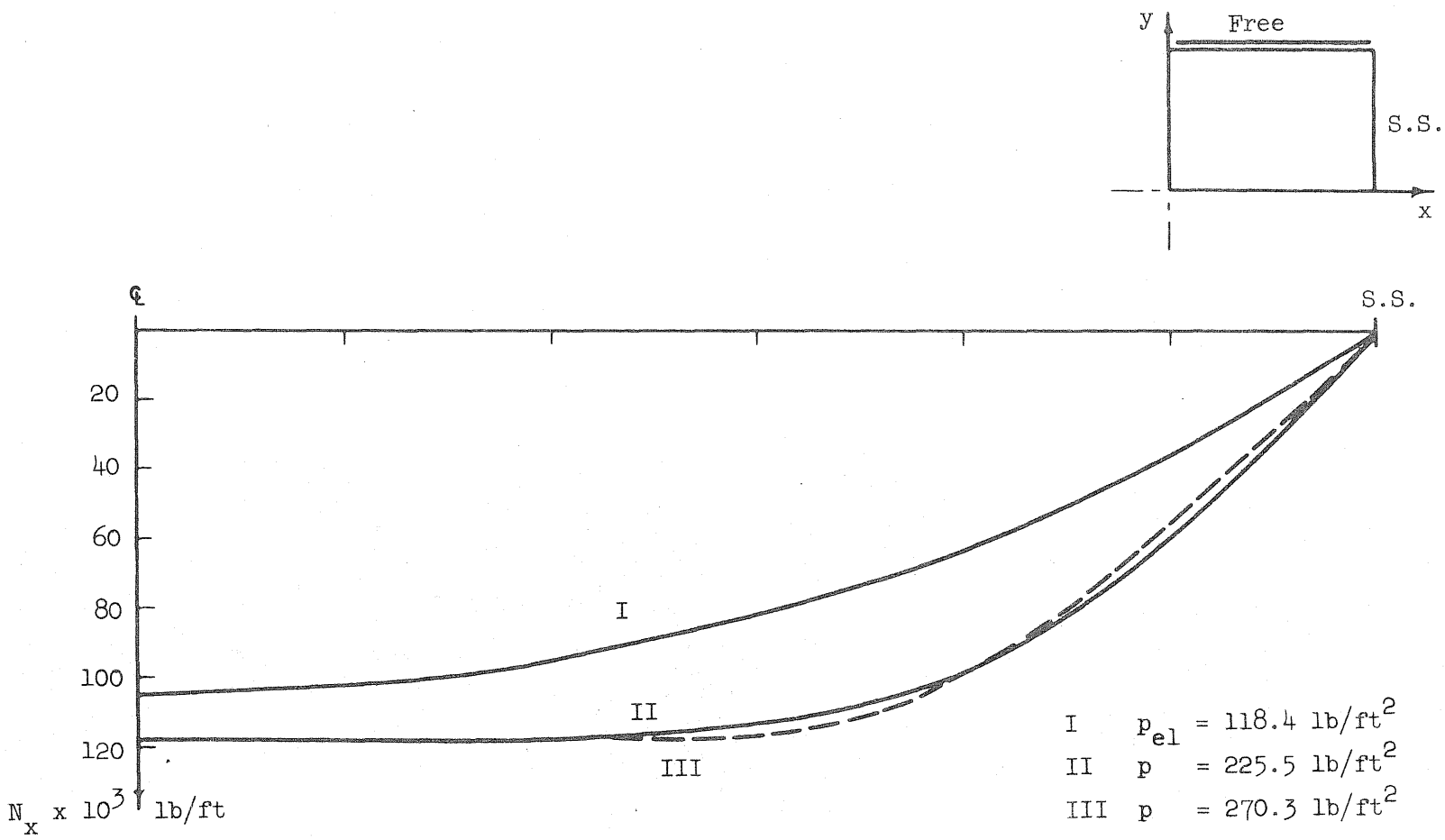

FIG. 27 VARIATION OF THE N_x FORCE ALONG THE FREE EDGE

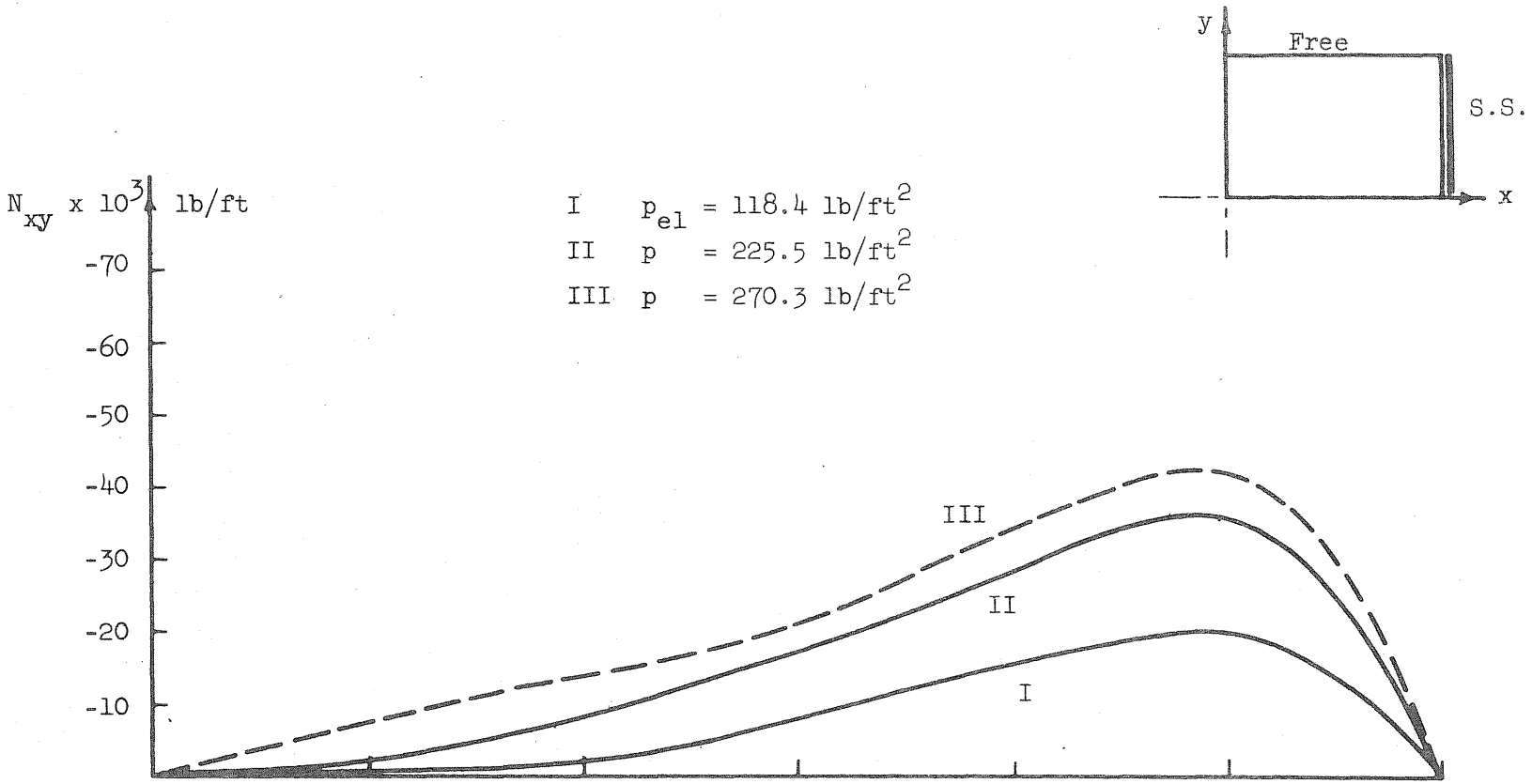

FIG. 28 VARIATION OF THE N_{xy} FORCE ALONG THE SIMPLY SUPPORTED EDGE

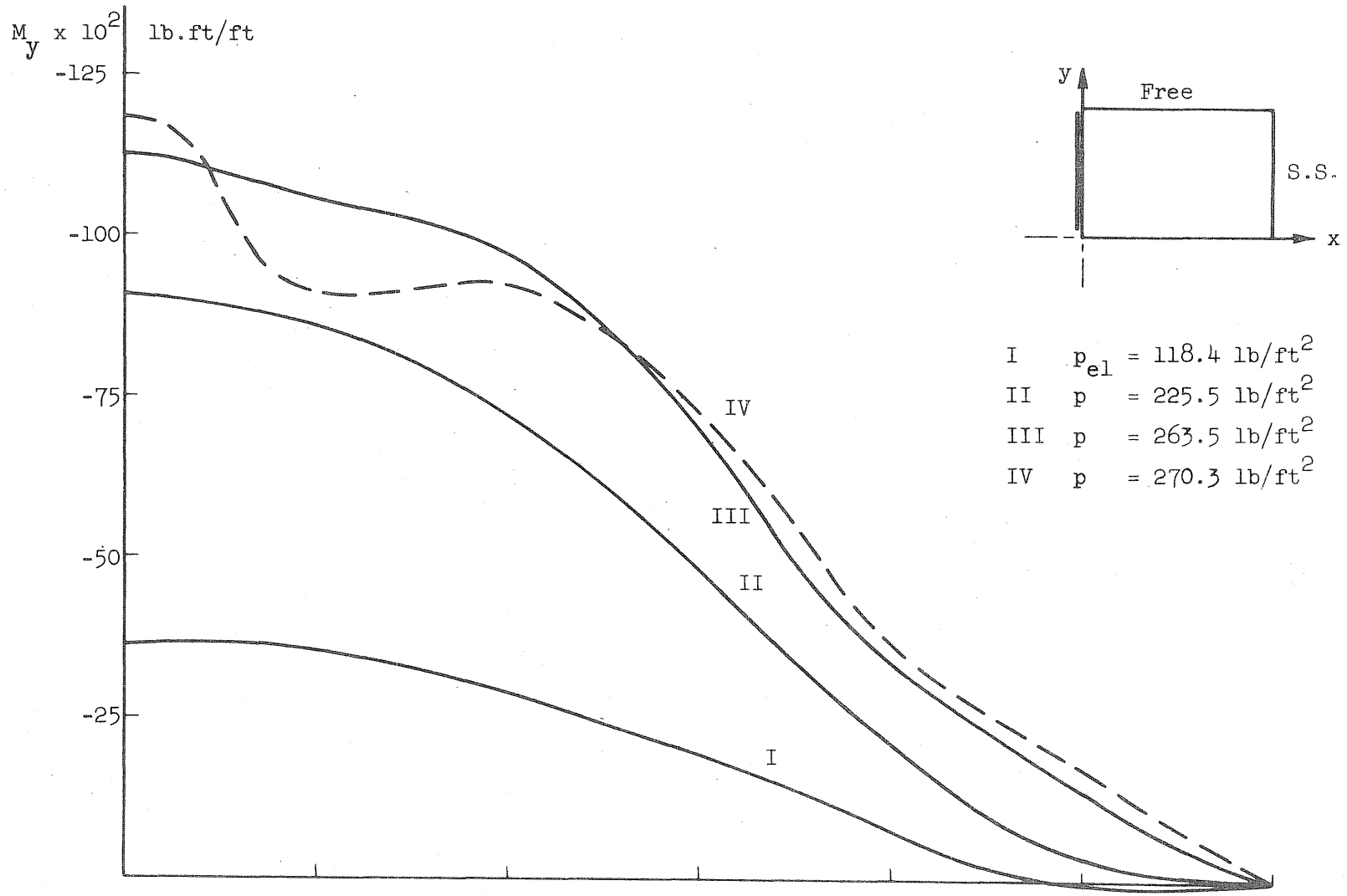

FIG. 29 VARIATION OF M_y AT MIDSPAN SECTION IN THE CYLINDRICAL SHELL WITH FREE LONGITUDINAL EDGES

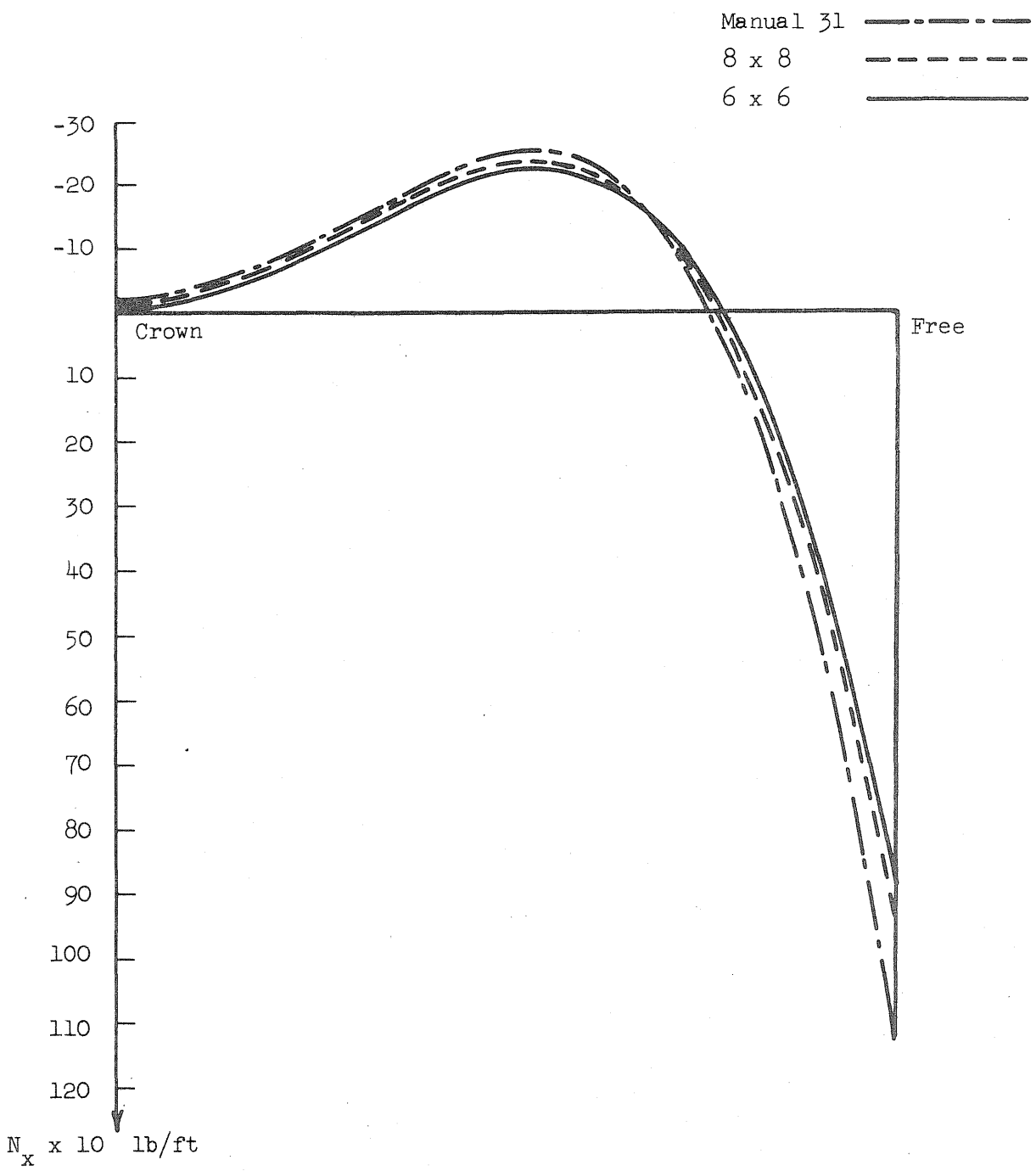

FIG. 30 COMPARISON OF THE N_x FORCE DISTRIBUTION AT MID SECTION AS DETERMINED BY THE MODEL AND BY MANUAL 31

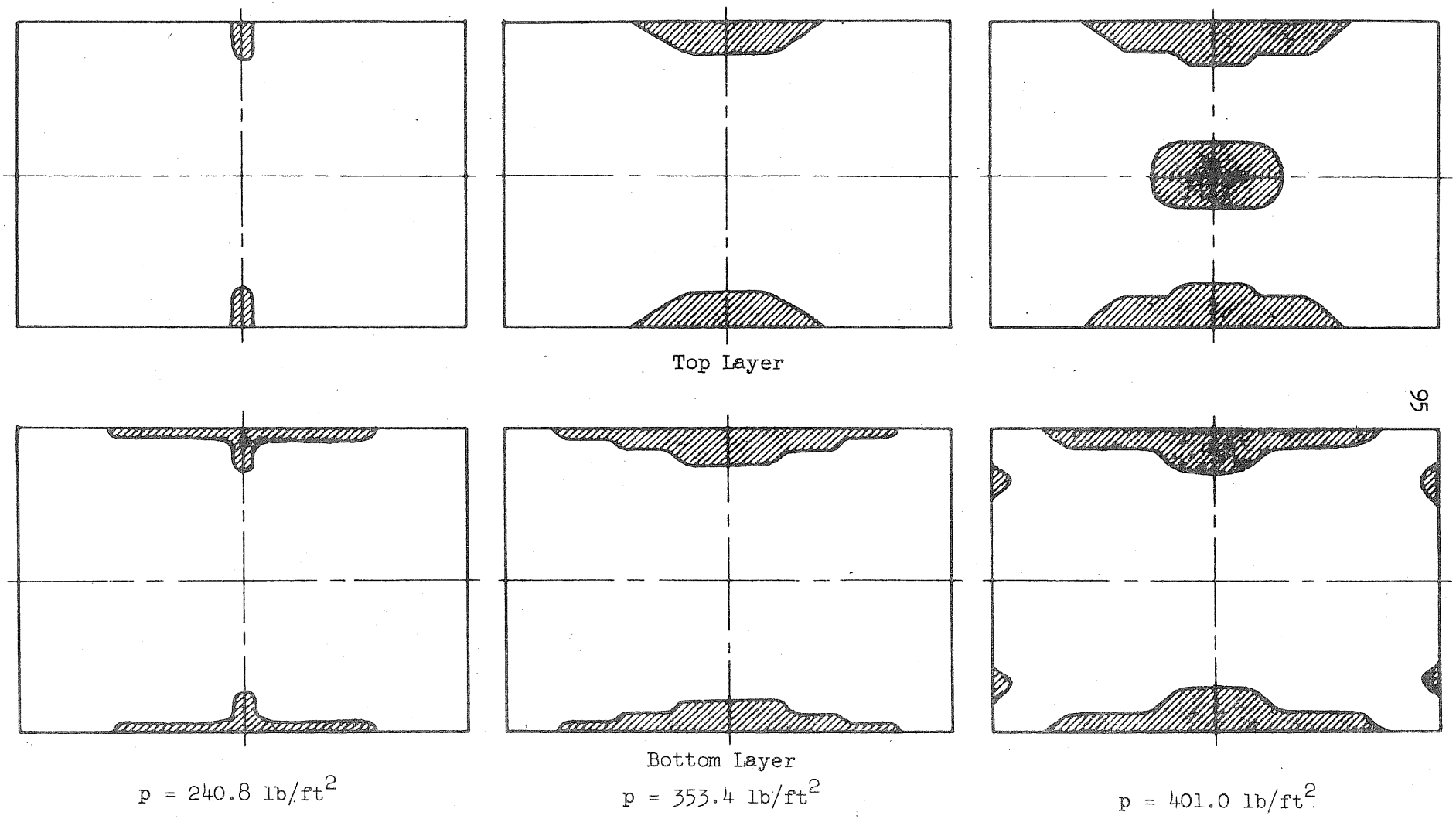

FIG. 31 PROGRESSION OF YIELDING FOR A CYLINDRICAL SHELL CONTINUOUS IN THE TRANSVERSE DIRECTION

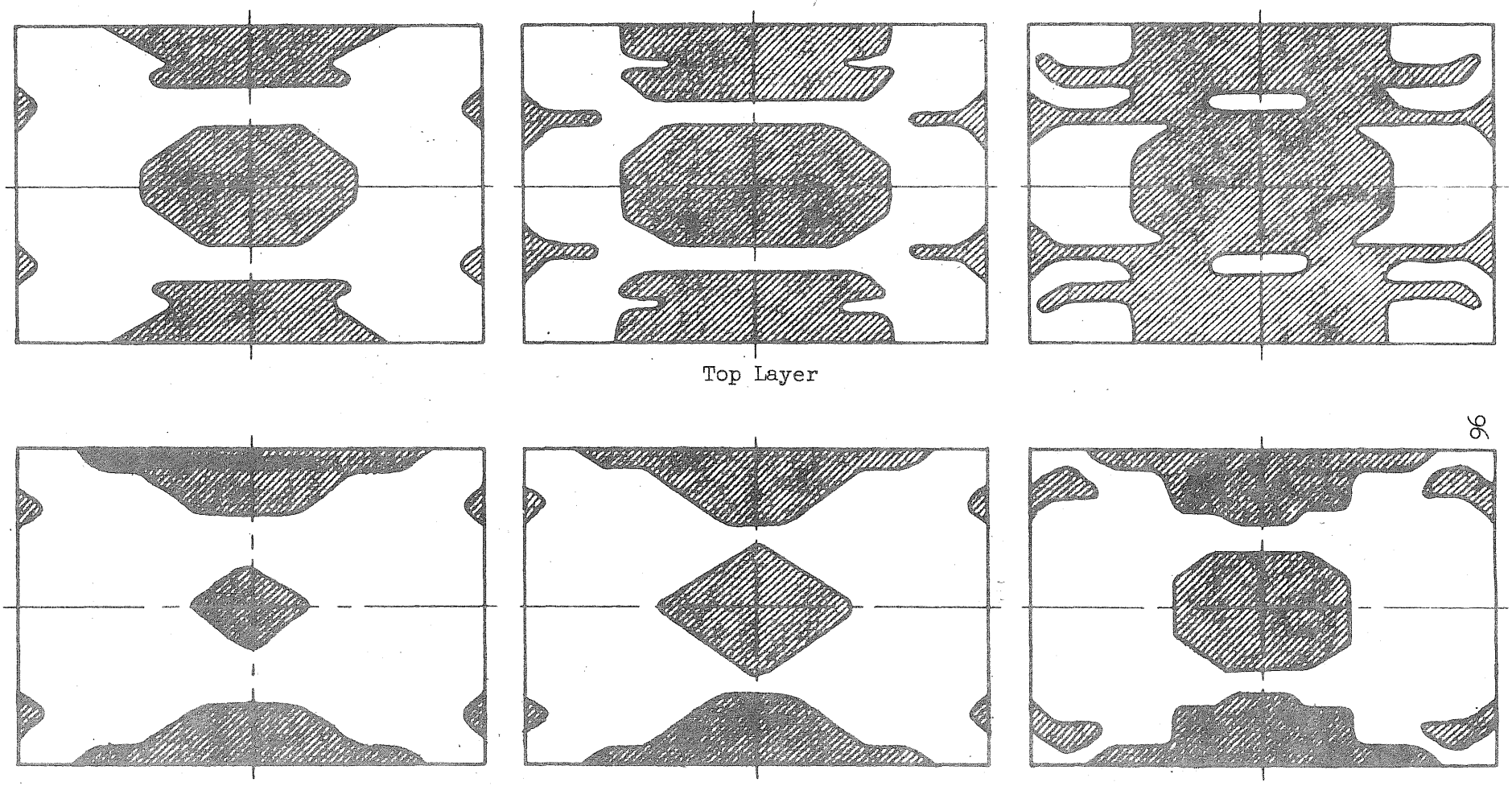

FIG. 31 (cont'd) PROGRESSION OF YIELDING FOR A CYLINDRICAL SHELL CONTINUOUS IN THE TRANSVERSE DIRECTION

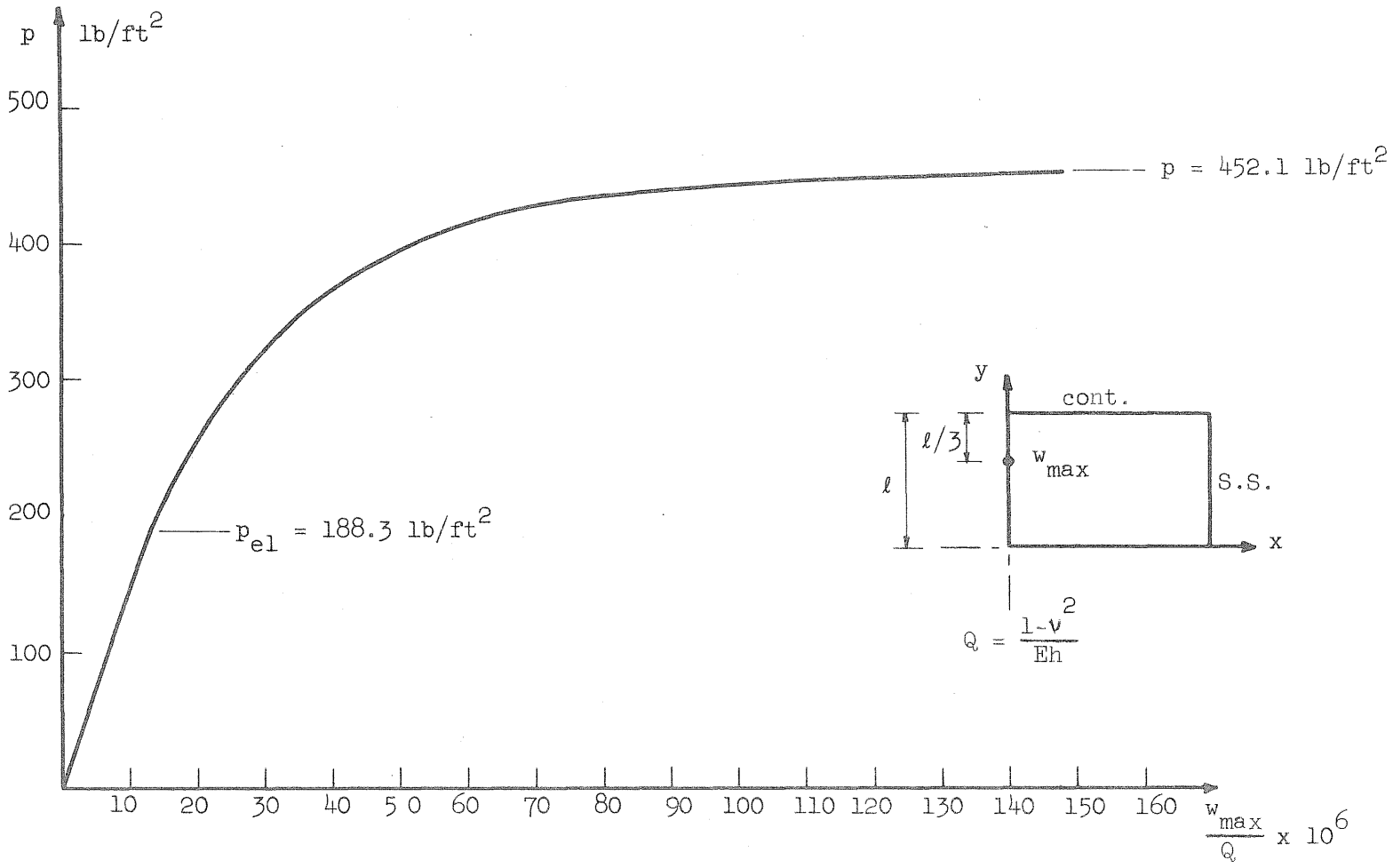

FIG. 32 LOAD-DEFLECTION CURVE FOR THE NODE WITH THE MAXIMUM DEFLECTION

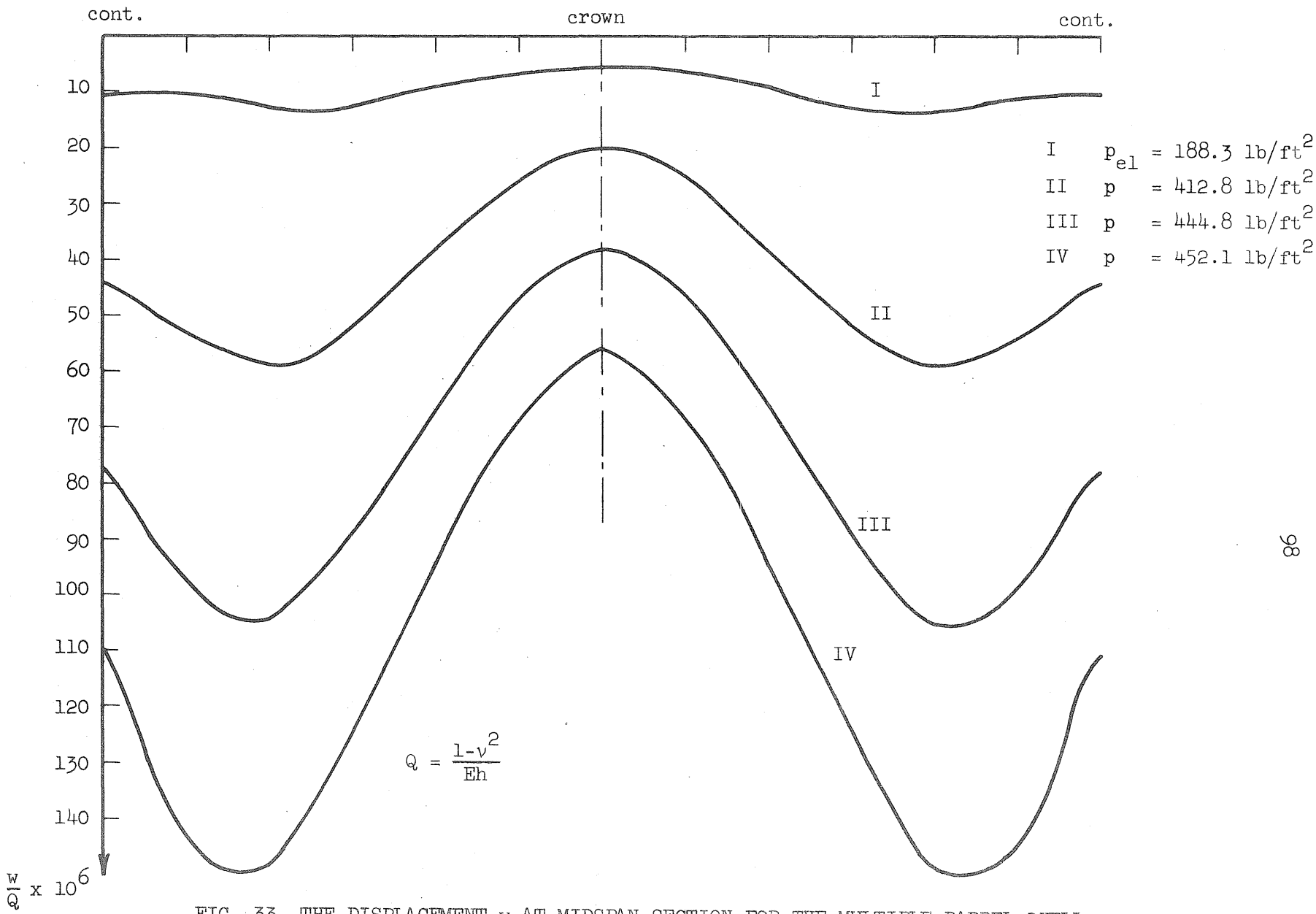

FIG. 33 THE DISPLACEMENT w AT MIDSPAN SECTION FOR THE MULTIPLE BARREL SHELL

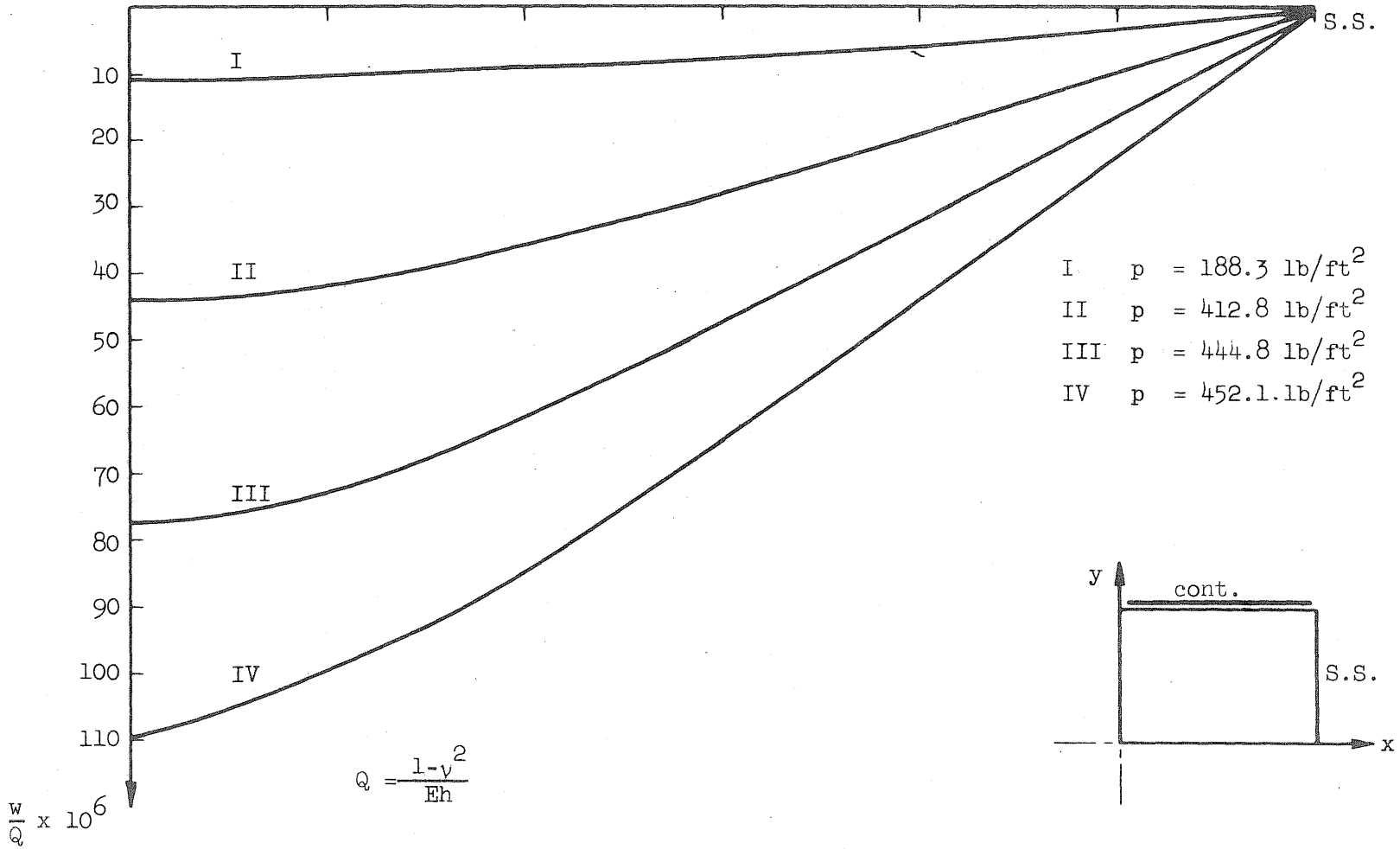

FIG. 34 THE DISPLACEMENT w ALONG THE VALLEY

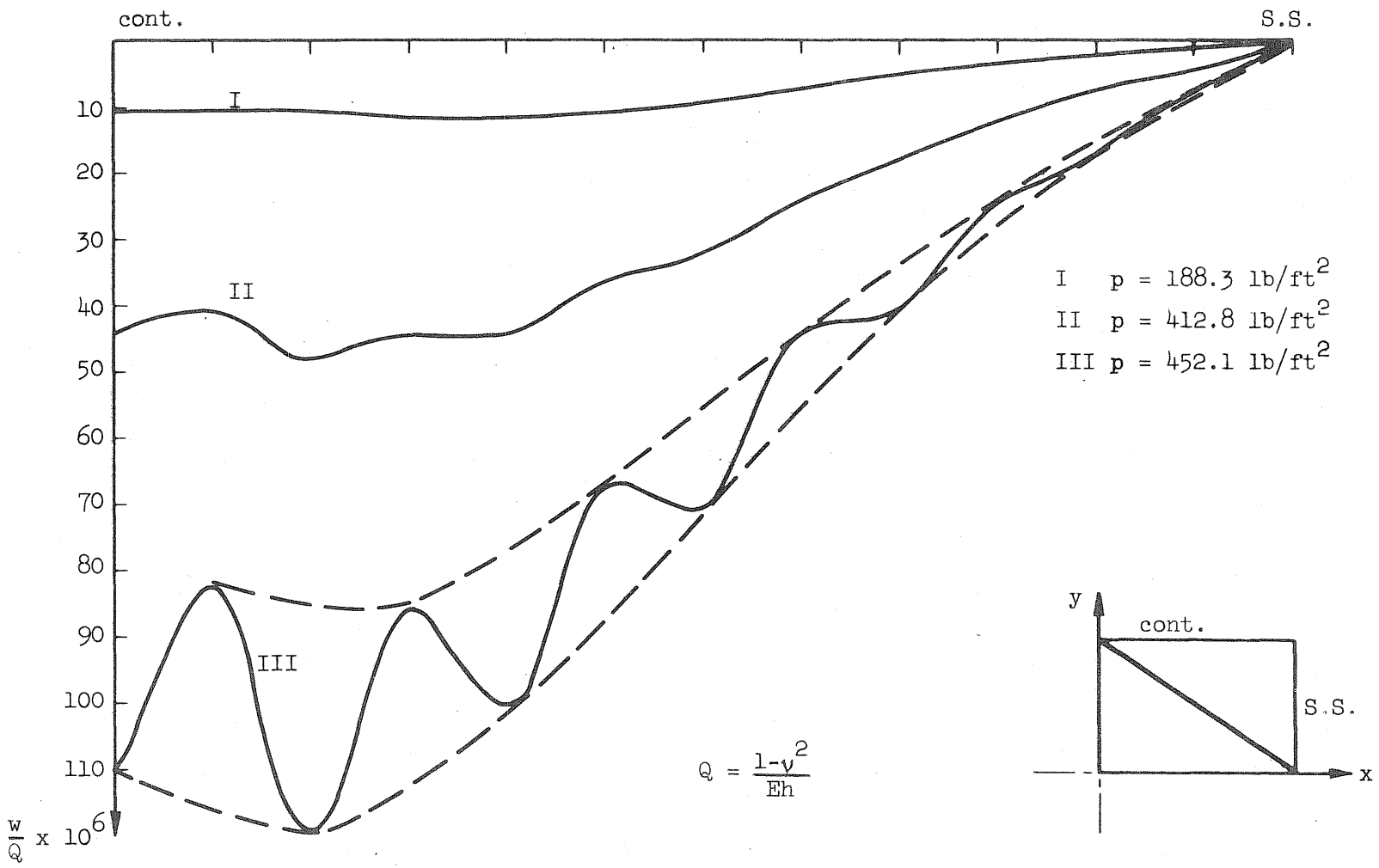

FIG. 35 THE DISPLACEMENT w ALONG A LINE EXTENDING FROM THE CONTINUOUS EDGE TO THE SIMPLY SUPPORTED EDGE

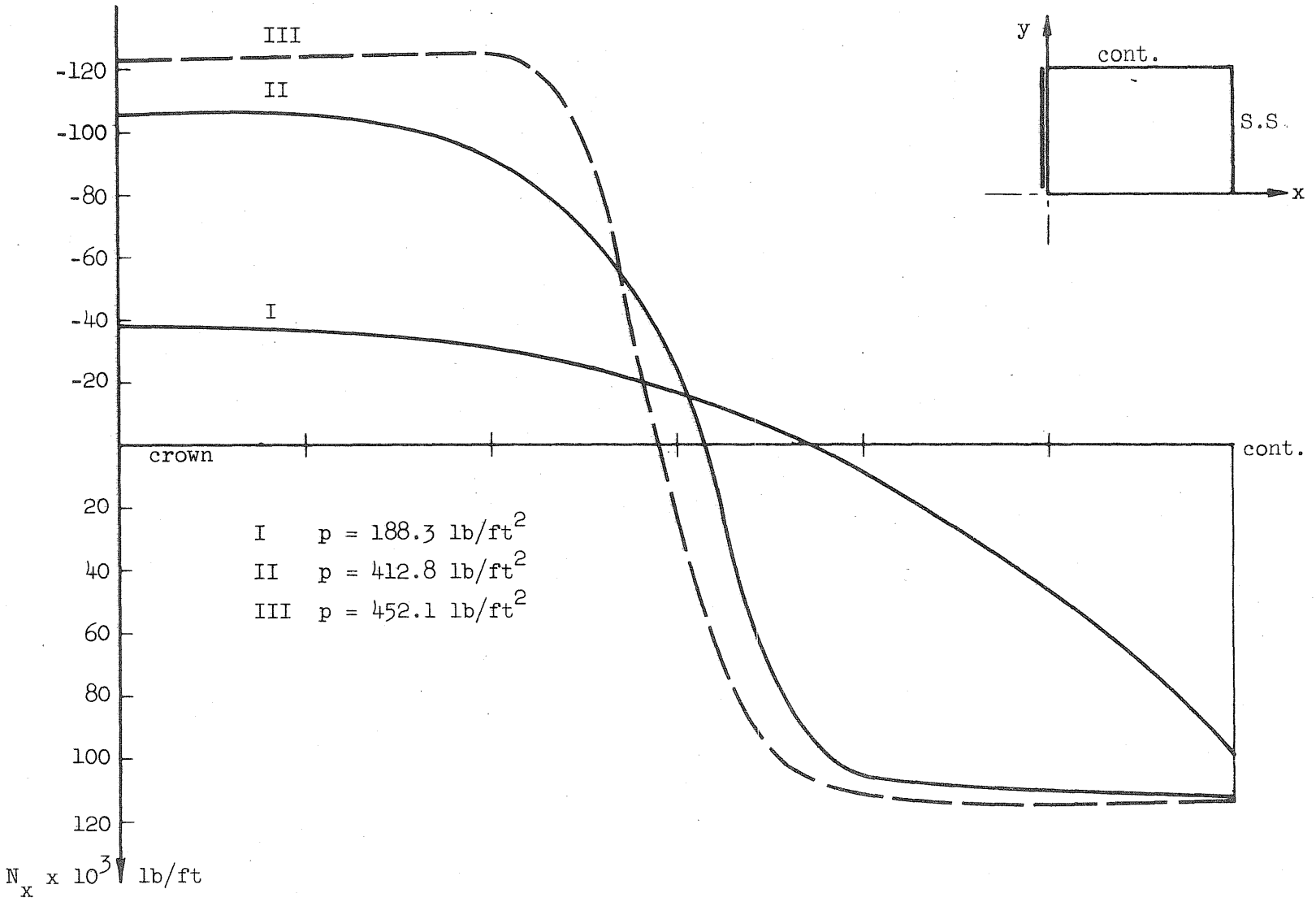

FIG. 36 VARIATION OF THE N_x FORCE AT MIDSPAN SECTION IN THE MULTIPLE BARREL SHELL

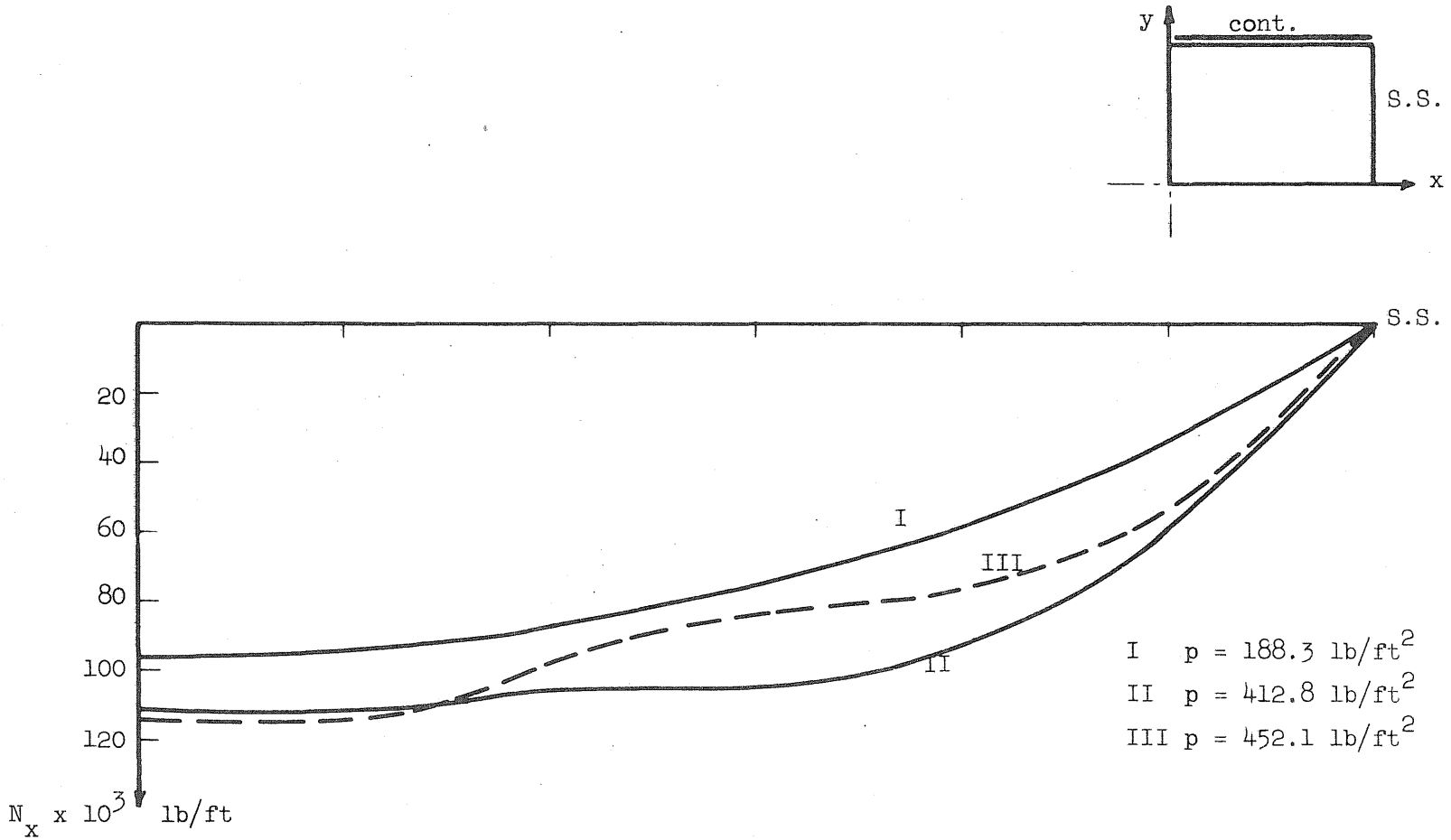

FIG. 37 VARIATION OF THE N_x FORCE ALONG THE VALLEY OF THE MULTIPLE BARREL SHELL

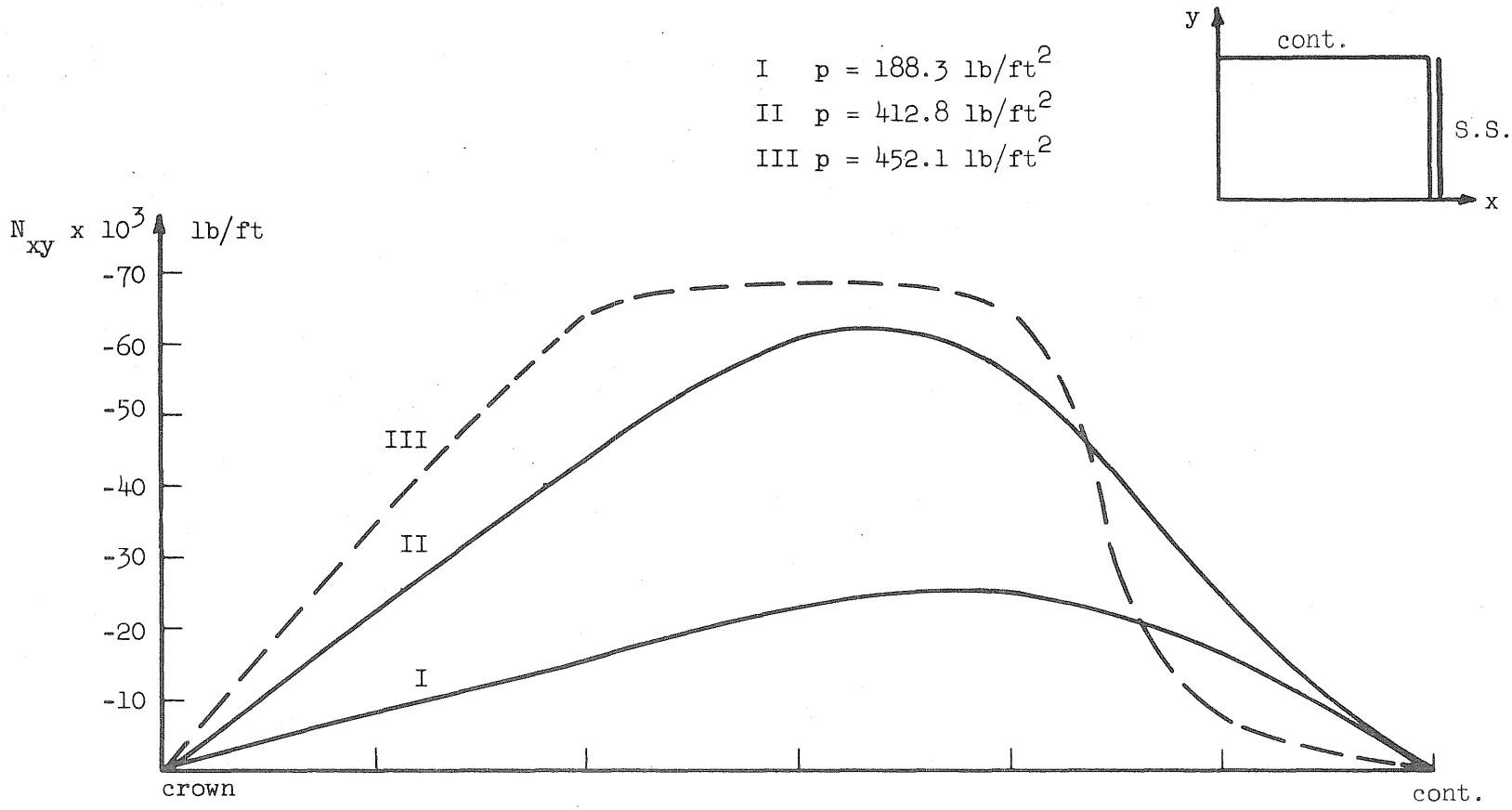

FIG. 38 VARIATION OF THE N_{xy} FORCE ALONG THE SIMPLY SUPPORTED EDGE OF THE MULTIPLE BARREL SHELL

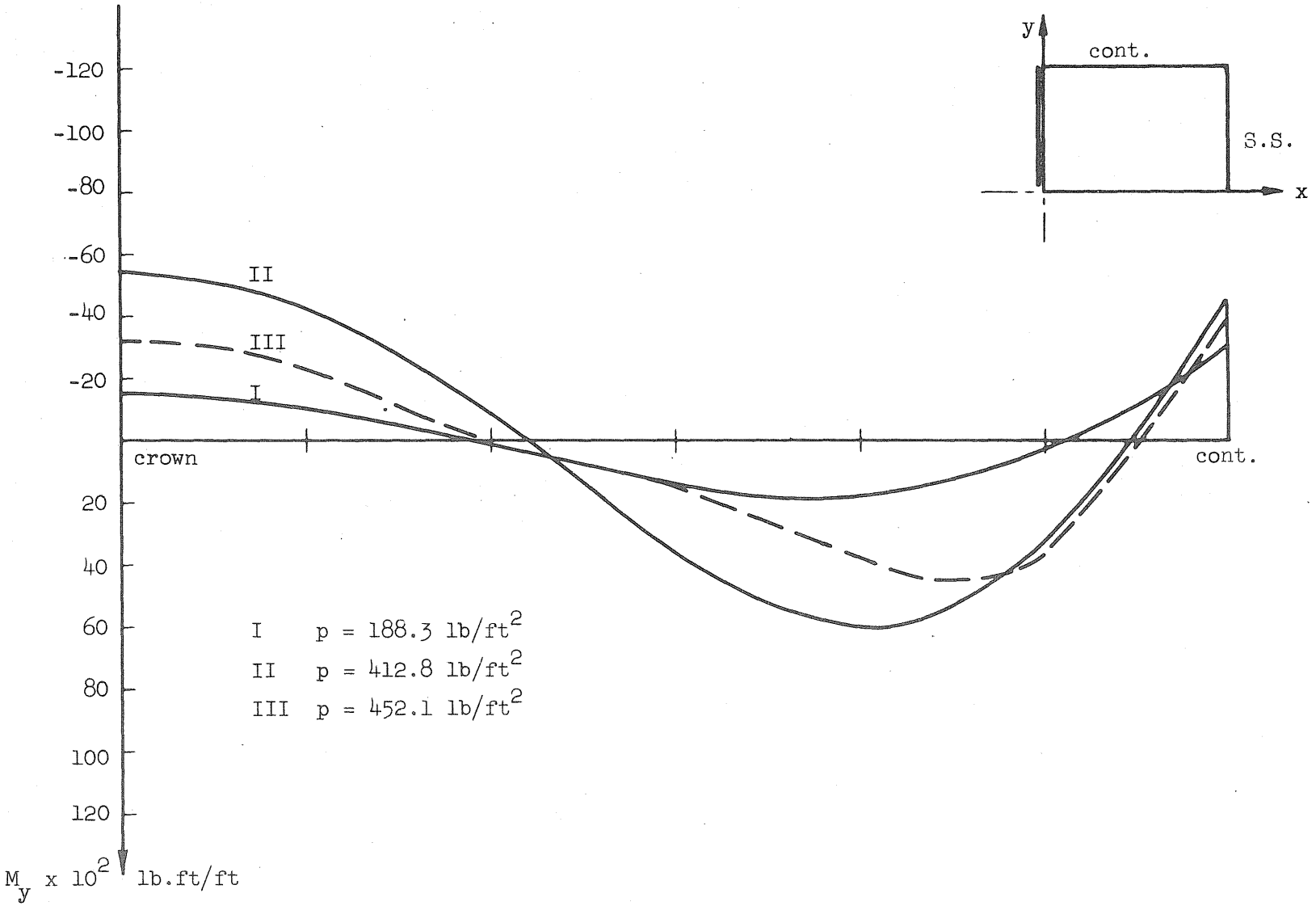

FIG. 39 VARIATION OF M_y AT MIDSPAN SECTION IN THE MULTIPLE BARREL SHELL

APPENDIX A

STRESS-DISPLACEMENT OPERATORS

The stresses in the top and bottom layers of a typical interior node are shown here in their operator form in terms of the displacements in Figs. A-1 through A-6:

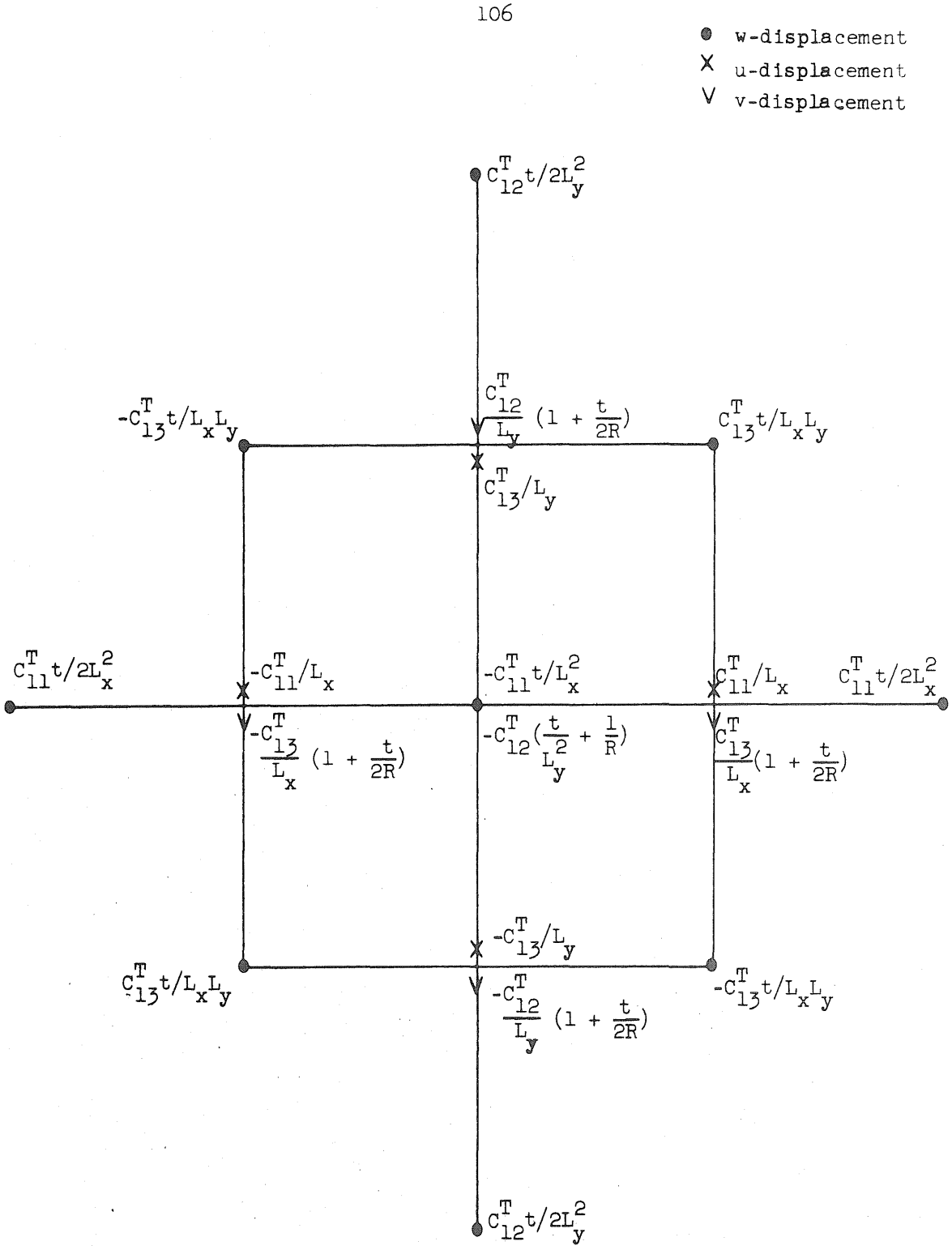

FIG. A-1 OPERATOR FOR σ_x^T

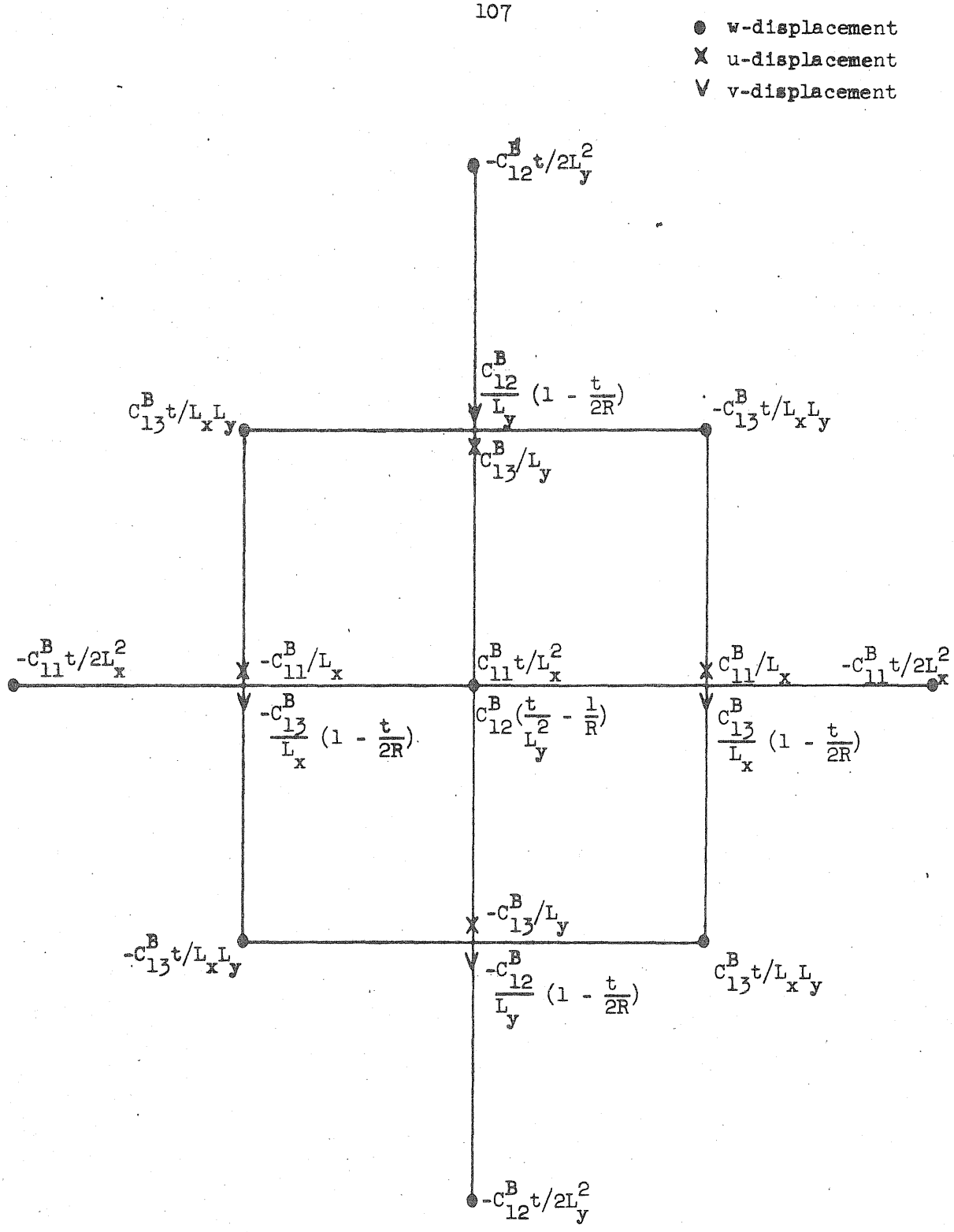

FIG. A-2 OPERATOR FOR σ_x^B

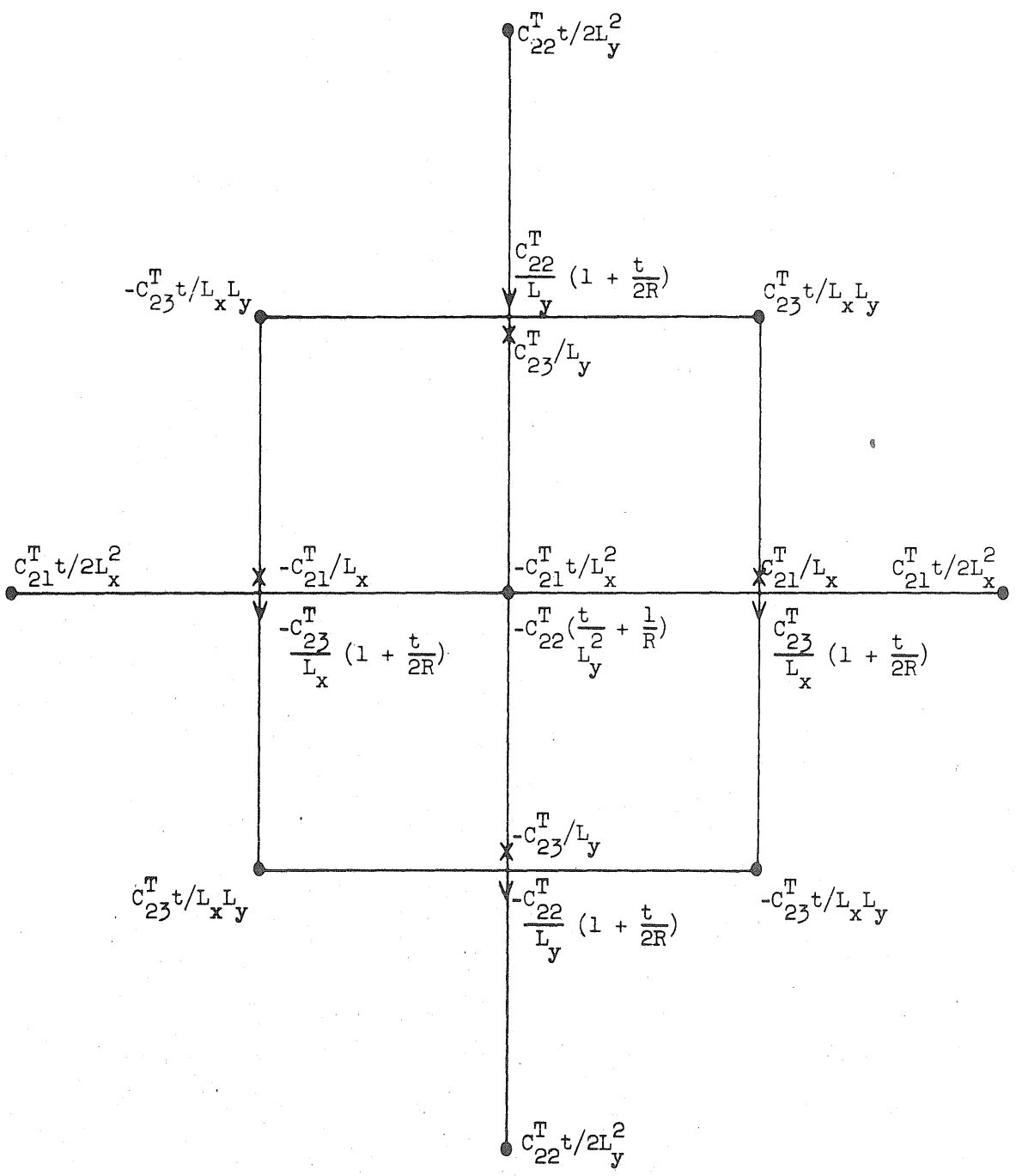

FIG. A-3 OPERATOR FOR σ_y^T

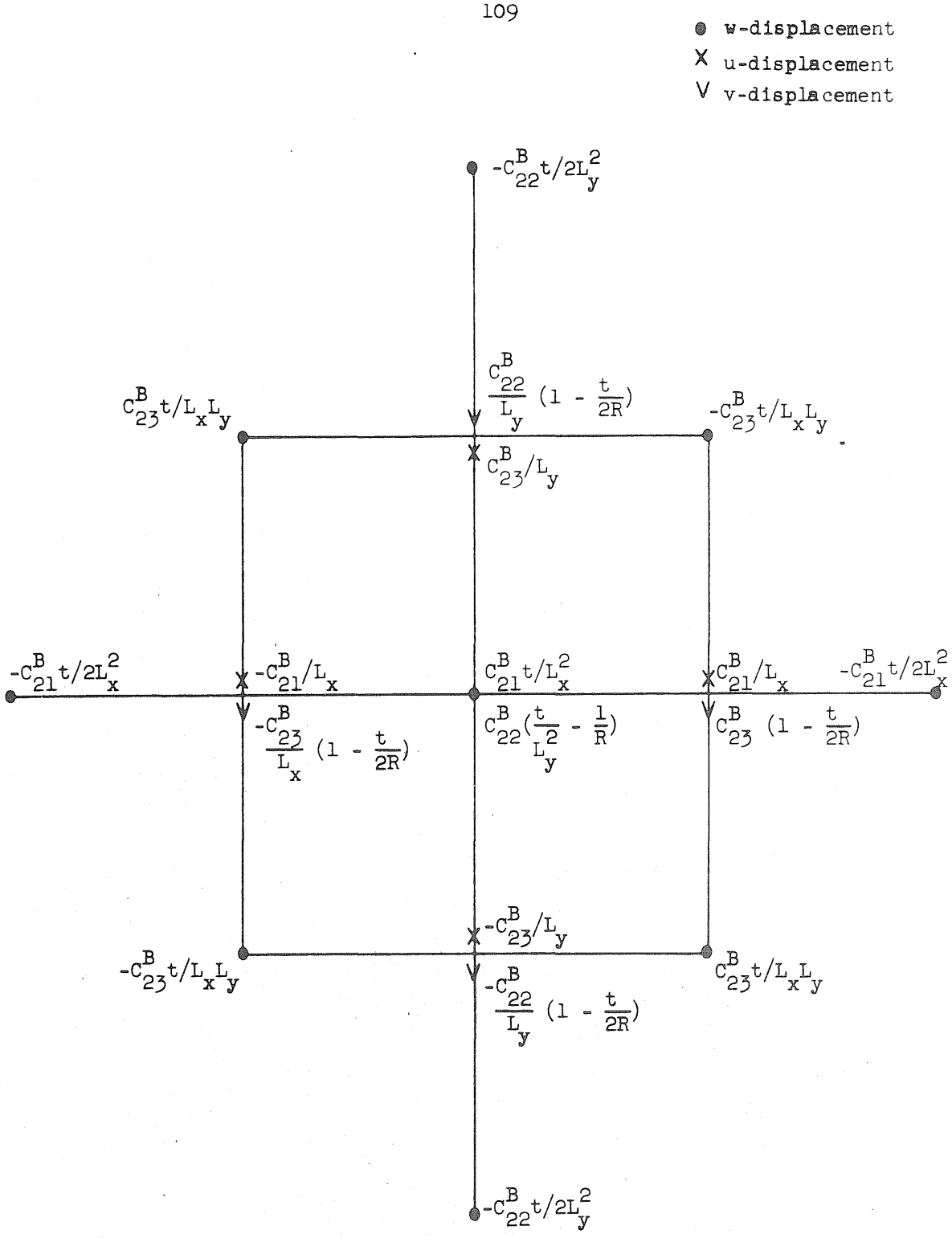

FIG. A-4 OPERATOR FOR σ_y^B

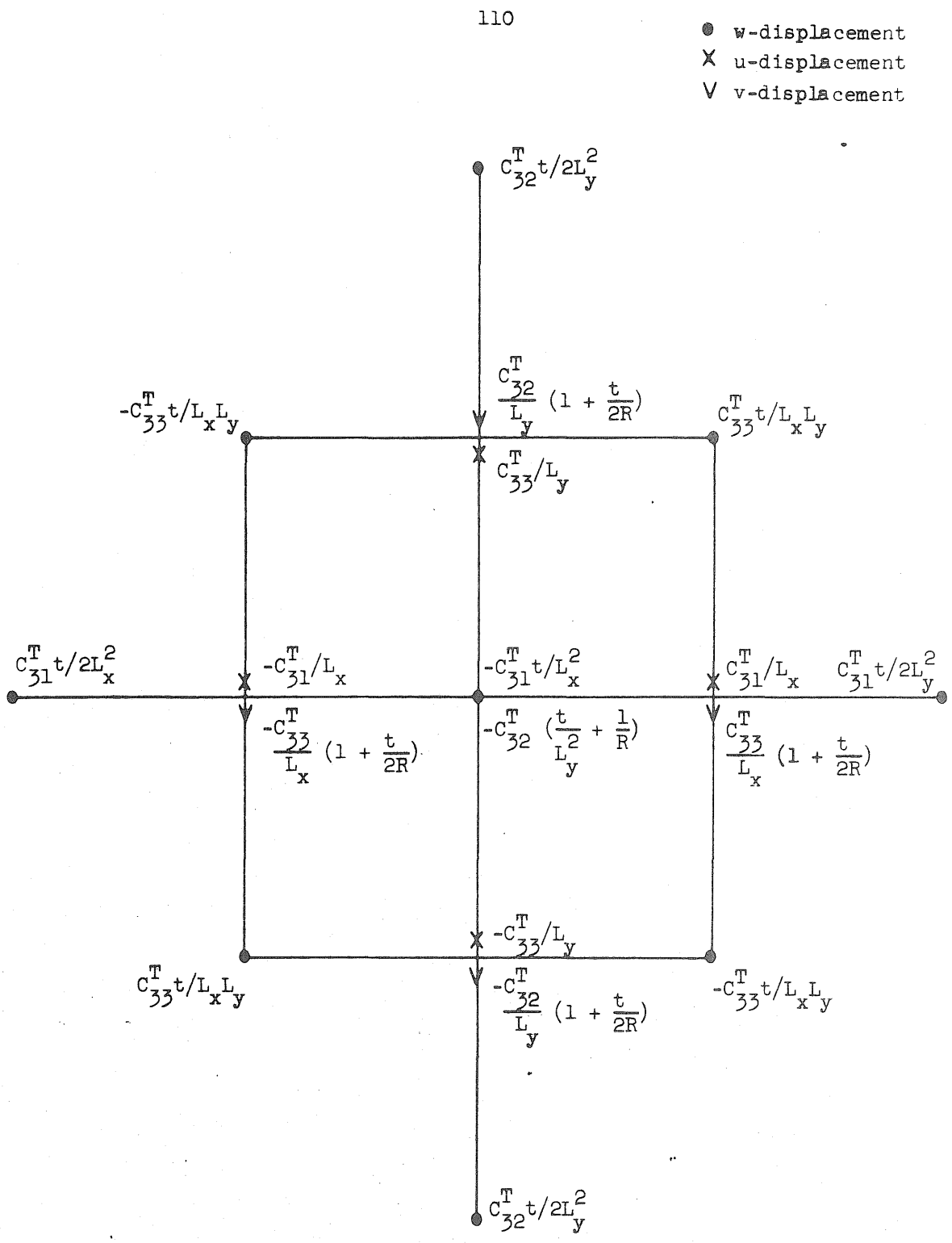

FIG. A-5 OPERATOR FOR τ_{xy}^T

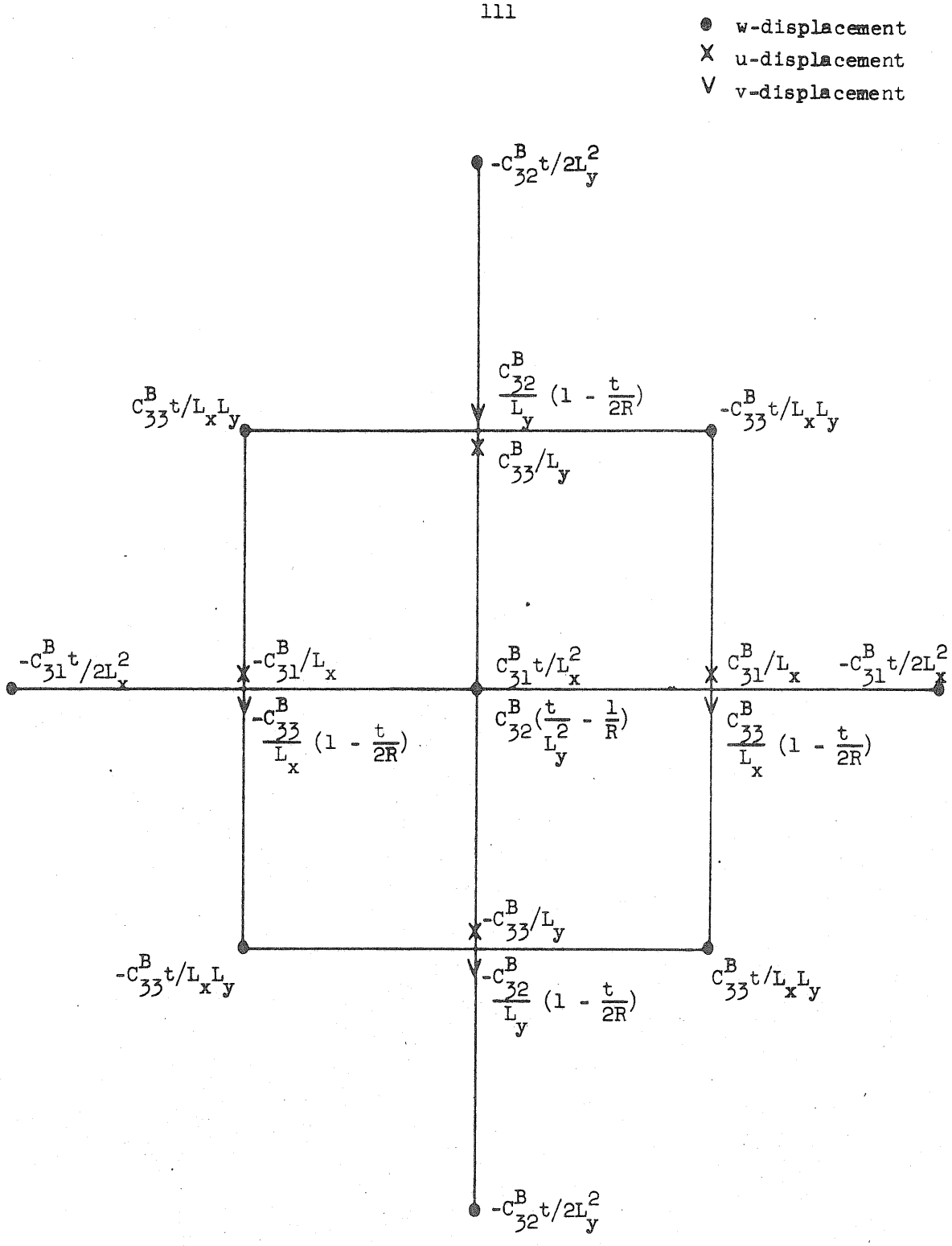

FIG. A-6 OPERATOR FOR τ^B_{xy}

APPENDIX B

FORCE-DISPLACEMENT OPERATORS

The forces and moments similar to the finite difference form developed about the middle surface of a real continuous shell are obtained by combining the stresses in the top and bottom layers of a node according to Eqs. (3.19). The operators for all the three forces and three moments are shown below in terms of the displacements in Figs. B-1 through B-6. In what follows A stands for $(C^T + C^B)$ and B stands for $(C^T - C^B)$.

$$N_x = \frac{L_y h}{4} \left[\quad \right]$$

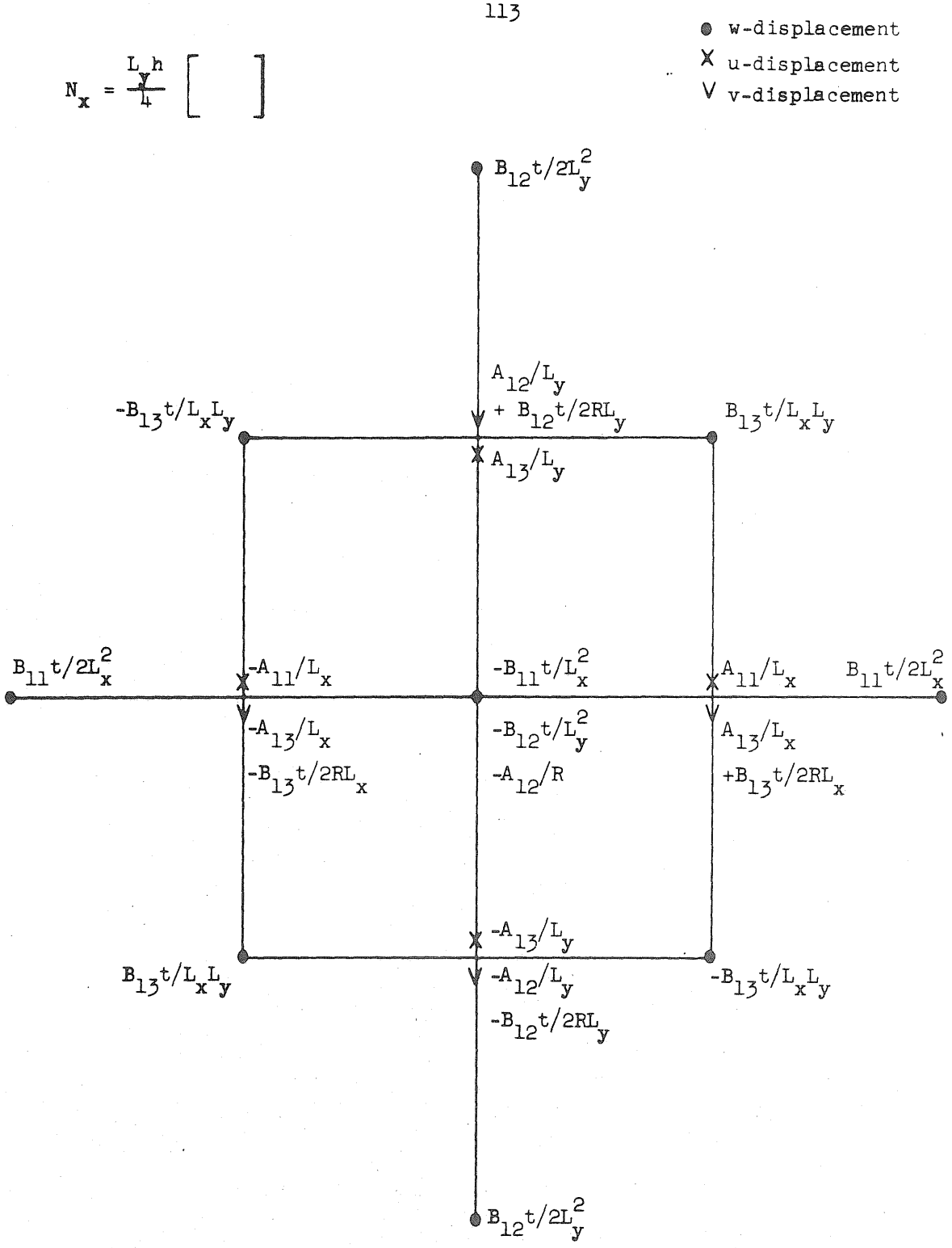

FIG. B-1 OPERATOR TO BE USED WITH N_x

$$N_y = \frac{L_x h}{4} \left[\quad \right]$$

● w-displacement
X u-displacement
V v-displacement

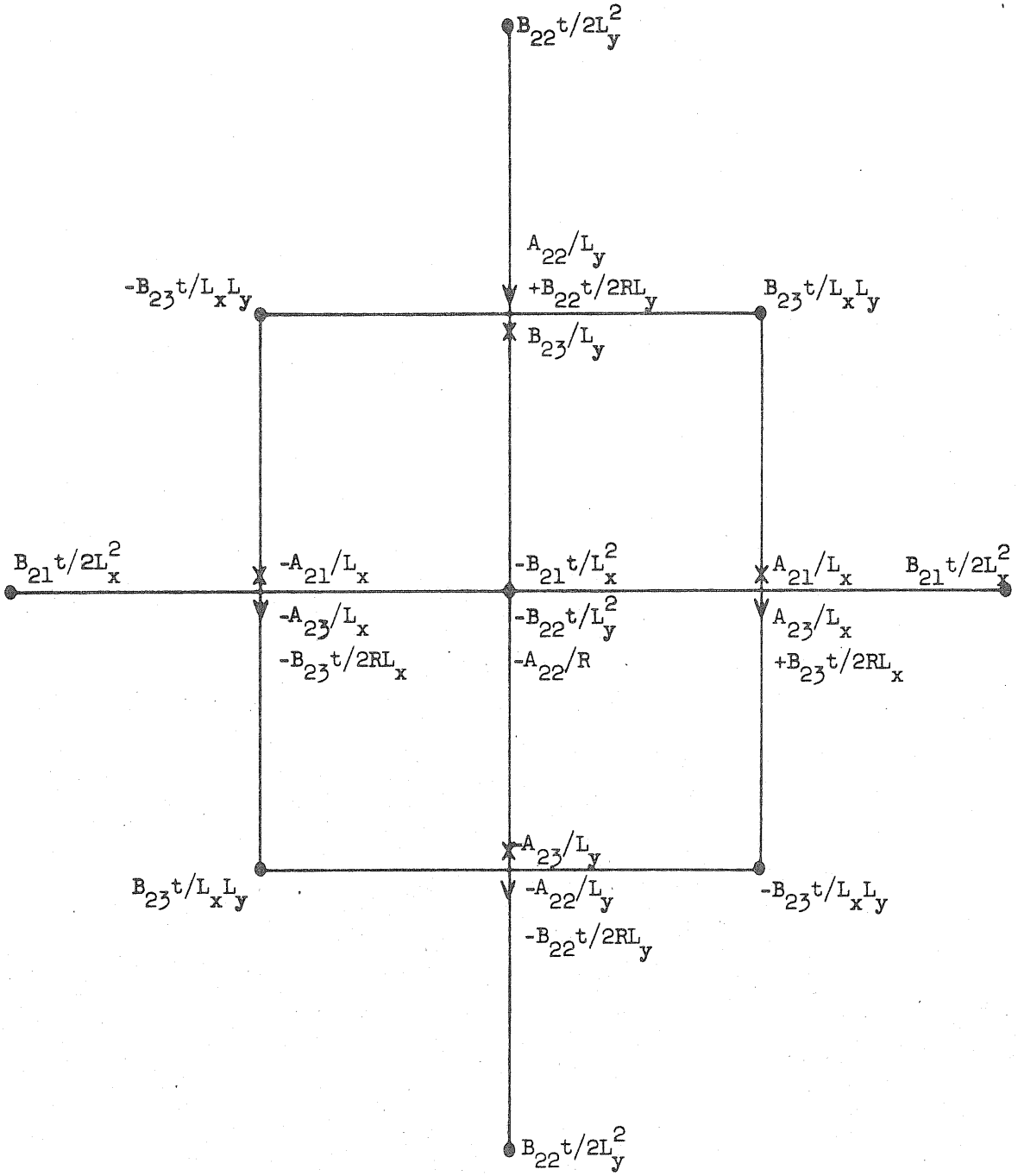

FIG. B-2 OPERATOR TO BE USED WITH N_y

$$N_{xy} = \frac{L_y h}{4} \left[\quad \right]$$

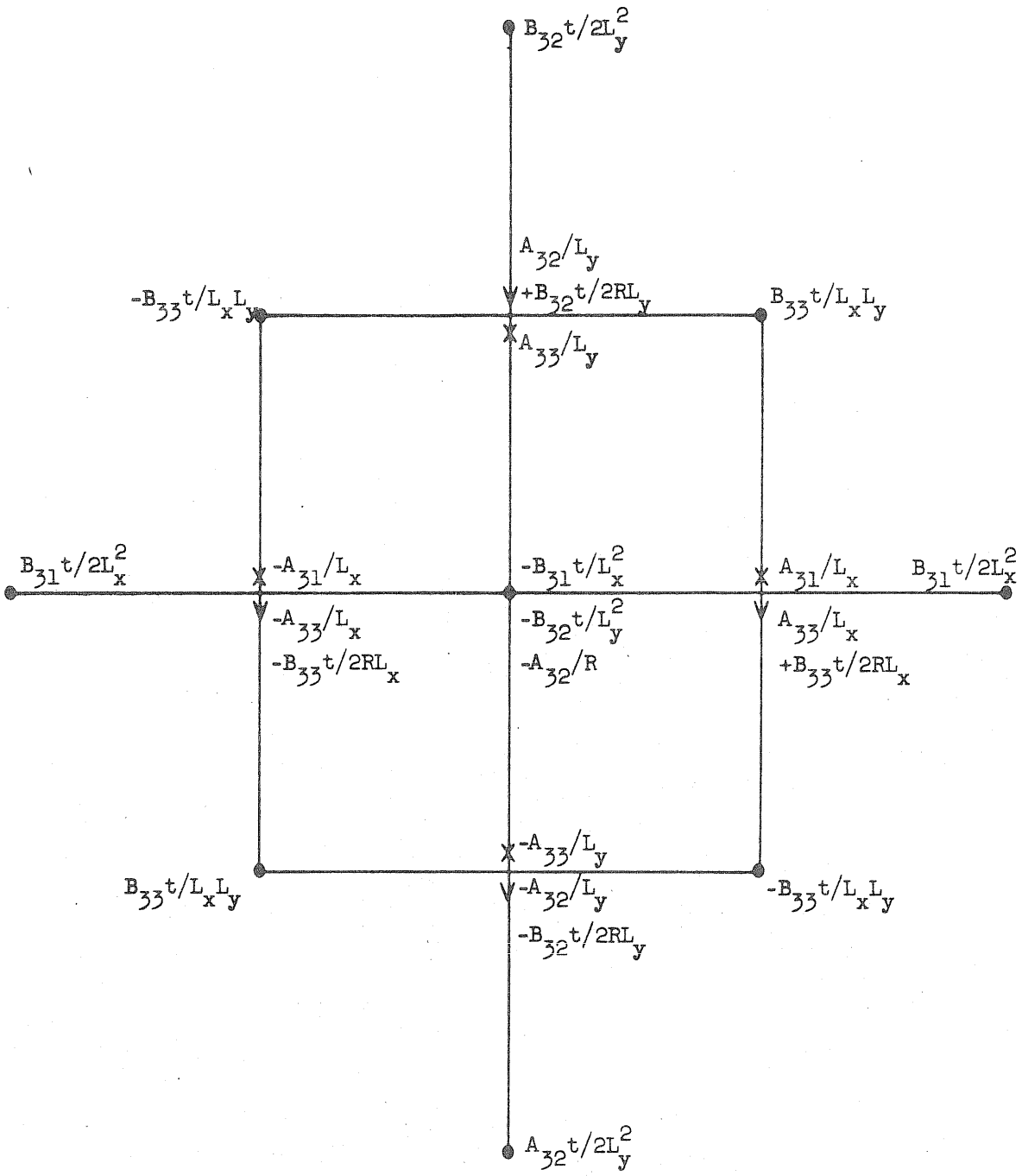

FIG. B-3 OPERATOR TO BE USED WITH N_{xy}

$$M_x = \frac{L_y ht}{8} \left[\quad \right]$$

● w-displacement
X u-displacement
V v-displacement

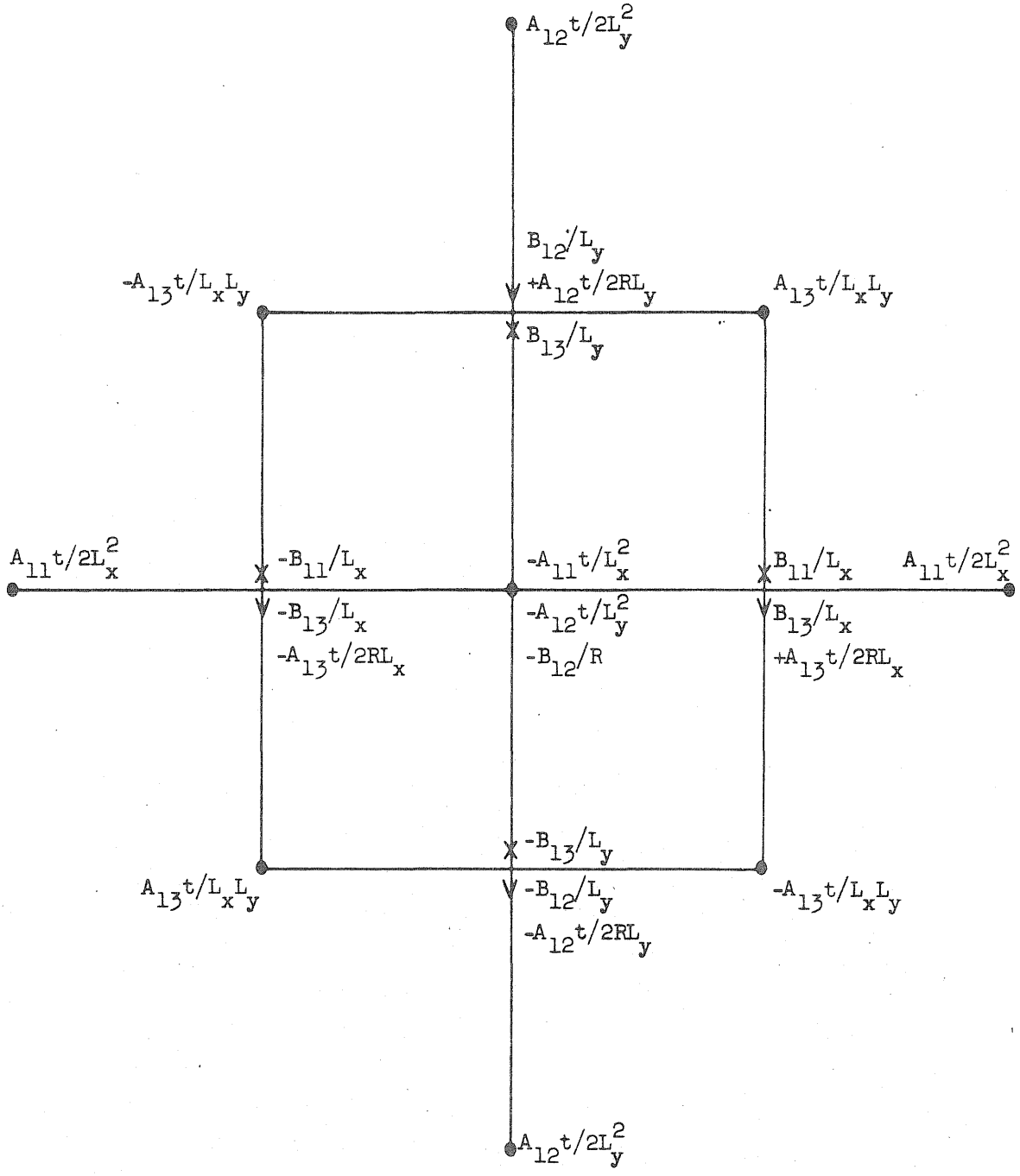

FIG. B-4 OPERATOR TO BE USED WITH M_x

$$M_y = \frac{L_x ht}{8} \left[\quad \right]$$

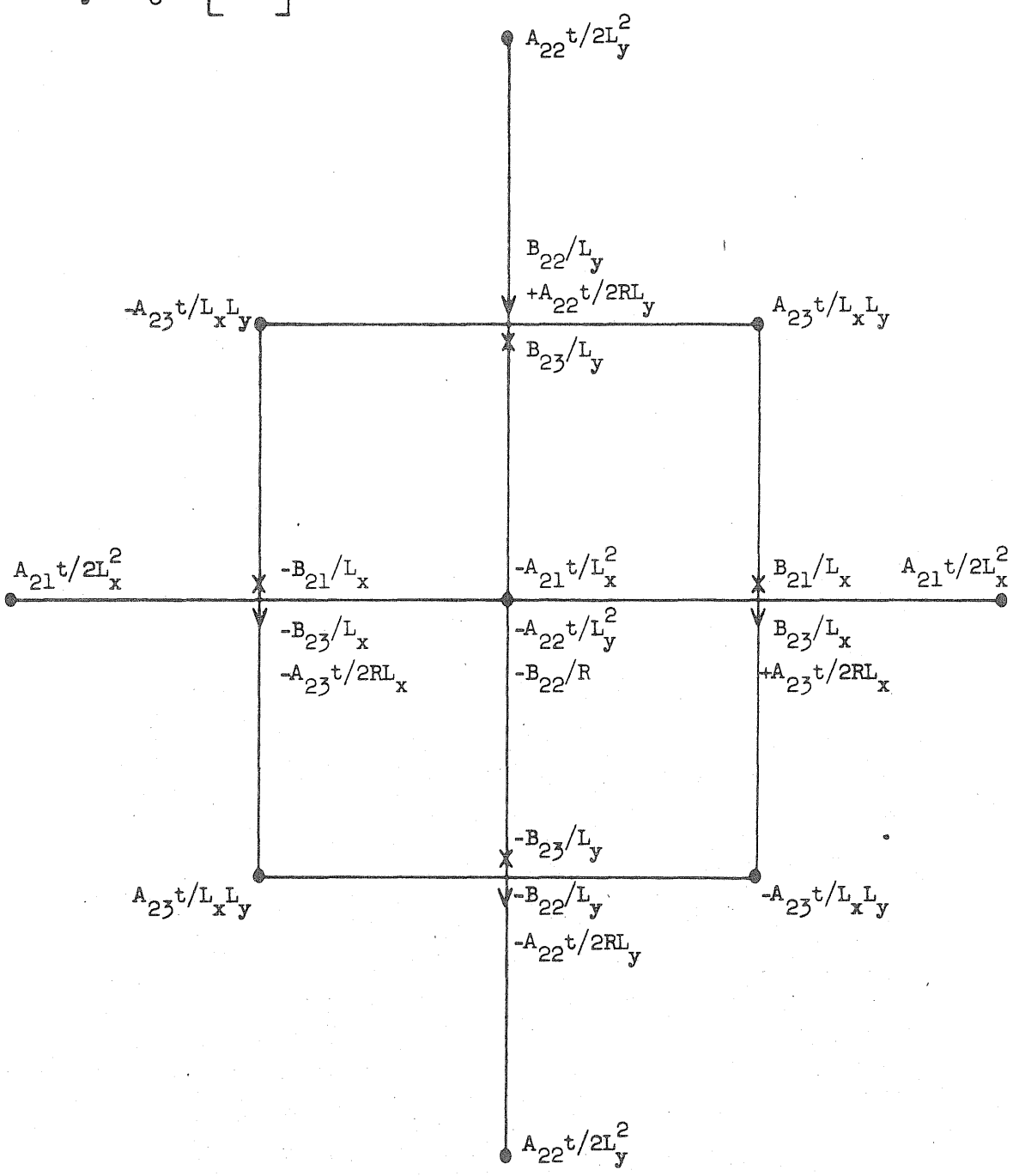

FIG. B-5 OPERATOR TO BE USED WITH M_y

$$M_{xy} = \frac{L_y ht}{8} \left[\quad \right]$$

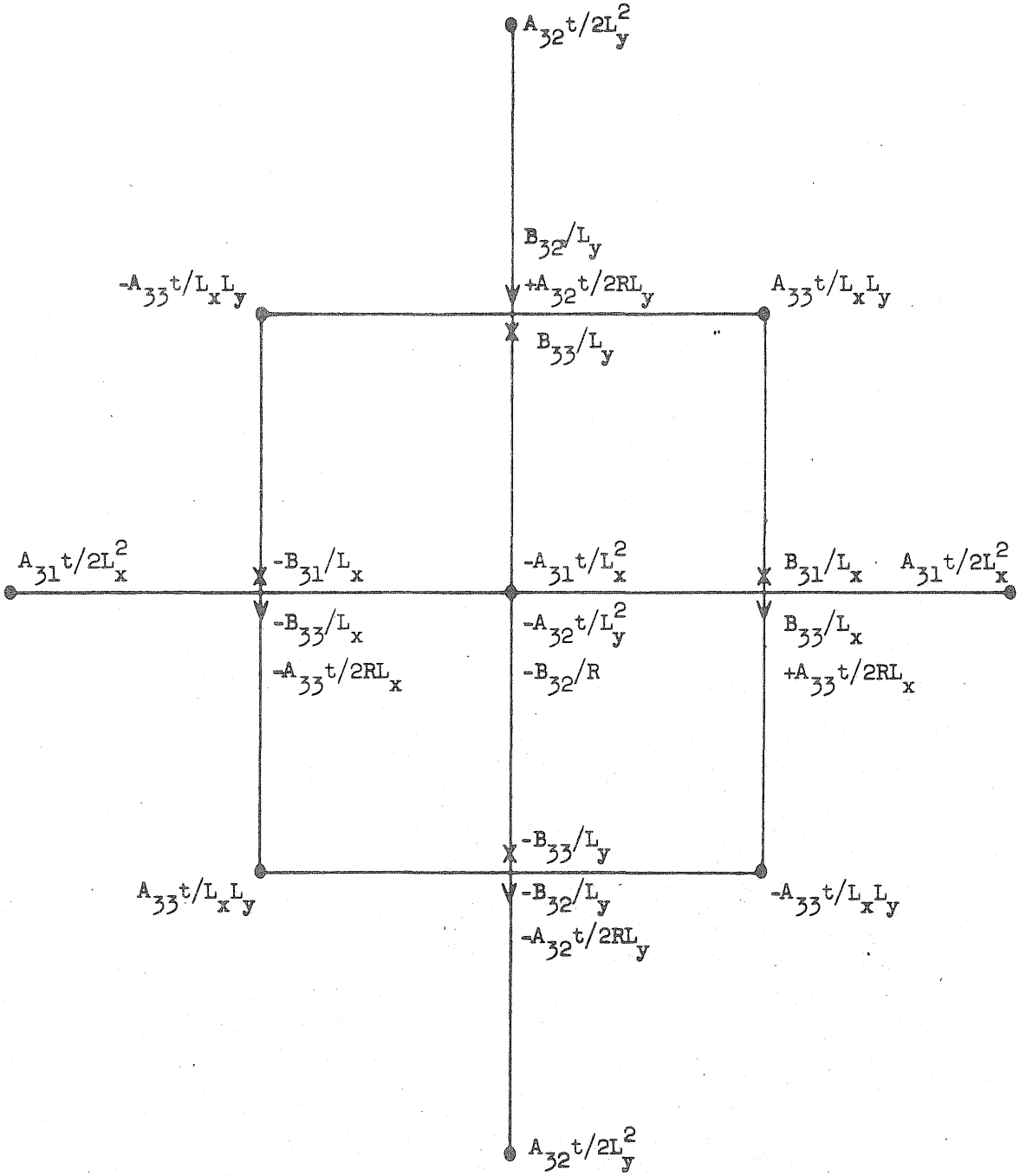

FIG. B-6 OPERATOR TO BE USED WITH M_{xy}